UCLouvain

École polytechnique de Louvain

Robustness study of patient-specific range modulators for conformal FLASH proton therapy

Authors: **Bérénice BESÈME, Mano PLETINCKX**
Supervisor: **John LEE**
Readers: **Edmond STERPIN, Sylvain DEFFET**
Academic year 2022–2023
Master [120] in Biomedical Engineering

Acknowledgements

First, we would like to thank our supervisor John Lee for giving us the opportunity to work on this topic. It was a great opportunity to work on an innovative and interesting subject that could have direct usefulness. It was also an excellent opportunity to work as a pair to improve our personal skills like teamwork or communication.

We also would like to offer special thanks to Sylvain Deffet for his support, advice, and time spent guiding us throughout this master's thesis.

We must also thank Edmond Sterpin for being a jury member and taking the time to be present for our oral defense.

Thanks go to IBA and the FLASH team for their advice, suggestions, and their welcome at all the meetings. Also thanks go to MIRO for giving us the opportunity to work together on their premises.

Finally, thanks go to our families and friends for their support throughout this master's thesis.

Abstract

Cancer is a leading cause of death worldwide and various treatment options are available to combat this disease. One commonly used approach is external radiation therapy, which aims to destroy cancer cells by damaging their DNA through radiation delivery. Proton therapy (PT), an advanced technique, offers the potential for improved precision in targeting the tumor volume compared to conventional radiotherapy methods. Recently, it has been shown that using ultra-high dose rates would less damage the healthy tissues while maintaining the same tumor control. The characteristic of this new method, also known as FLASH, is to deliver the prescribed dose in a much shorter time window. In order to administer the dose within a limited time frame, an additional component must be incorporated. This component is a 3D patient-specific range modulator that passively degrades proton beam energy in order to perfectly match the tumor shape. The addition of a new component can create uncertainties due to various factors. In this master's thesis, we will study the impact of 3 types of uncertainties on dose delivery in FLASH-PT: spot size uncertainties, spot position uncertainties, and analysis of air inclusions when printing the patient-specific range modulator. To achieve this goal, we computed simulations of beam delivery in OpenTPS (an open-source treatment planning system developed at UCLouvain). Following the analysis of the results, we observe that some characteristics, particularly the spot size, are more important to be heeded of but the field still seems to be promising. However, this study did not cover all the uncertainties that could appear. Further studies still need to be made in order to validate this technique.

Keywords: Radiation therapy, proton therapy, FLASH, uncertainties, patient-specific range modulators, IMPT, OpenTPS

Contents

List of Figures

Acronyms

BDL Beam Data Library.

CT Computed Tomography.

CTV Clinical Target Volume.

DMF Dose Modifying Factor.

DR Dose Rate.

DVH Dose-Volume Histogram.

ESS Energy Selection System.

FMF FLASH Modifying Factor.

GTV Gross Target Volume.

GUI Graphic User Interface.

HI Homogeneity Index.

HU Hounsfield Unit.

IMPT Intensity Modulated Proton Therapy.

IMRT Intensity Modulated Radiotherapy.

MC Monte Carlo.

OAR Organ At Risk.

PBS Pencil Beam Scanning.

PT Proton Therapy.

PTV Planned Target Volume.

ROI Region Of Interest.

RT Radiotherapy.

SOBP	Spread Out Bragg Peak.
TPS	Treatment Planning System.
UHDR	Ultra-High Dose Rate.
VMAT	Volumetric Modulated Arc Therapy.
VOI	Volume Of Interest.
WET	Water Equivalent Thickness.

Chapter 1

Introduction

Cancer is a leading cause of death worldwide, accounting for nearly 10 million deaths in 2020 and more than 19 million cases reported ([1]) ([2]). Although this disease is becoming increasingly widespread, it largely remains a mystery and is difficult to treat due to its complexity. Many innovative treatments have been developed over the last few years to fight cancer but research is still ongoing to find increasingly effective treatments.

Nowadays, various approaches are implemented in treating this disease, but our focus lies on external radiation therapy. This kind of therapeutic method involves delivering radiation to the patient from an external source to eradicate cancer cells by damaging their DNA. While photons are commonly used in conventional radiotherapy (RT), it has been demonstrated that protons possess interesting characteristics for cancer treatment. The advantage of protons over photons is the energy deposition along the pathway. While the energy of photons decreases as they pass through matter, the main fraction of the protons' energy is released at a certain depth (which we call the Bragg Peak) which depends on the speed of the particle (and thus on its initial energy). Using protons allows to better spare healthy tissues around cancerous ones during treatment delivery.

To deliver protons, the current gold standard method is performing the Pencil Beam Scanning (PBS) at various energy layers. Also called Intensity Modulated Proton Therapy (IMPT), this method consists in painting the target layer by layer, line by line. On each layer, the beam scans the tumor line by line to cover the entire layer. To change layers in depth, an Energy Selection System (ESS) is used to deliver protons with a different energy. By having a different energy, protons will stop at a different depth, which leads to the irradiation of another layer. The process resumes until the whole tumor is covered.

Recent research has shown promising results for a novel treatment approach known as Ultra-High Dose Rate (UHDR) radiation therapy, or FLASH. This innovative technique has the potential to minimize damage to healthy tissues surrounding the cancer while achieving comparable tumor control to conventional delivery methods. This method exists for various types of external radiation therapy, such as conventional proton therapy (PT). FLASH therapy involves delivering the dose in a much shorter time frame. This requires a significantly higher dose rate than conventional PT. Ongoing research aims to understand the biological mechanisms that contribute to FLASH therapy's ability to spare healthy tissues. Research at UCLouvain is being conducted to assess the potential of FLASH-PT.

The challenge with FLASH therapy lies in the requirement of delivering an extremely high-intensity dose within a very short timeframe. This limited time window poses a constraint on the energy selection system to swiftly switch between different configurations, so as to adjust the energy of the delivered protons. To address this challenge, a novel component called a range modulator, also known as a hedgehog due to its shape, is incorporated into the treatment machine. This range modulator is a patient-specific 3D component designed to accurately match the shape of the tumor. By integrating this component, the depth-wise dose delivery is passively achieved through the range modulator and is no longer actively performed by the ESS.

The aim of this study is to evaluate the effects of various types of uncertainties on the administration of the dose using this 3D patient-specific range modulator. To achieve this goal, we tested various parameters:

- Impact of spot size on dose distribution.

  Our objective by evaluating this parameter is to assess whether altering the spot size will have an impact on the predicted dose distribution in the treatment plan. Spot sizes are linked to the beam data library (BDL) which contains beam parameters for various energy settings.

- Impact of spot position on dose distribution.

  If the hedgehog is not well positioned, the dose at each point could be degraded differently from what it should be. Therefore, it is important to evaluate the difference in dose distribution with a small shift of the hedgehog, and whether this has an impact on the treatment plan.

- Impact of air inclusions during 3D printing of the range modulator on dose distribution.

  During the 3D printing process, air inclusions can be formed inside the hedgehog, which can affect the quality of the printed component. When protons pass through air instead of material, their energy will not be degraded as necessary, which can affect the final dose delivery.

Based on the results obtained, we will discuss whether the patient's treatment needs to be adjusted if the uncertainties significantly alter the initial treatment plan.

Chapter 2

External Radiation Therapy

In this chapter, we will provide an introduction to cancer and discuss one of the commonly employed treatments, external radiation therapy. Currently, radiotherapy serves as a fundamental treatment for cancer, but there is ongoing progress in proton therapy due to the unique properties of protons. We will also provide a brief overview of the proton journey from creation to delivery and address the uncertainties associated with dose delivery. Towards the end of this chapter, we will introduce the concept of FLASH delivery method from a biological point of view. We will illustrate this concept with an example and discuss the challenges associated with implementing this technique in existing proton therapy facilities.

2.1 Cancer

Cancer arises from the transformation of normal cells into tumor cells via a multi-stage process that generally progresses from a pre-cancerous lesion to a malignant tumor ([1]). It is a disease in which some of the body's cells grow uncontrollably and spread to other parts of the body, as shown in Figure 2.1 ([3]). This is a clear and simple definition but in reality, a cancer is a very complex organism much more complex than just a mutated cell that replicates. Currently, cancers remain enigmatic and their nature is not fully understood, with limited knowledge at our disposal.

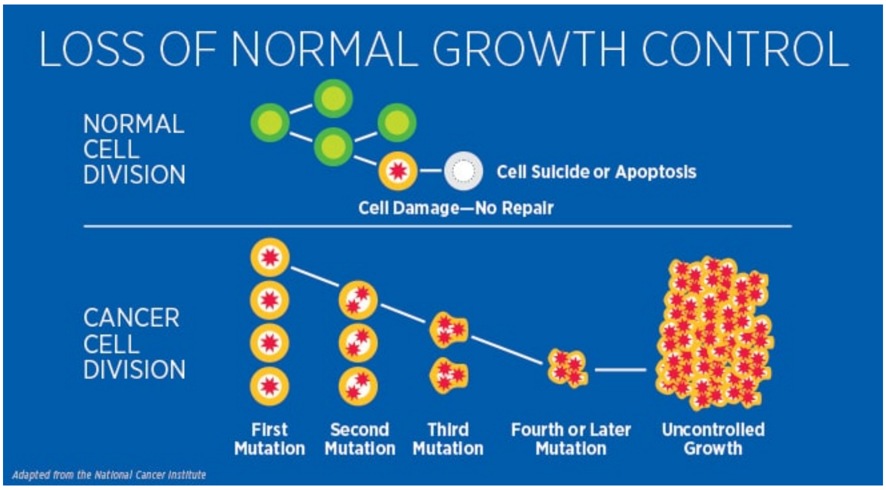

Figure 2.1: Development of a cancer cell ([4])

Over time, scientists tried to better understand cancer's characteristics. In 2000, they created the

"Hallmarks of cancer" which are characteristics that generally appear during the development of cancer. Initially, 6 hallmarks were found to characterize cancer, they are shown in Figure 2.2.

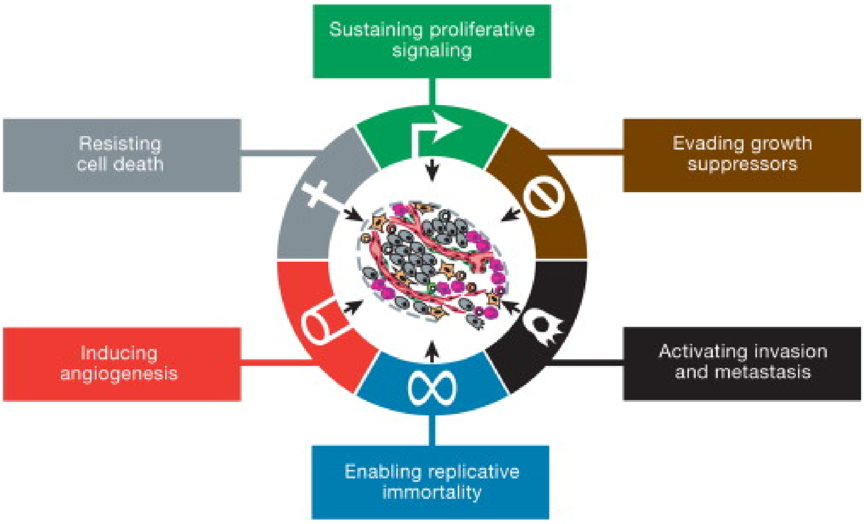

Figure 2.2: Hallmarks of cancer in 2000 (5)

In 2011, they updated the document with 4 new characteristics which resulted in 10 hallmarks of cancer as in Figure 2.3.

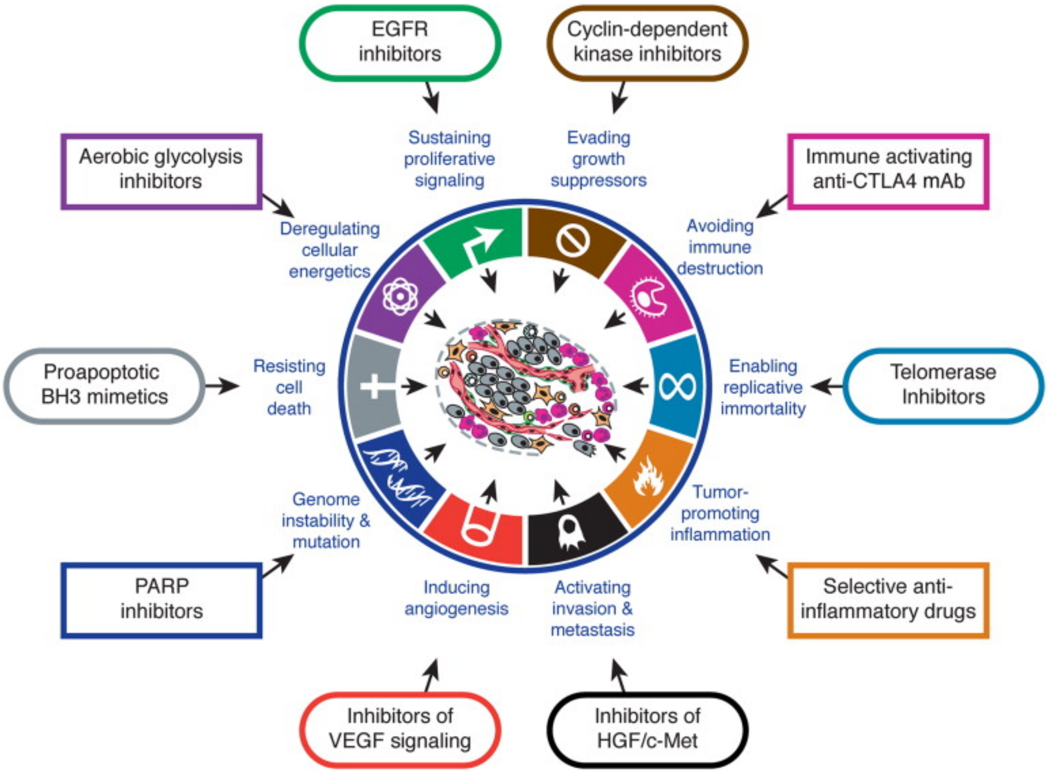

Figure 2.3: Hallmarks of cancer in 2011 (5)

Last year, in 2022, a new version was published with 4 new hallmarks, which shows that our understanding of cancer is still ongoing. It is difficult to determine the exact number of hallmarks required to diagnose cancer as not all types of cancer exhibit all the hallmarks.

Various techniques exist to treat cancer (6), the most common being

- Surgery: remove the cancer or as much of the cancer as possible.
- Chemotherapy: use drugs to kill cancer cells.
- Radiation therapy: use high-powered energy beams, such as X-rays or protons, to kill cancer cells. Radiation treatment can come from a machine outside the body (external beam radiation), or it can be placed inside the body (brachytherapy).
- Immunotherapy: use the body's immune system to fight the cancer.

The kind of therapy administered to a patient is contingent upon the type and stage of cancer they are afflicted with.

External radiation therapy, which is the main subject of this paper, can be used to treat primary cancer or advanced cancer. It can also be used to reduce the size of the tumor and relieve pain, discomfort, or other symptoms, depending on the type of cancer and how far it has spread ([7]). It is often combined with another technique to increase the chance of recovery for the patient.

Various types of radiation are used ([8])

- photons: the most used technique (radiotherapy).
- protons: thanks to the physical properties of protons, they have the potential to better spare the Organ At Risk (OAR) around the tumor. This will be explained in the section 2.2.
- electrons: currently, beams of electrons cannot travel very far through the body, so their use is limited to tumors on the skin or near the body surface.

2.2 Radiotherapy

The objective of radiotherapy is to irradiate cancer so as to break the DNA brand in order to stop cancer replication without harming the patient too much or damaging the surrounding healthy tissues.

In Figure 2.4 we can see the curve of the tumor control and the curve for the normal tissue complication. Raising the dosage is good for killing cancer cells but it also affects the healthy cells around, therefore a balance must be struck to ensure patient safety. The aim is to widen the gap between the two curves: a maximum level of tumor control and a minimum risk of normal tissue complications. This optimal window allows for the highest radiation dose to be delivered to the tumor while minimizing exposure of healthy tissue. The goal is to eradicate the cancer without inducing secondary malignancies.

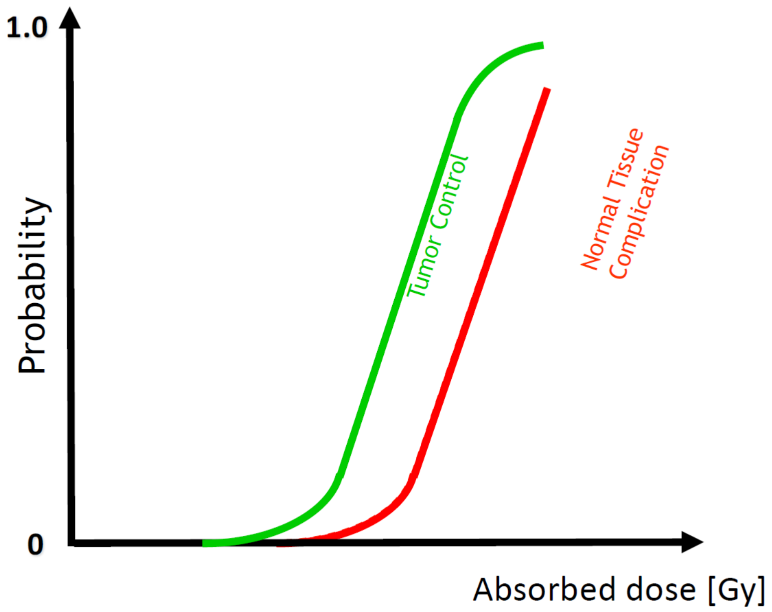

Figure 2.4: Therapeutic window ([9])

To allow sufficient time for healthy tissues to recover, dividing the radiation dosage into fractions is essential. As we can see in Figure 2.5, by breaking up the treatment into fractions, the same level of cell survival can be achieved with a higher overall dosage than would be possible with a single, large dose. Healthy tissue possesses a distinct advantage in the form of DNA repair mechanisms, which are led by the p53 protein, often referred to as the "guardian of the genome". Cancer cells lack this restorative ability. Thus, when fractioning the dosage, it is necessary to strike a balance between allowing sufficient time for healthy cells to repair themselves and not providing an excessive window for cancer cells to proliferate.

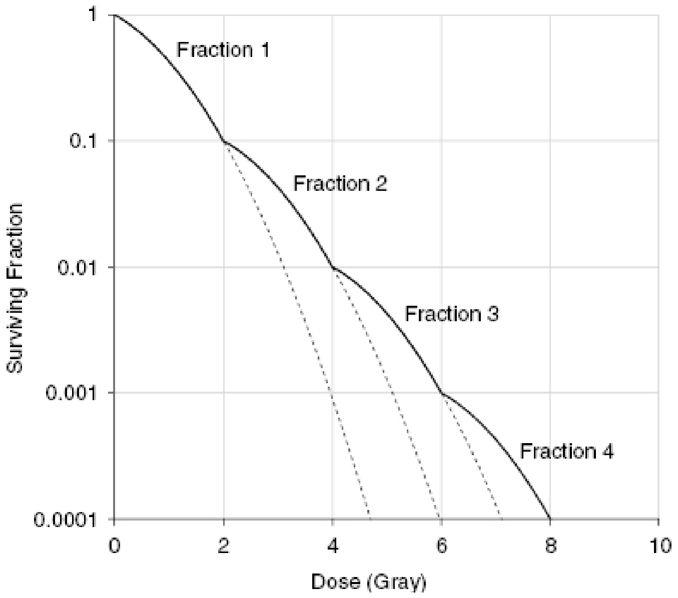

Figure 2.5: Dose fractioning ([10])

When healthy cells do not receive adequate time for repair, or when the damage is extensive, the level of surviving cells decreases, leading to toxicity in the healthy tissues. Figure 2.6 displays the various toxicity levels, with the primary objective of always keeping the lowest number in the table below ([11]). It is obvious that radiation treatment requires careful control and can have severe consequences if not properly administered.

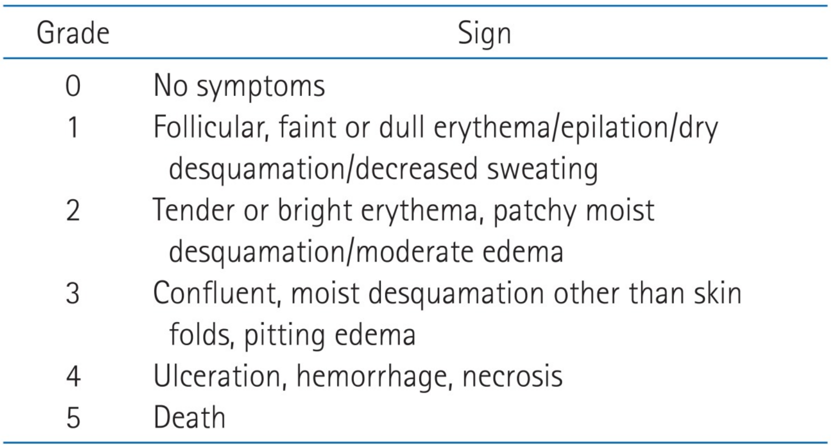

Grade	Sign
0	No symptoms
1	Follicular, faint or dull erythema/epilation/dry desquamation/decreased sweating
2	Tender or bright erythema, patchy moist desquamation/moderate edema
3	Confluent, moist desquamation other than skin folds, pitting edema
4	Ulceration, hemorrhage, necrosis
5	Death

Figure 2.6: Toxicity levels for radiation treatment (11)

Typically, in patients undergoing conventional radiotherapy, the skin is the primary organ impacted as it receives the highest dosage. This is attributed to the way photons deposit energy when traveling through matter. Depending on the particle type, energy deposition into the travel material can vary.

As we can see in Figure 2.7, particles release their energy at different moments. Electrons, for instance, discharge most of their energy at very shallow depths, making them suitable for treating skin cancer or lesions close to the surface as previously mentioned. Electrons are also preferable to photons for treating proximal cancer, since their curve decreases rapidly, resulting in lower doses for organs located beyond the tumor site.

Following the electron curve is the curve for photons, which has its top not very far from the top of the electron curve. However, the key distinction is that the delivery of photon doses decreases gradually, which implies that doses remain relatively high even as photons travel through matter. This characteristic has both benefits and drawbacks: it is advantageous for irradiating tumors located at any depth, but it also results in the irradiation of many healthy tissues along the pathway. To reduce the dose on healthy tissues but keep the full dose on the cancer, Intensity Modulated Radiotherapy (IMRT) is used. IMRT employs multiple angles to deliver the dose, sculpting the radiation beams so as to conform closely to the cancerous area and spreading the undesired dose to healthy tissues. The beams are shaped to match the shape of the cancer and can move through an arc while they deliver the radiation (12). IMRT can be very helpful in areas such as the head and neck, for example, to avoid the spinal cord or salivary glands. Volumetric Modulated Arc Therapy (VMAT), also known as Rapid Arc, is a new type of IMRT that is increasingly being utilized. VMAT differs from traditional IMRT in that the radiation beam is delivered in an arc shape, with the radiotherapy machine rotating around the patient. As it moves around the body, the machine continuously adjusts the shape and intensity of the radiation beam (13). The main advantage of VMAT is a shortened delivery time, which leads to improved patient comfort and possibly smaller intra-fraction movements (14). A comparison of dose distributions between 3D conventional RT, IMRT and VMAT is shown in Figure 2.8.

Compared to electrons and photons, protons and carbon particles display a significantly different energy distribution. The Bragg Peak of protons and carbon particles provides a significant advantage over photons, as the majority of the dose is concentrated at a specific depth (for a given energy) and drops off almost instantly. As for RT, Intensity Modulated proton therapy (IMPT) exists for protons. Today, IMPT is the standard way to deliver PT.

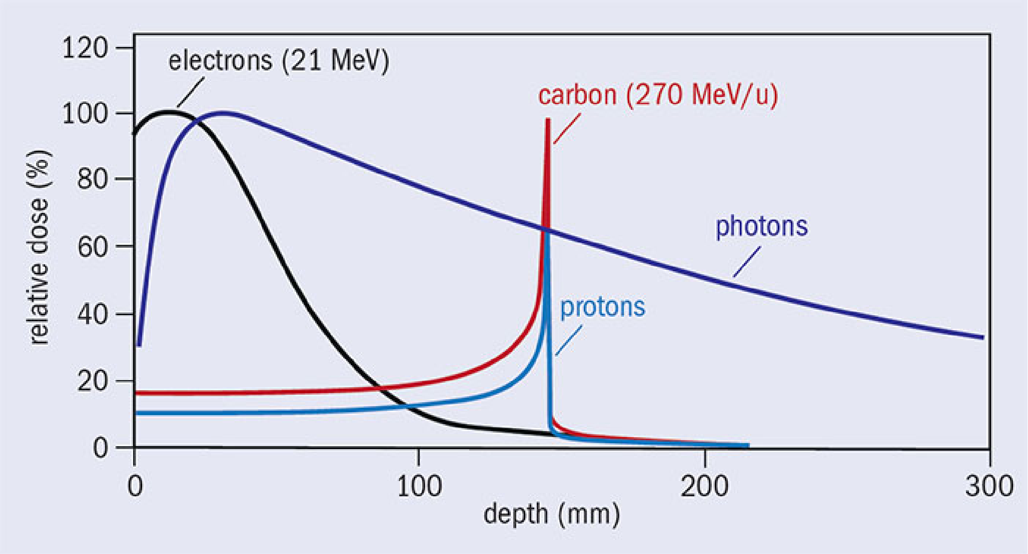

Figure 2.7: Energy deposition of various particles into matter ([15])

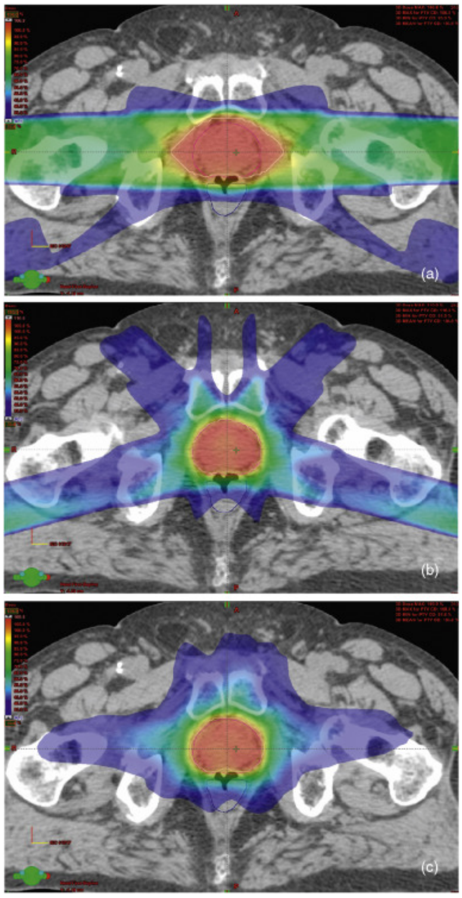

Figure 2.8: Comparison of dose distribution for (a) 3D-CRT, (b) IMRT and (c) VMAT ([16])

Figure 2.9 shows the dosimetric advantage of protons over photons. Less excessive dose is given to healthy tissues with protons leading to the sparing of most of the OAR around the cancer.

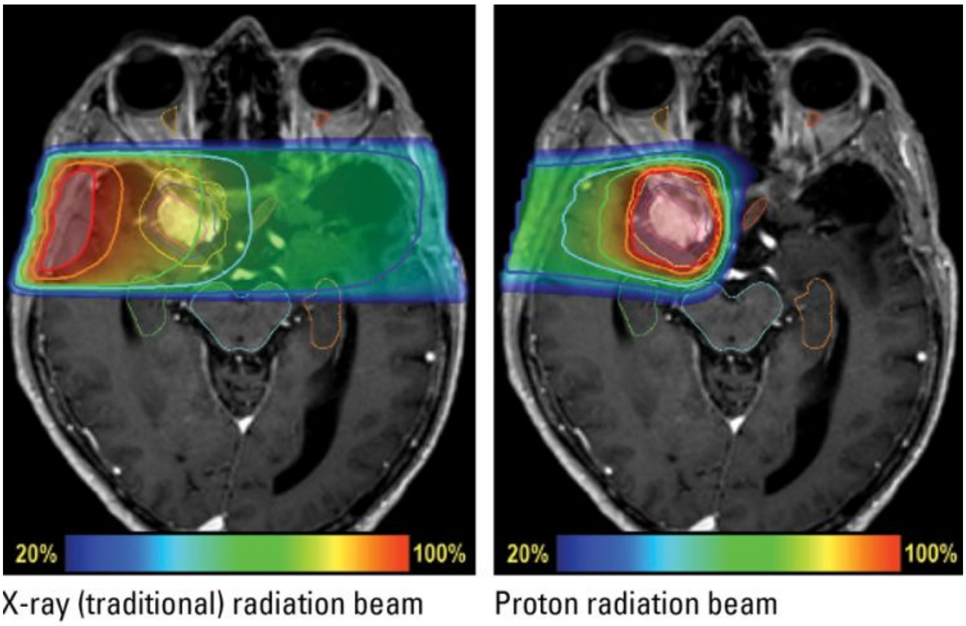

Figure 2.9: Dose deposition on MRI image for a patient with meningioma (17)

2.3 Proton therapy

Ensuring a uniform dose distribution on the target volume is crucial as cancer is not limited to a single point or surface. This uniformity is achieved through the creation of a Spread Out Bragg Peak (SOBP) in which several Bragg peaks of different ranges are combined. These peaks correspond to different entrance energies and have specific intensities or weights, as shown in Figure 2.10 (18).

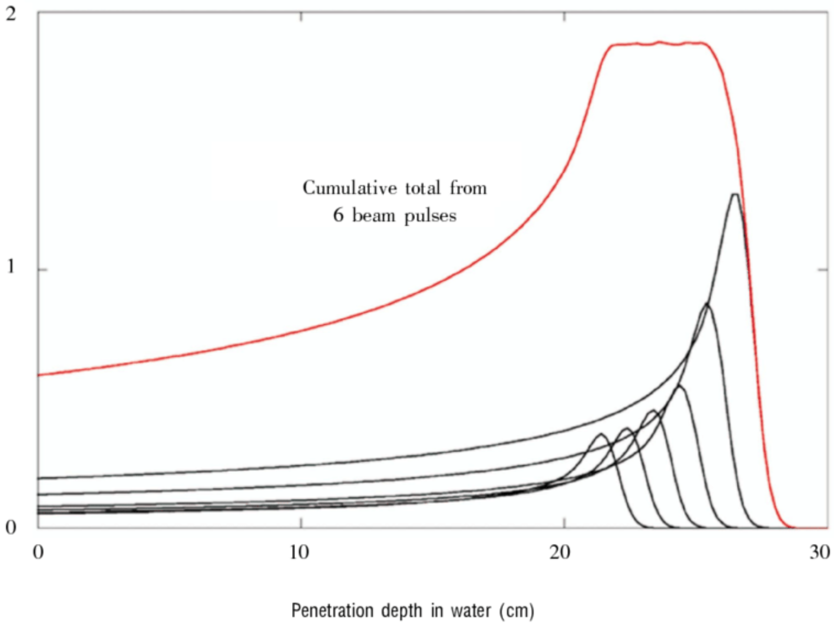

Figure 2.10: Spread out Bragg peak (SOBP) (19)

Figure 2.11 illustrates the advantage of using proton therapy over conventional radiotherapy with X-rays for treating cancer. The grey area indicates the depth at which the cancer is located and where the maximum dose is desired. The blue curve represents the dose distribution for X-rays, and the red curve represents the dose distribution for protons with SOBP. The blue shaded area represents the amount of healthy tissue spared by using protons instead of X-rays. This difference in healthy tissue sparing can be significant, especially when surrounding tissues are considered OAR.

IBA builds their machines based on the principle of using the Bragg Peak to treat cancer, while their competitor Varian takes a different approach. Varian uses transmission beam PT and lets the protons traveling through the body to have the Bragg Peak outside, without relying on the Bragg Peak characteristic to treat cancer ([20]).

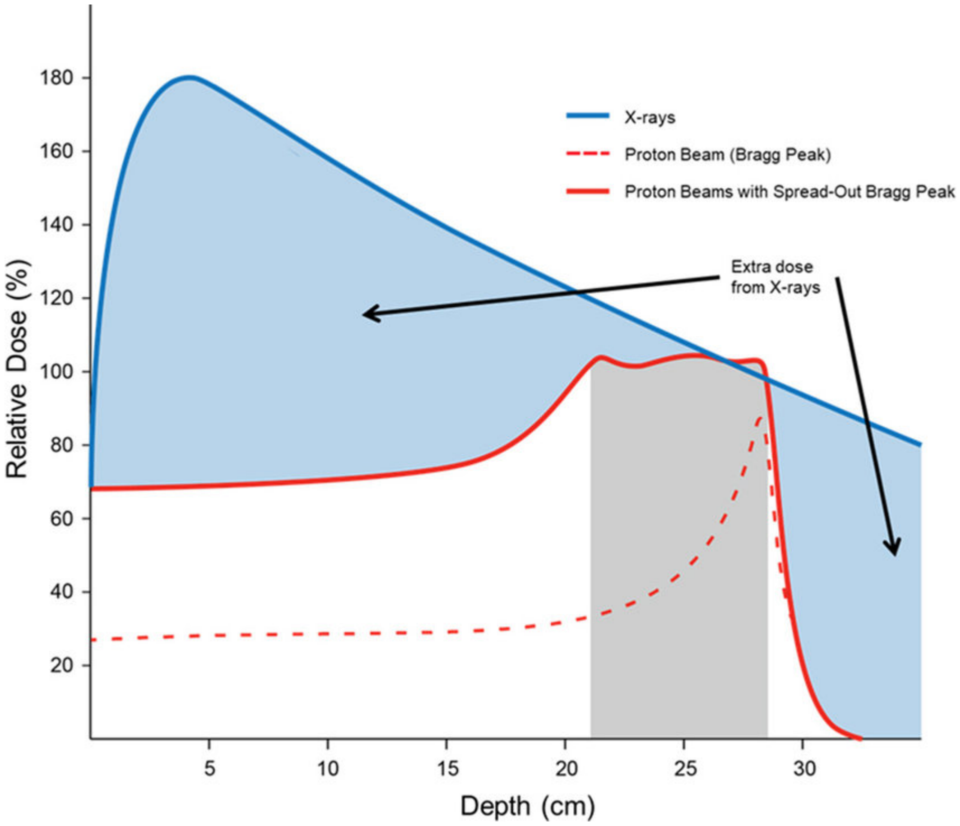

Figure 2.11: Spread out Bragg peak and spared dose ([21])

In order to attain the desired energy level, protons need to undergo a process of acceleration to reach high energies (using devices like cyclotrons). Subsequently, the protons are decelerated to attain the intended energy level.

2.3.1 Set-up

To generate accelerated protons, a hydrogen particle is used because it contains only one proton and one electron. An electric field is applied to separate the proton and the electron. The proton is then placed in a cyclotron to be accelerated up to the desired energy, which corresponds to a specific speed. Following the acceleration of protons, the beams are guided towards the gantry using electromagnets. In the treatment room, the gantry, which is the third component of the delivery system, can rotate around the patient to deliver treatment from the desired angle. Finally, the beam is delivered to the patient through the nozzle.

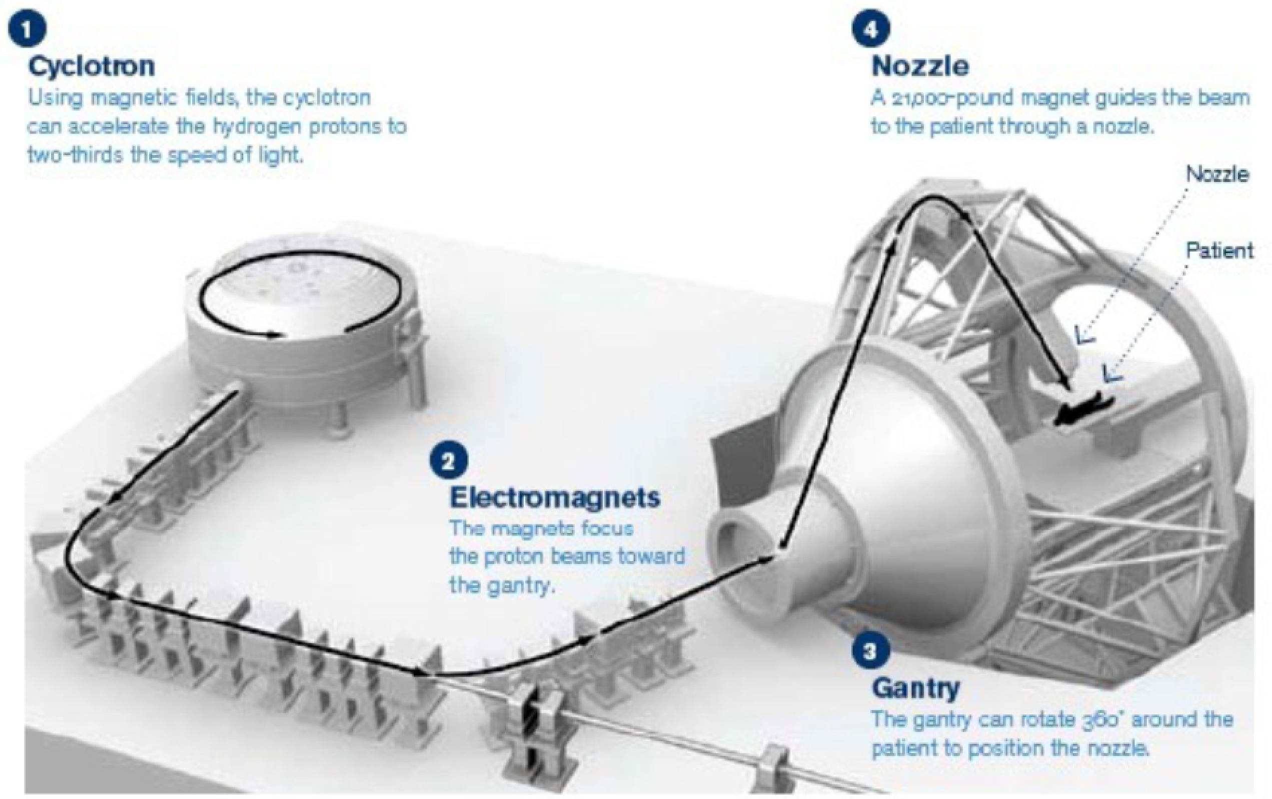

Figure 2.12: Proton pathway for treatment delivery ([22])

As previously discussed, using protons in radiation therapy has numerous advantages. However, it is still crucial to deliver the correct dose to the target area. The state of the art PT technique is PBS IMPT in which the tumor is painted laterally with a so called Pencil Beam Scanning (PBS) and in depth by changing the energy of the protons between successive layers.

2.3.2 Pencil Beam Scanning (PBS)

The PBS technique is illustrated in Figure 2.13. As the name suggests, it involves a single beam that travels all along the tumor in depth and over each layer. This beam is used to paint the tumor with small and discrete spots of radiation. The intensity and position of the pencil beam can be carefully controlled so as to deliver the desired radiation dose to the target while minimizing exposure of surrounding healthy tissue. The principle is to use 2 pairs of magnets (in green) to direct the beam onto each layer. For a given energy, the beam is maintained at a specific depth, and the magnets direct it towards each point on the layer.

The beam that exits the cyclotron has constant energy, but an Energy Selection System (ESS) allows protons to vary in energy and consequently stop at different depths. The ESS, depicted in Figure 2.14, takes some time to reconfigure and provide protons at different energy levels at the output of the nozzle. Energy layer switching may be of the order of 1s ([23]).

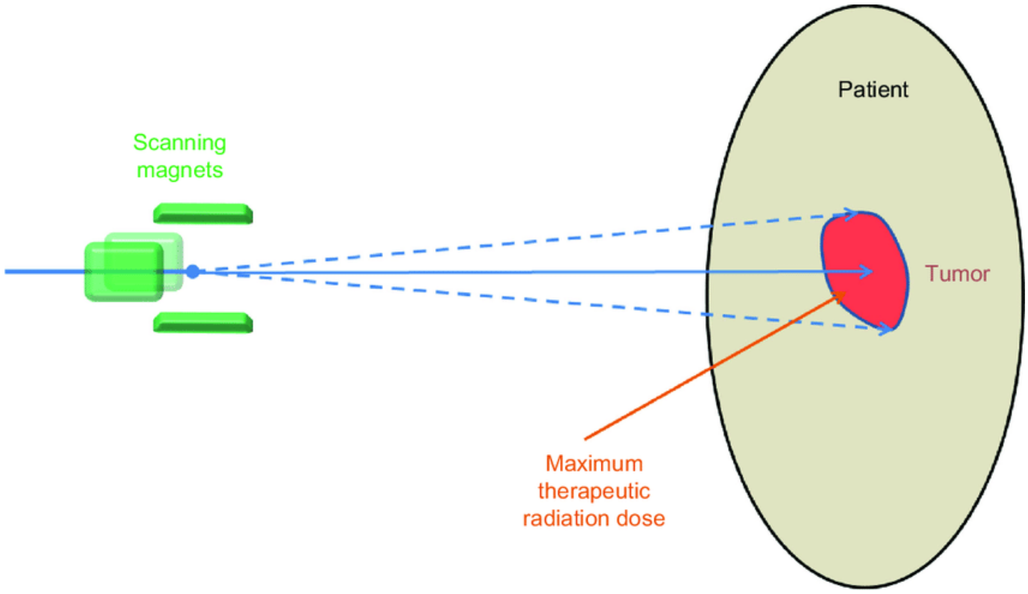

Figure 2.13: Pencil Beam Scanning (PBS) ([24])

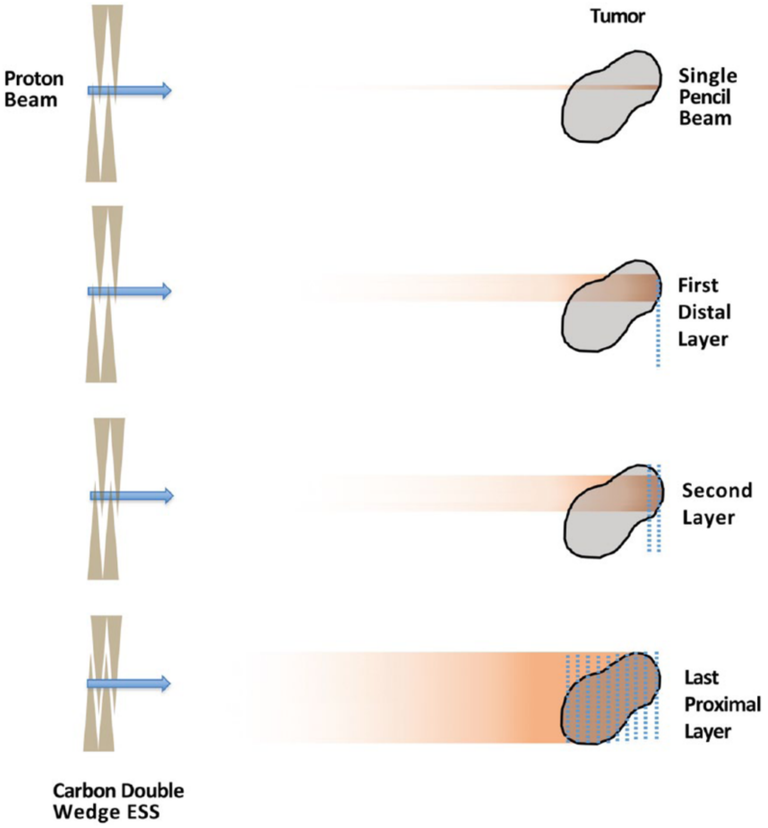

Figure 2.14: Energy Selection System (ESS) ([25])

In order to deliver the desired dose to a specific layer using the magnets, the proton beam is directed to all spots of the target line by line, layer by layer. in Figure 2.15 we can see the beam's eye view of an arbitrary target contour superimposed with a grid pattern for proton delivery that has a fixed 2 mm spot spacing.

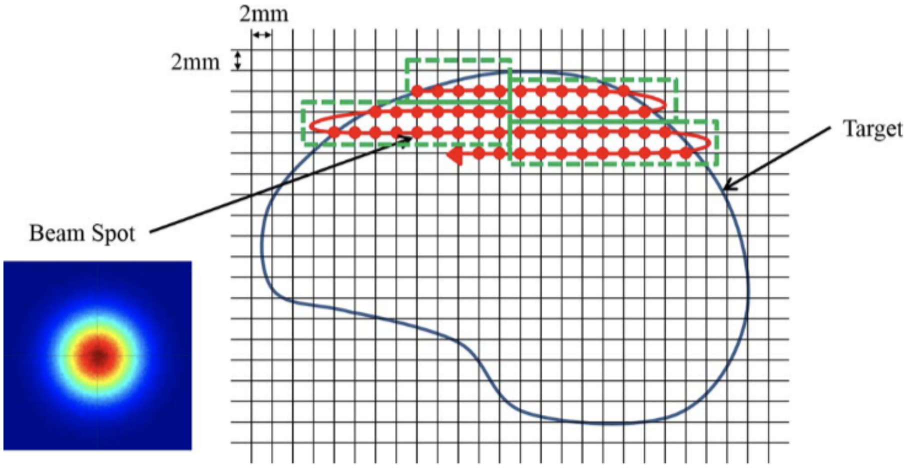

Figure 2.15: PBS scanning pattern in conventional PT ([26])

In PBS, the amount of dose received by a particular spot is not constant throughout the treatment delivery, as demonstrated in Figure 2.17. The dose is delivered to different areas of the volume at different times, with contributions from nearby spots as well as from the low-dose penumbra of neighboring spots. With multiple energy layers the dose to a given point may have contributions from the entrance region of multiple different energy layers ([27]).

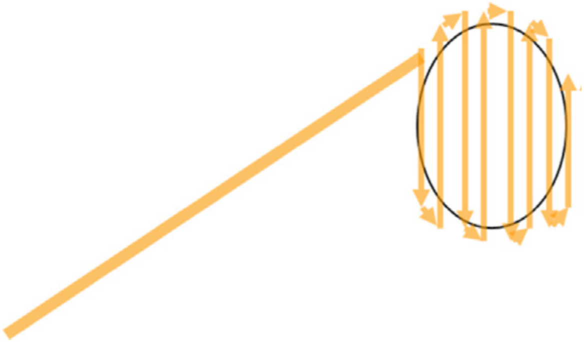

Figure 2.16: PBS ([27])

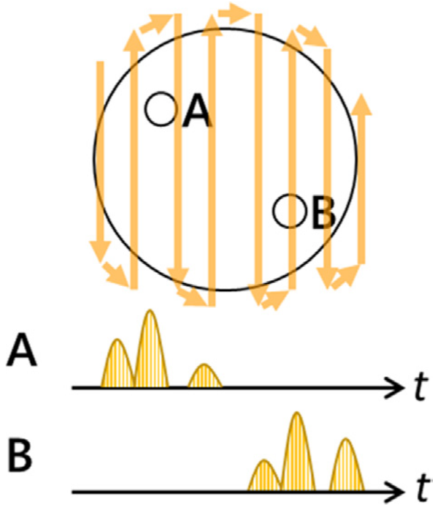

Figure 2.17: Dose for different spots according to time ([27])

The PBS technique offers high precision in delivering radiation to a specific spot. While it is theoretically excellent, in practice, several uncertainties need to be taken into account.

2.3.3 Uncertainties

Radiation therapy is associated with uncertainties that originate from various sources. If these uncertainties are not properly considered and controlled, they can pose a risk to the patient. PT is particularly affected by uncertainties due to the need for precise delivery of protons to achieve the Bragg Peak at the intended location and not just in its vicinity. Uncertainties can lead to overshooting or undershooting the target in PT, as opposed to conventional RT. If we refer to Figure 2.11 when the beam misses the target due to uncertainties, the tumor location (grey zone) is no longer covered by the dose, which poses a greater challenge for PT compared to RT due to the sharpness of the SOBP.

The first source of uncertainty in radiation therapy is related to imaging. There are limitations in the resolution of the images and imperfect conversion of imaging data into quantities required to compute the dose distribution. Additionally, patient anatomy changes, such as displacement or shrinkage of the tumor, weight gain/loss, or cavity filling, which can have a significant impact on the heterogeneity of the pathway. The impact of heterogeneity on dose delivery can be seen in Figure 2.18.

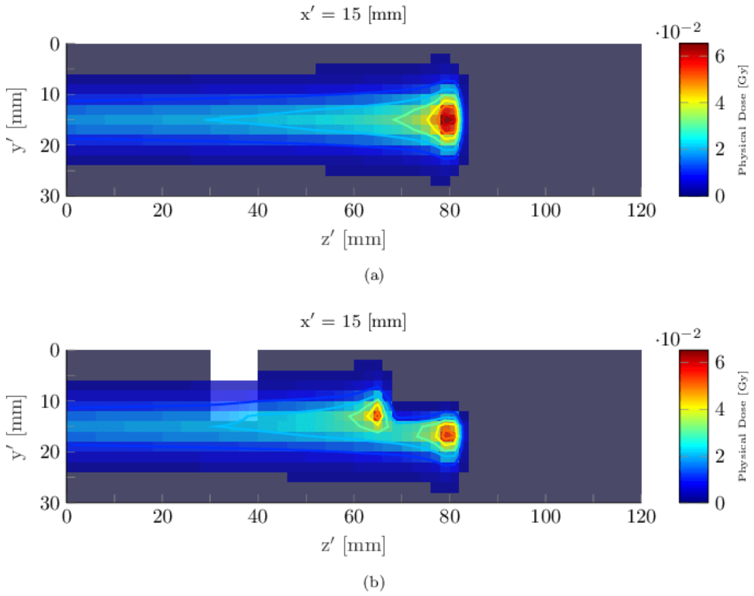

(a)

(b)

Figure 2.18: Effect of heterogeneity on dose distribution ([28])

Another source of uncertainty is patient motion during treatment, such as breathing or organ movement. Patient positioning is also a factor that can introduce uncertainty.

They are two types of errors that can arise from patient positioning: systematic errors that are patient-specific and random errors, which are illustrated in Figure 2.19. The first type of error is the systematic error which occurs consistently in all treatment fractions and leads to misalignment of the dose delivery to the target. The second type of error is the random error which occurs in each delivery fraction and results in a blurring of the dose when all fractions are combined.

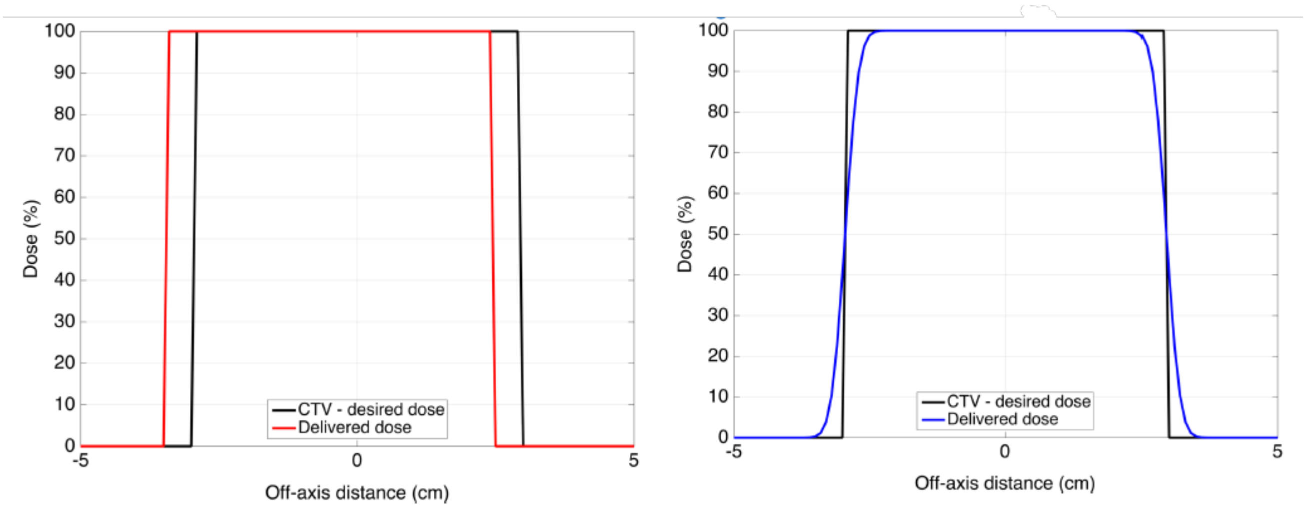

Figure 2.19: The effect of systematic and random errors (respectively) on the dose ([29])

In order to ensure proper coverage of the target, a margin is added to the irradiated zone, which includes not only the tumor volume, but also some surrounding tissue. The target volume is therefore no longer just the cancer but the cancer as well as a margin.

GTV, CTV and PTV

Defining the target volumes is a crucial aspect of treatment planning ([29]). Three important concepts, as depicted in Figure 2.20 and 2.21, are used to establish the treatment zone.

The first volume to be considered is the Gross Target Volume (GTV), which refers to the location and extent of the malignant growth that is palpable, visible, or clinically demonstrable.

Next, we have the CTV or Clinical Target Volume, which includes an extended area around the GTV where cancerous cells are highly likely to be present.

The final volume is the PTV or Planning Target Volume which is an extension of the CTV. In this zone, the presence of cancerous cells is uncertain, but it accounts for the delivery uncertainties of the treatment. The tissues present in this zone are usually healthy, but it is better to irradiate a small amount of healthy tissue than to miss cancer cells and risk the possibility of regrowth.

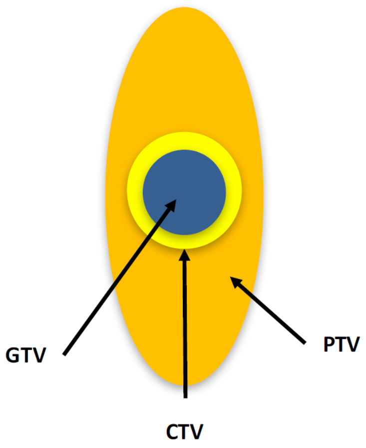

Figure 2.20: GTV, CTV and PTV ([29])

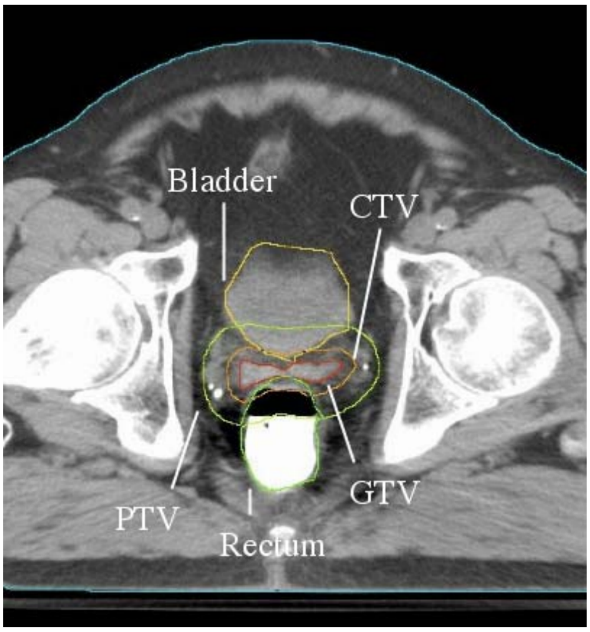

Figure 2.21: GTV, CTV, and PTV on CT slice for a prostate treatment plan ([30])

Measuring both the quantity and quality of the delivered dose is crucial when administering radiation to the PTV. A graphical representation of the simulated radiation distribution within a patient's region of interest (PTV), which is a result of a proposed radiation treatment plan, is called a cumulative dose-volume frequency distribution or a Dose-Volume Histogram (DVH). DVHs are effective tools for comparing alternative treatment plans for a specific patient as they depict the uniformity of dose in the target volume and reveal any high-dose regions in neighbouring normal tissues or organs.

2.3.4 DVH

A DVH example for prostate cancer is illustrated in Figure 2.22. The aim is to achieve the higher dose for the larger volume of the target (i.e., PTV) while minimizing the dose to the OAR. Thus, the PTV curve on the graph should be as sharp as possible and located in the upper right region. On the other hand, for healthy surrounding tissues, the objective is to have the curve as low as possible and located in the bottom left region of the graph.

Important values can be extracted from this graph which are useful for further analysis. We have D_5, D_{95} or D_{mean} which are the values of the dose to cover 5%, 95% of the target or the mean dose to cover the target.

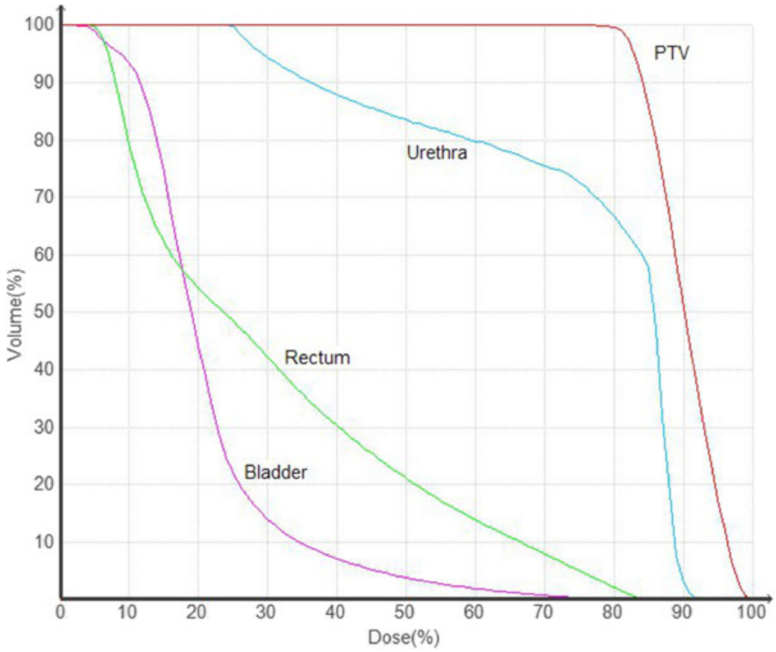

Figure 2.22: DVH example ([31])

Conventional PT and RT have demonstrated their efficacy in treating cancer, but a new delivery method called FLASH is gaining attention due to its potential to spare healthy tissues more effectively than conventional delivery modes.

2.4 FLASH method

In recent years, FLASH radiation therapy has garnered considerable attention because of its ability to potentially minimize the adverse effects associated with radiation therapy administered at conventional dose rates. To qualify as a FLASH treatment, a high dose of radiation must be delivered within an extremely brief time frame. Although further investigation is necessary to gain a comprehensive understanding of the advantages and drawbacks of FLASH proton therapy (FLASH-PT), as well as the underlying mechanism, an increasing number of research studies are exploring treatment planning and delivery ([32]).

This method entails administering the same treatment dose as conventional PT within a much shorter timeframe and fewer fractions compared to conventional PT. As a result, dose rates that are thousands of times greater than those in conventional PT are used. The proton therapy irradiation process typically lasts a few minutes, while in FLASH it is less than one second, but the dose delivered is significantly higher.

The FLASH delivery method is also being explored in radiotherapy and it even started with this. Before 2014, FLASH-RT was referred to as the flash effect, which was first reported by Dewey and Boag in 1959. Dewey and Boag's study outlined that ultra-high dose-rate irradiation can protect bacteria when compared to conventional dose-rate irradiation. In 2014, Favaudon reported that using FLASH-RT to treat lung tumors can lead to a complete response and reduce the early and late toxicity affecting normal lung tissue; subsequently, FLASH became a topic of particular interest in radiation research ([33]).

In Figure 2.23 we can see that the irradiation time can affect organisms at different levels. Current theories suggest that the FLASH effect is protective in normal tissues due to several hypothetical mechanisms including transient oxygen depletion resulting from radiolytic oxygen consumption, differential activation of metabolic and detoxification pathways in response to reactive oxygen and nitrogen species between normal and tumor cells, or radical-radical recombination [34].

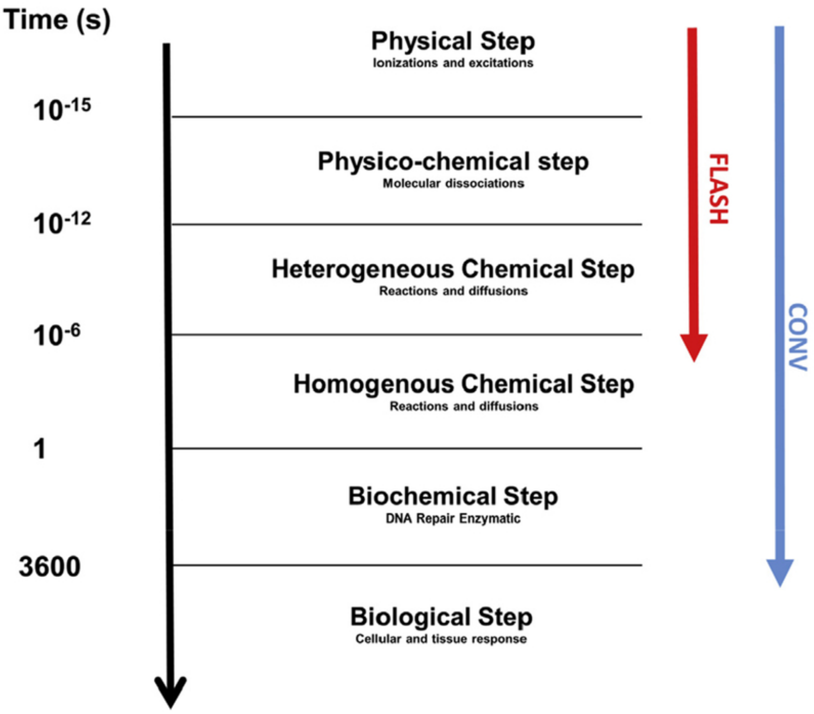

Figure 2.23: Effect of irradiation time on biological tissues [35]

2.4.1 Radiobiological effects

As previously mentioned, the FLASH delivery mode is advantageous in that it preserves a greater amount of healthy tissue surrounding the tumor. Radiation exposures at ultra-high dose rates at several orders of magnitude greater than in current clinical radiotherapy have been shown to manifest differential radiobiological responses compared to conventional dose rates.

The varying radiobiological reactions to a fixed dose lead us to consider the concept of dose modifying-factor, which is fundamental to the utilization of FLASH.

The difference in response between the two delivery methods can be expressed through the FLASH Modifying Factor (FMF). This factor represents the ratio of doses required to achieve an isoeffect (causing the same level of biological effect) for a specific biological system, with one dose administered at conventional dose rates (CONV) and the other at ultra-high dose rates (UHDR) [36]. This FLASH Modifying Factor is defined as [36]

$$FMF = \frac{D_{CONV}}{D_{UHDR}}|_{isoeffect} \tag{2.1}$$

An FMF smaller than 1 indicates that an ultra-high dose rate results in better preservation of normal tissue compared to a conventional irradiation dose rate.

Figure 2.24 displays the FMF values for various organs and animals exposed to a single-fraction ultra-high dose rate dose. It is observed that the FMF values for doses less than 20Gy are approximately 0.9 (almost 1). Although the research presents findings for doses greater than 40Gy, it is impractical for radiation therapists to administer such a high dose since it will cause tissue damage.

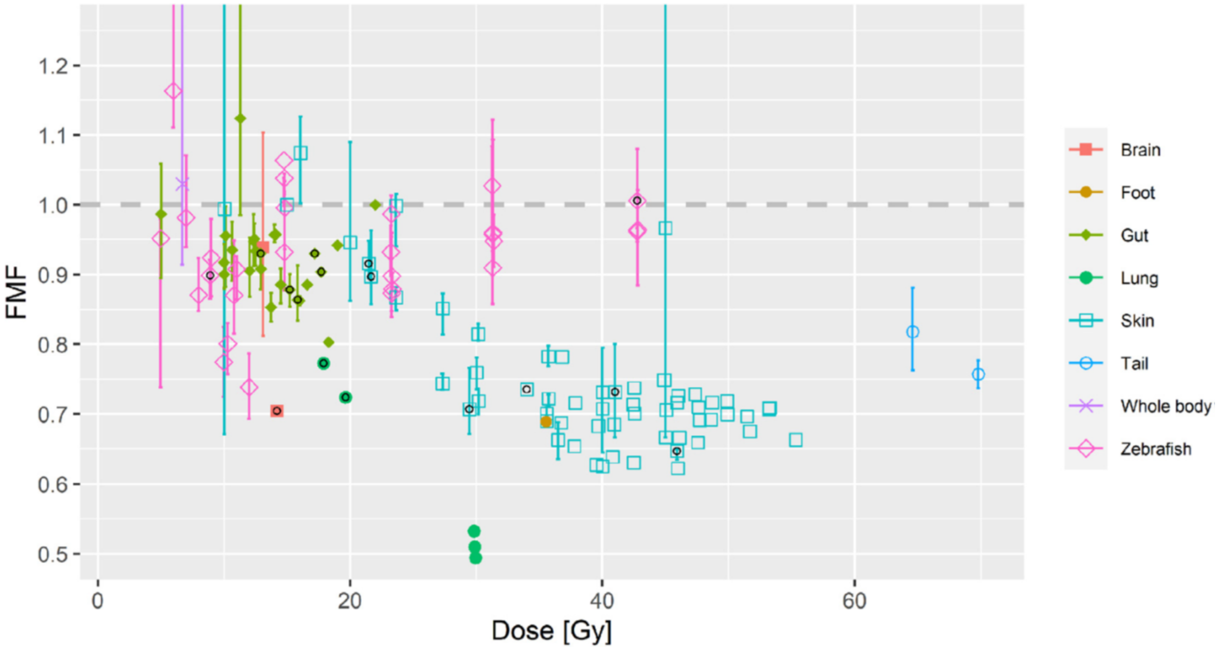

Figure 2.24: FMF values of normal tissues as a function of single-fraction ultra-high dose rate dose, grouped by species and organ/body region (ie, mouse brain, rat foot, mouse gut, mouse lung, mammalian skin, mouse tail, mouse whole body, and zebrafish whole body). Datapoints obtained by small extrapolation of conventional dose rate data or interpolating UHDR data are indicated by black open circles ([36]).

The dose-modifying factor (DMF) is the reciprocal of the FMF. A dose-modifying factor greater than 1 indicates that ultra-high dose rates result in better preservation of normal tissue compared to conventional irradiation dose rates ([36]).

Pre-clinical studies have shown that FLASH radiotherapy can cause a dose-modification factor of 1.2–1.6 in various systems, as shown in Figure 2.25, thereby inducing a sparing effect in healthy tissue of about 20–40% compared to conventional dose rates ([27]).

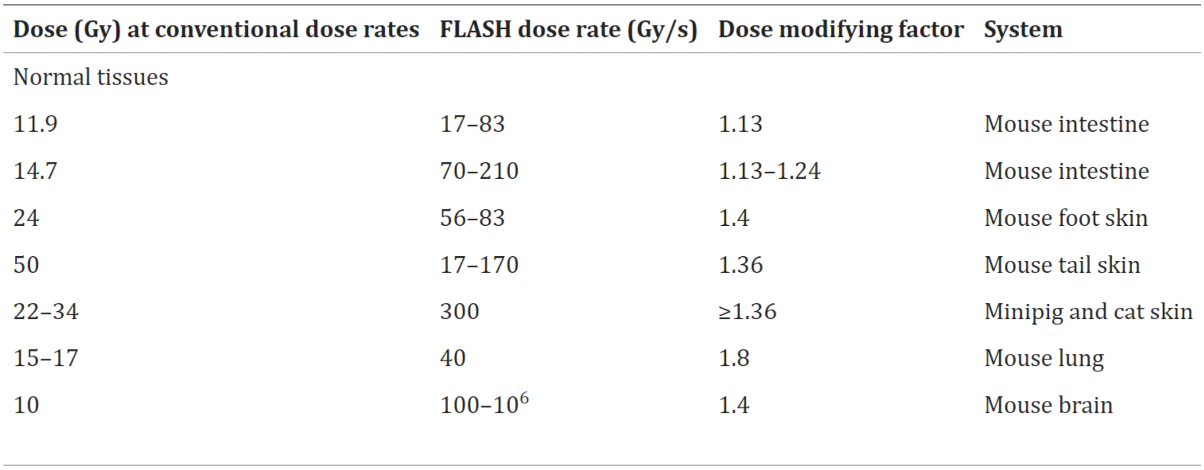

Dose (Gy) at conventional dose rates	FLASH dose rate (Gy/s)	Dose modifying factor	System
Normal tissues			
11.9	17–83	1.13	Mouse intestine
14.7	70–210	1.13–1.24	Mouse intestine
24	56–83	1.4	Mouse foot skin
50	17–170	1.36	Mouse tail skin
22–34	300	≥1.36	Minipig and cat skin
15–17	40	1.8	Mouse lung
10	$100–10^6$	1.4	Mouse brain

Figure 2.25: Dose modifying factor ([35])

Long-term effects are also crucial to investigate. Therefore, the following section presents an example of zebrafish growth after exposure to a conventional dose with and without a radio-protective drug, as well as a FLASH dose. The zebrafish were exposed to the treatments when they were embryos, and their length was measured as they grew to evaluate the long-term effects of the treatments.

2.4.2 Example

In Figure 2.26, it is observed that the use of the FLASH delivery method has an effect on the size of zebrafish, indicating that biological tissues are better preserved with FLASH compared to conventional RT. In particular, FLASH-RT is even more effective in protecting normal tissues than Amifostine, a selective radio-protective drug commonly used in radiotherapy and chemotherapy to minimize normal tissue toxicity ([37]).

Amifostine was added to the zebrafish embryos' water 1h before irradiation and the irradiation was performed 4 hours post-fertilization. Embryos were given 8 Gy delivered with FLASH-RT (1 pulse of 1.8×10^{-6}s) or conventional dose-rate irradiation (0.1 Gy/s). Radiation-induced alteration of zebrafish morphology was assessed 5 days post-fertilization by body length measurement ([38]).

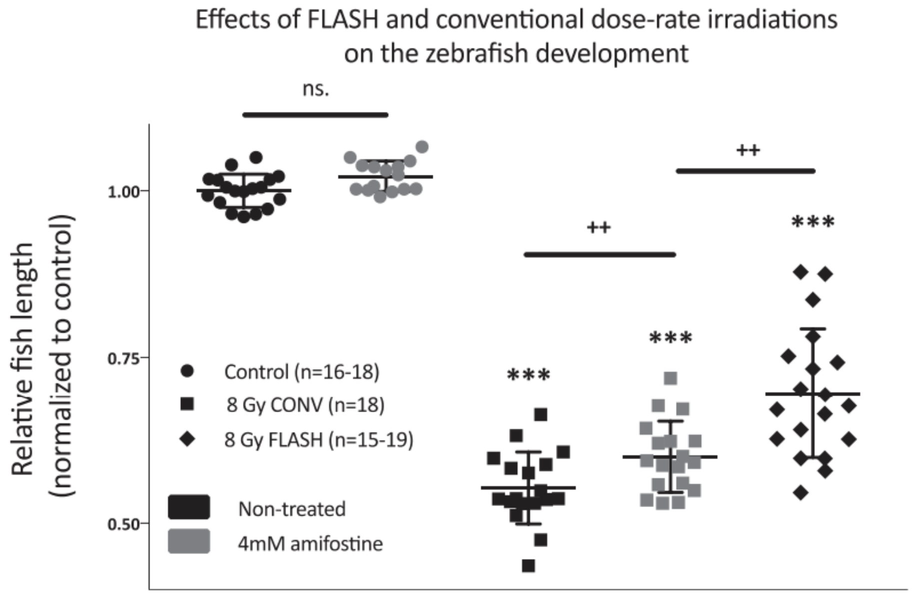

Figure 2.26: Effects of FLASH on zebrafish development ([38])

FLASH is a very promising technique that has demonstrated great performances. However, a significant hurdle arises due to the inability of current proton therapy systems to deliver radiation within the extremely short timeframes required for FLASH treatment. To overcome this challenge, a new component is incorporated into the delivery machine to enable the achievement of ultra-high dose rates.

2.4.3 3D patient-specific range modulator

One challenge in using the FLASH delivery method is that it relies on the PBS method, which involves changing the energy with the ESS. The time required to change the ESS configuration is too long for the fast delivery time required by the FLASH method.

In order to solve this issue, a new component called a 3D patient-specific range modulator, also called hedgehog because of its shape (as shown in Figure 2.27 and 2.28) is added to the nozzle of the device.

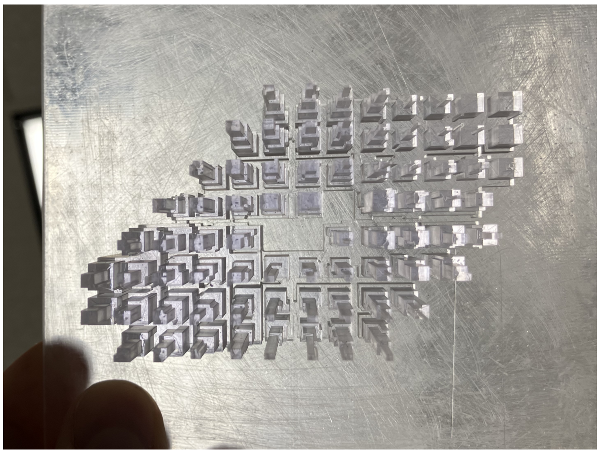

Figure 2.27: Top view of a 3D range modulator

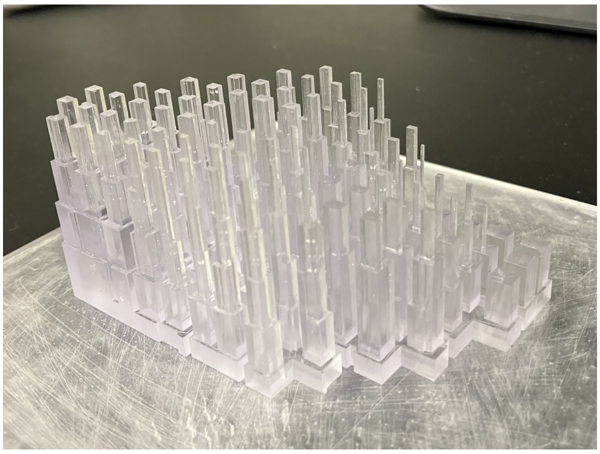

Figure 2.28: Side view of a 3D range modulator

This 3D range modulator is used to shape the beam to the target with the SOBP without the need of an ESS.

This hedgehog consists of 2 main parts as we can see in Figure 2.29:

- The range shifter is used to slow down protons to reach the desired speed so that protons deliver their energy at the desired depth thanks to the Bragg Peak.
- The spikes/tower of the range modulator, as shown in Figure 2.30, have the shape of a pyramid and they create an SOBP due to the distance that the protons travel in the material.

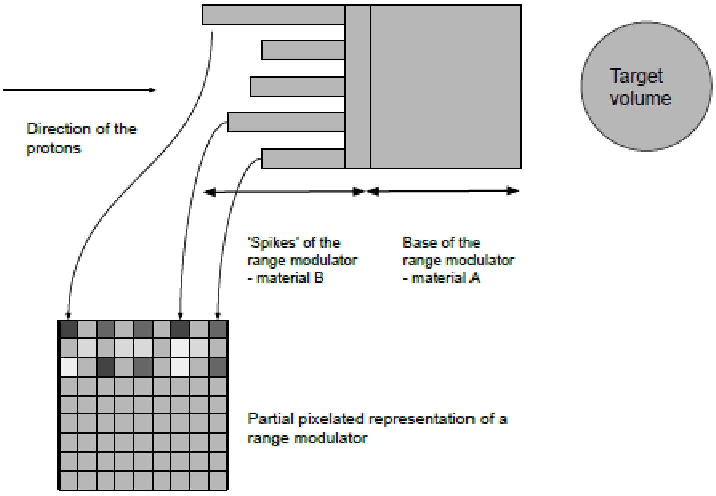

Figure 2.29: 3D range modulator split into towers/spikes in material B and the base of the range modulator (range shifter) material A ([39])

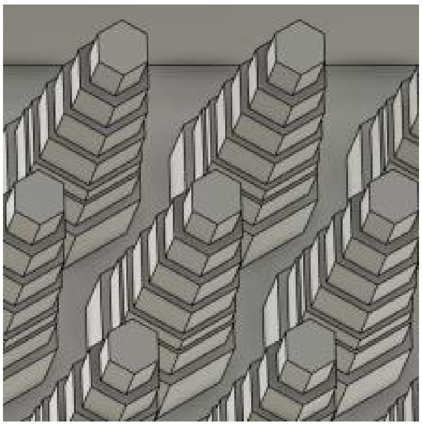

Figure 2.30: Multiple pyramid-shaped pin ([40])

At IBA, the two parts of this 3D range modulator are made of the same material (Accura ClearVue) and are printed using 3D printing technology, which can introduce uncertainties related to the quality of the printing. Moreover, the addition of a new component to the existing proton therapy system can introduce other sources of uncertainty, such as the improper placement of the hedgehog, which can have an impact on patient treatment.

Chapter 3

FLASH

As described in Chapter 2, IMPT (PBS) is used for proton therapy delivery. With this technique, the tumor is painted at various depths by adjusting the energy of the protons. In conventional PT, an ESS is used to change the energy, while in FLASH-PT, a 3D patient-specific range modulator, known as a hedgehog, is used. After protons are generated in the cyclotron, they have maximum energy and must be slowed down to achieve the desired energy level. It is important to study how the speed of protons affects the dose deposition along the beam path. We will thus begin by exploring some fundamental principles governing the behavior of protons in physics. Following this, we will look at the distinct advantages of FLASH compared to conventional delivery methods from a physics perspective. A more comprehensive discussion on the concept of dose rate will be provided, and we will conclude with an examination of the optimization methodology for the hedgehog component.

3.1 Physics background of protons

As explained in section 2.2, PT has a significant advantage over RT which due to the Bragg Peak, which refers to the specific energy deposition of protons during their travel through matter. This characteristic Bragg Peak can be explained with some physics. At this point, our focus is solely on the physics aspect since it was not necessary earlier for a comprehensive understanding. However, we will now delve into the subject matter with precise and in-depth discussions that align with our interests.

3.1.1 Fluence

First, the fluence is the number of particles (dN) incident on a surface over a certain period of time divided by the area of the surface (da):

$$\phi = \frac{dN}{da} \tag{3.1}$$

3.1.2 Stopping power

When a charged particle travels through matter, it loses energy along the pathway. This is the concept of Stopping Power: the average loss of energy (dE) per unit distance (ds) along the path is, in $[MeV cm^{-1}]$.

$$S = -\frac{dE}{ds} \tag{3.2}$$

The energy loss of a particle depends on all the interactions that take place during its travel through matter.

3.1.3 Interactions of protons with matter

There are four types of interactions for protons, which are illustrated in Figure 3.1. These include Inelastic Coulomb scattering, Elastic Coulomb scattering, Nuclear reactions, and Bremsstrahlung.

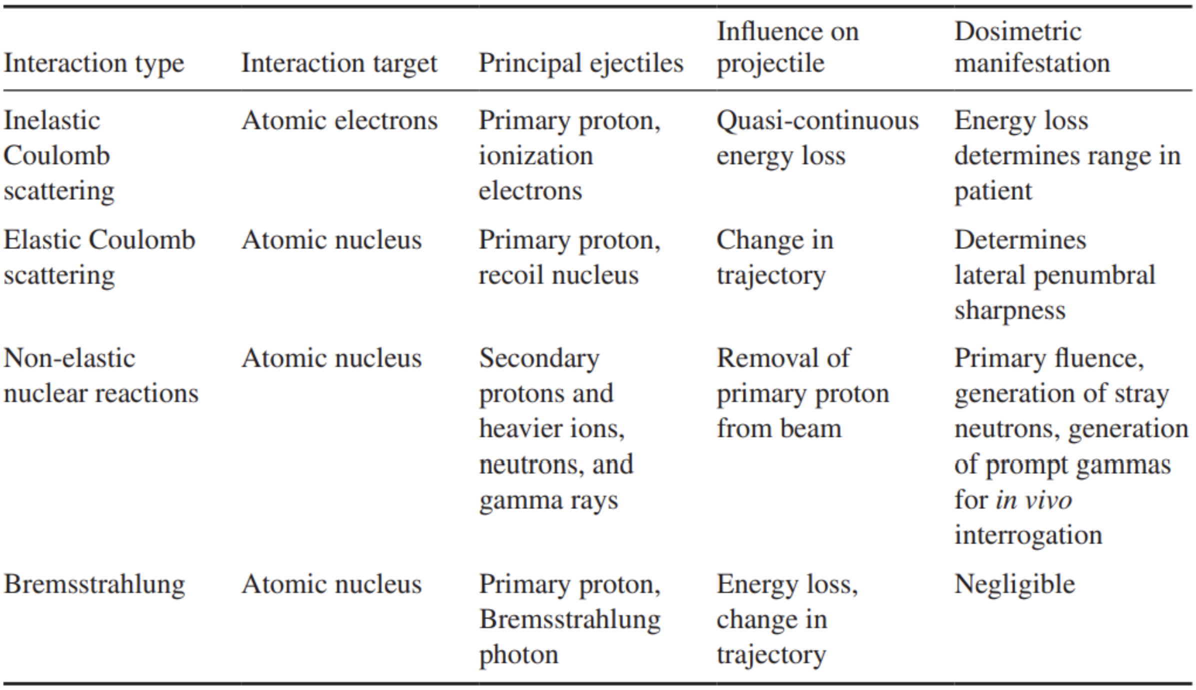

Interaction type	Interaction target	Principal ejectiles	Influence on projectile	Dosimetric manifestation
Inelastic Coulomb scattering	Atomic electrons	Primary proton, ionization electrons	Quasi-continuous energy loss	Energy loss determines range in patient
Elastic Coulomb scattering	Atomic nucleus	Primary proton, recoil nucleus	Change in trajectory	Determines lateral penumbral sharpness
Non-elastic nuclear reactions	Atomic nucleus	Secondary protons and heavier ions, neutrons, and gamma rays	Removal of primary proton from beam	Primary fluence, generation of stray neutrons, generation of prompt gammas for *in vivo* interrogation
Bremsstrahlung	Atomic nucleus	Primary proton, Bremsstrahlung photon	Energy loss, change in trajectory	Negligible

Figure 3.1: Summary of proton interaction types, targets, ejectiles, influence on projectile, and selected dosimetric manifestations (41).

For PT, Bremsstralhung is completely negligible because of the level of energy used. In Figure 3.2 are represented the 3 types of interactions for a proton at medical level:

(a) Inelastic Coulomb scattering: when the proton hits an electron. Due to the difference of mass between the two (a proton is approximately 2000 times heavier than an electron), the electron is ejected from the electronic cloud of the atom and the proton continues most of the time straight forward. This is the main cause of energy loss by protons and it creates a transfer of energy to matter, resulting in energy absorption and dose deposition.

(b) Elastic Coulomb scattering: when the proton is deflected from its trajectory due to the larger mass and charge of the nucleus. It results in a change of energy loss and direction of the incident charged particle.

(c) Nuclear interactions: the primary proton hits a nucleus and ejects a secondary proton (p'), a neutron (n), and γ-rays. The primary proton gives up all its energy and does not continue to travel after this collision.

All of these interactions with matter are important in general, but particularly for this master's thesis, as all of these phenomena will occur within the range modulator. The range modulator passively degrades the energy of the protons to achieve the dose conforming to the expected dose calculated during treatment planning.

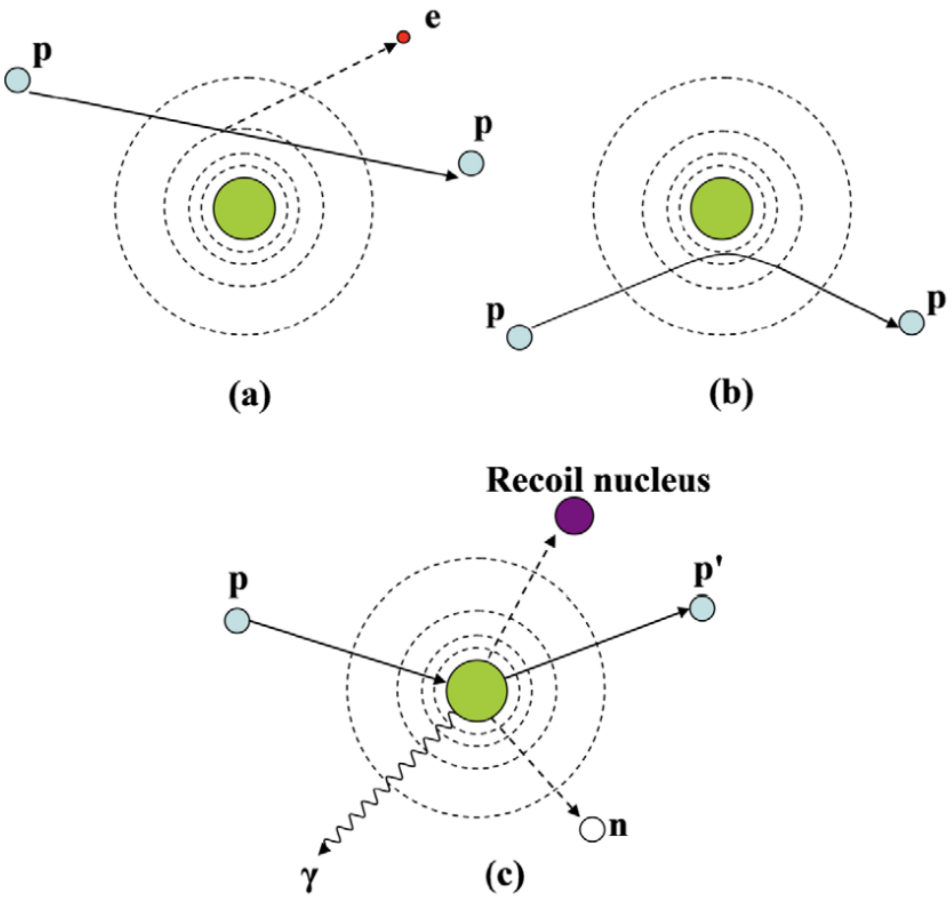

Figure 3.2: (a) inelastic Coulomb scattering, (b) deflection of proton trajectory by repulsive Coulomb elastic scattering with a nucleus, (c) removal of primary proton and creation of secondary particles via non-elastic nuclear interaction ([41]).

3.1.4 Collision stopping power

As previously mentioned, collisions of protons with atomic electrons are the primary cause of energy deposition in matter, as shown in Figure 3.3. This leads to the concept of collision stopping power, which can be estimated using the Bethe(-Bloch) formula

$$\left(\frac{S}{\rho}\right)_{col} = -\frac{1}{\rho}\left(\frac{dE}{ds}\right)_{col} = 0.1535\frac{z^2}{\beta^2}\left[27.675 + 2ln\left(\frac{\beta^2}{1-\beta^2}\right) - 2\beta^2 - \delta - 2lnI - 2\frac{C}{Z}\right]\left(\frac{Z}{A}\right) \tag{3.3}$$

expressed in $[MeVcm^2g^{-1}]$ where $\beta = \frac{v}{c}$, $\frac{C}{Z}$: shell effect, z: atomic number of the projectile, Z: atomic number of target atom, A: mass number of the target atom.

The most dominant term in the formula is $\frac{z^2}{\beta^2}$. Since the incident particle is a proton with $z = 1$, the collision stopping power is proportional to the inverse square of its velocity ($\frac{1}{\beta^2}$).

The collision stopping power is a critical factor in the optimization of the range modulator, making it a key aspect of this master's thesis.

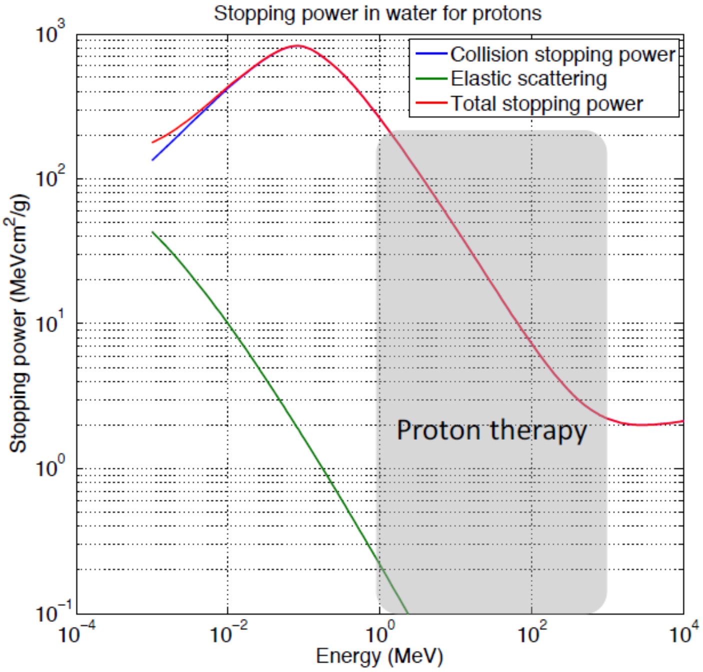

Figure 3.3: Stopping power of protons ([42])

The impact of elastic scattering on stopping power and dose delivery through matter is minimal, as illustrated in Figure 3.3. However, elastic scattering is primarily responsible for angular deflections of protons, resulting in a blurred effect on the dose, as shown in Figure 3.4.

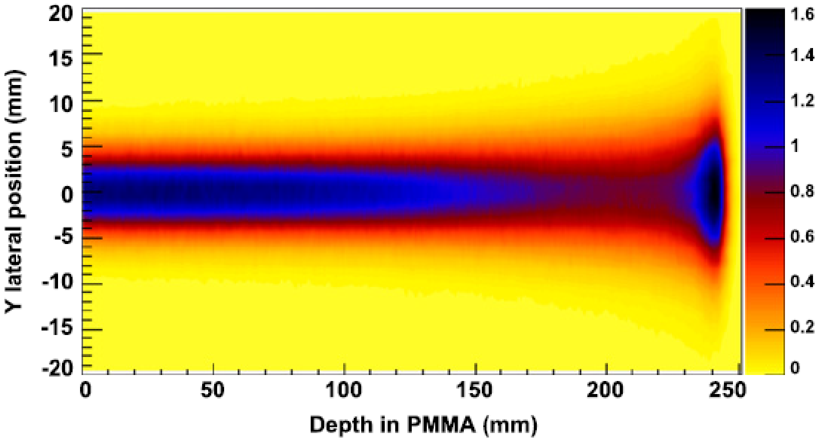

Figure 3.4: Elastic scattering of protons through PMMA ([42])

As demonstrated earlier, the energy of protons, which is closely associated with their velocity, plays a significant role in determining their interactions as they travel through matter. This difference of interaction has a major impact on energy delivery and thus on dose deposition in patient treatment. In the next section, we will show the advantage of the FLASH effect on dose distribution over the healthy tissues.

3.2 FLASH effect

Over the past years, there has been significant interest in FLASH radiation therapy due to its potential to reduce the side effects associated with conventional radiation therapy. FLASH treatment involves delivering a high radiation dose within an extremely short time frame. While more research is needed to fully understand the benefits and limitations of FLASH-PT and its underlying mechanisms, there is a growing number of studies investigating treatment planning and delivery.

Compared to conventional PT, FLASH-PT involves delivering the same treatment dose in a much shorter time frame and with fewer fractions. This requires using dose rates that are thousands of times higher than those used in conventional PT. In conventional PT treatment, the dose is typically administered at rates of 1-4 Gy/min over several minutes. However, in FLASH-PT, the dose is delivered at a significantly higher rate of at least 40 Gy/s for less than one second.

In section 2.4, it was also mentioned that reducing the duration of irradiation can have positive effects on biological tissues. Figure 3.5 illustrates this concept, where we observe a therapeutic window for FLASH that is wider compared to conventional PT. For the same tumor control (TC) (green curve), the normal tissue complication (NTC) curve for FLASH is shifted further to the right. This indicates a greater potential to treat cancer while minimizing the impact on healthy tissues, resulting in an expanded therapeutic window for FLASH.

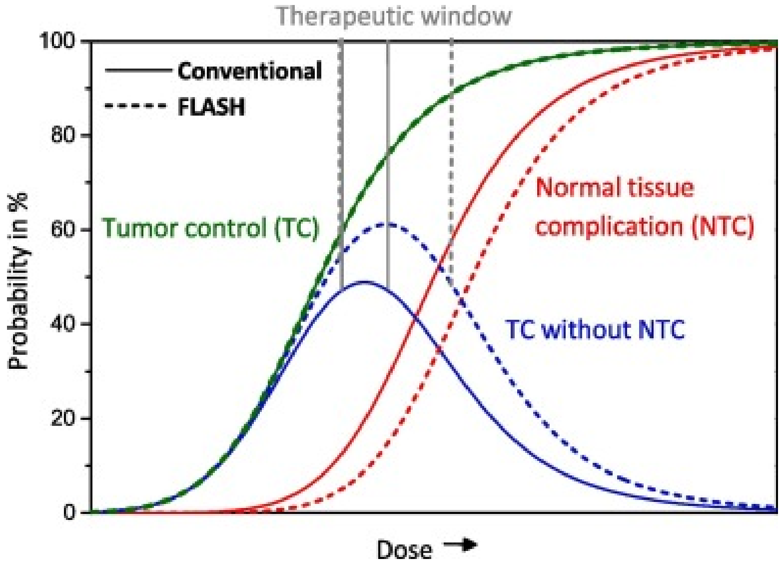

Figure 3.5: Therapeutic window with conventional and FLASH in RT (43)

The challenge with FLASH is to deliver a significantly higher dose within a very short timeframe, necessitating a higher global dose rate.

3.3 Dose rate

In the context of FLASH, both delivery time and beam intensity play crucial roles, leading to the introduction of the concept of dose rate. Dose rate refers to the rate at which radiation is delivered to a specific voxel within a given time frame. It is commonly expressed in units such as gray per second (Gy/s) or milligray per minute (mGy/min).

A spot refers to specific coordinates around which the dose will be distributed. Each spot is assigned a specific dose quantity, which follows a Gaussian distribution. The parameters of this distribution will determine the size of the spot. This distribution indicates that the majority of the dose is applied to the planned spot, but there is still some dose delivered to the surrounding locations as shown in Figure 3.6. As a beam is not confined to a finite size due to the Gaussian distribution, a particular voxel within the tumor will receive doses at various times during the treatment.

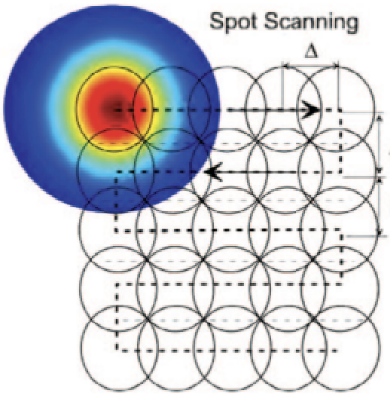

Figure 3.6: Scanning pattern [44]

Figure 3.7 illustrates the cumulative dose as a function of time for a specific spot. It clearly appears that the curve is not constant due to the contribution of different spots and the Gaussian distribution of the energy of protons when they release their energy.

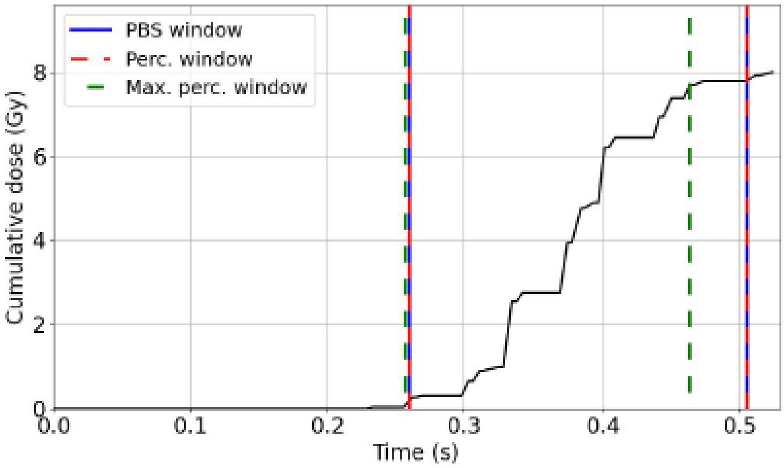

Figure 3.7: Accumulated dose and time windows as used by the PBS [32]

In Figure 3.8, the cumulative dose is shown as a function of space, highlighting that the dose is not evenly distributed over the surface due to scattering effects during the beam's travel through matter. This scattering contributes to the blurring effect in the dose delivery, resulting in a Gaussian distribution of the beam.

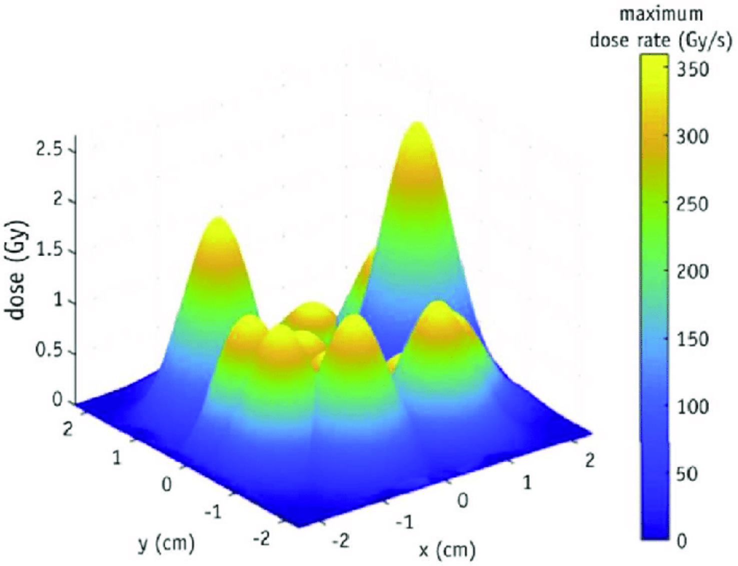

Figure 3.8: Spatial distribution of dose-rate within a pencil beam scanned proton beam illustrating the role of scatter contribution from adjacent spots, which leads to an inhomogeneous distribution of dose-rate (45).

3.3.1 Optimization pattern in PBS

In contrast to conventional PT, FLASH therapy requires a patient-specific irradiation pattern using PBS that needs to be individually optimized for each treatment. Unlike the traditional line-by-line scanning approach, the optimization in FLASH takes into account the importance of delivery time and the significantly higher global dose rate associated with this method. Various optimization patterns for various PTV are shown in Figure 3.9.

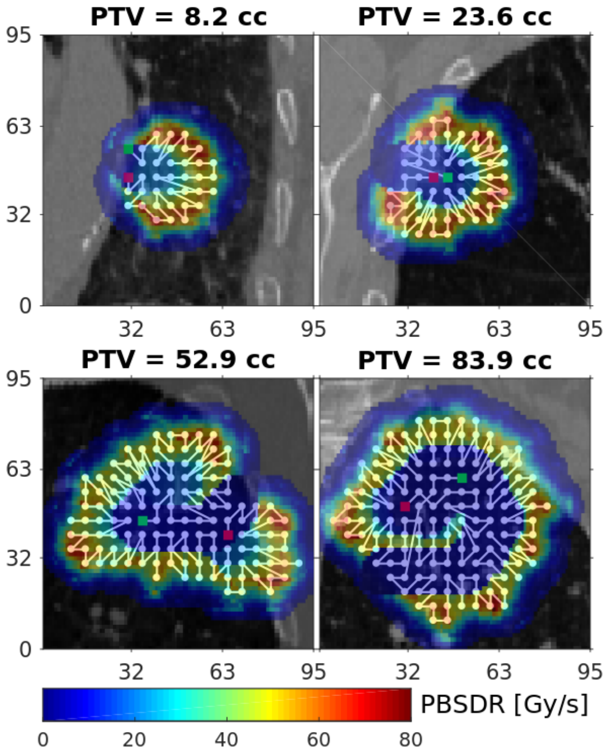

Figure 3.9: Optimized scanning patterns with initial (green) and final (red) positions, overlaid with the resulting PBS-DR distribution in a beam transverse plane through various PTV (46).

The investigation of dose delivery to each voxel is a key factor investigated in this master's thesis. It encompasses alterations in the overall dose deposition, which can have a major impact on patient treatment.

3.4 Adapting IMPT for FLASH

The FLASH effect relies on delivering a high dose within a narrow timeframe. Achieving this requires a significantly higher dose rate compared to conventional treatments, necessitating advanced beam-shaping technologies. As mentioned in section 2.4.3, the time required for energy switching in PBS is impractical for FLASH treatment. To overcome this limitation, a 3D patient-specific range modulator is employed to replace the energy selection system, enabling a significantly faster dose delivery. This new component consists of a collection of towers with varying heights, which convert individual Bragg peaks into SOBP and deliver protons at different energies.

3.4.1 3D range modulator definition and function

Currently, the PBS method is used to achieve the required level of precision in PT, ensuring uniformity and conformity. However, the current technology is unable to attain the necessary dose rate for the Flash effect when using IMPT treatment.

As a solution, the current approach for FLASH therapy involves using a single energy layer and a 3D patient-specific range modulator, also known as a hedgehog due to its distinctive shape (see Figure 3.11). This approach addresses the limitations and enables the delivery of high-dose radiation in a short timeframe.

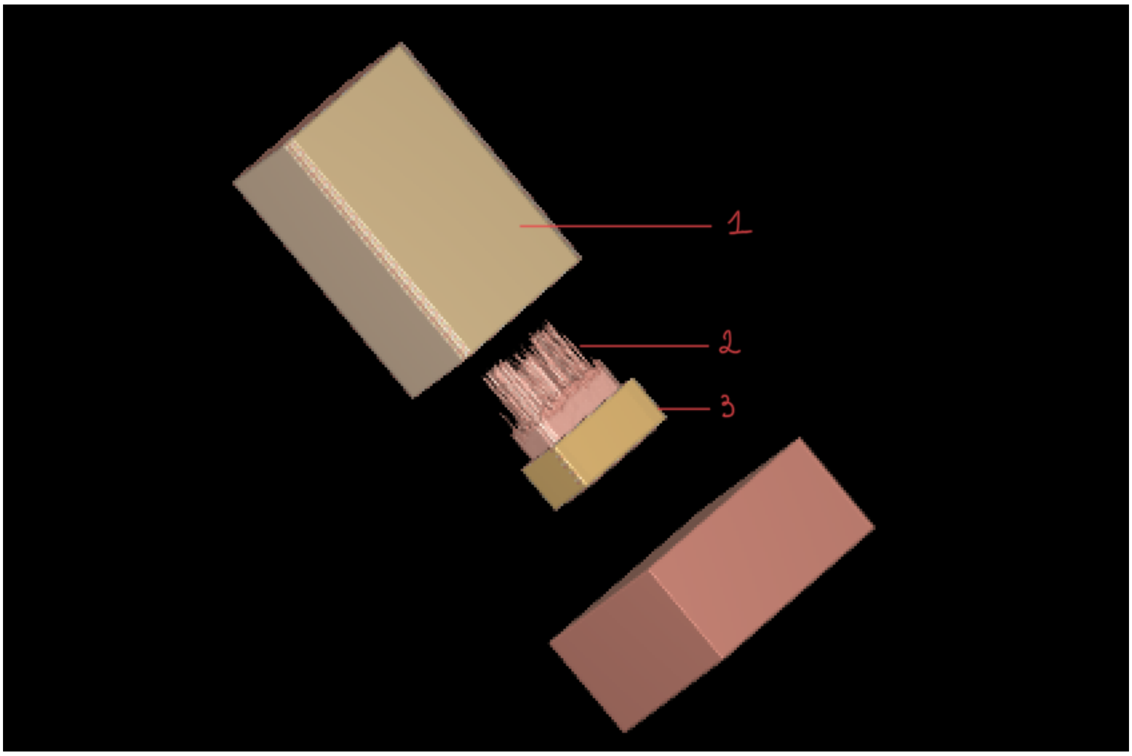

Figure 3.10: 3D image of an optimized hedgehog in OpenTPS

As we can see in Figure 3.10, the total process consists of several parts. The first part is a huge range modulator that is used to degrade the energy of the protons a first time in order to reach the desired energy.

The second part is actually what we call the hedgehog. It consists of multiple towers of varying heights, as illustrated in Figure 3.11. The specific example shown in the figure corresponds to a hedgehog designed for a spherical target with a diameter of 5 cm (47).

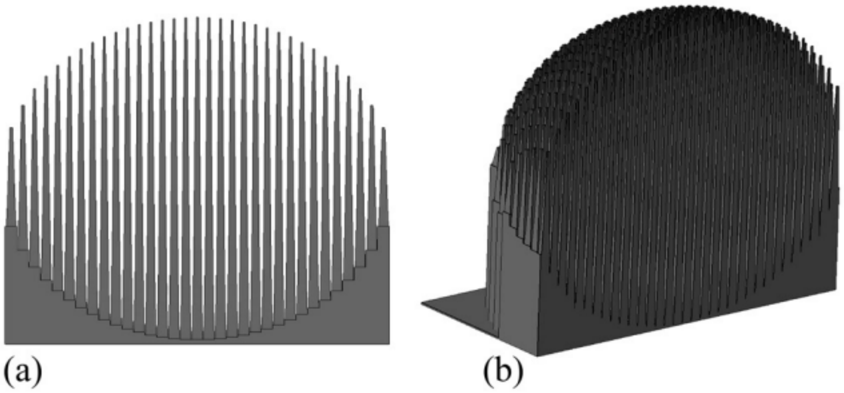

Figure 3.11: Frontal view (a) and oblique view (b) of a 3D range-modulator for a spherical target (47)

Each of these towers has a thicker base and a thinner top. This is due to the fact that we wish to use only one single layer of energy but still intend to reach a 3D volume which is the tumor. The aim behind this concept is that there will be protons that pass through a gap, an air gap, and will then travel further, and some protons will pass through the tower, will then be more degraded, and will then travel less deeply into the patient. This will create a SOPB that allows delivering the dose to a 3D volume using a single 2D pattern of PBS scanning. This concept is illustrated in Figure 3.12 (47). Furthermore, it is worth mentioning that the lateral conformity of the dose is maintained through the scattering of protons.

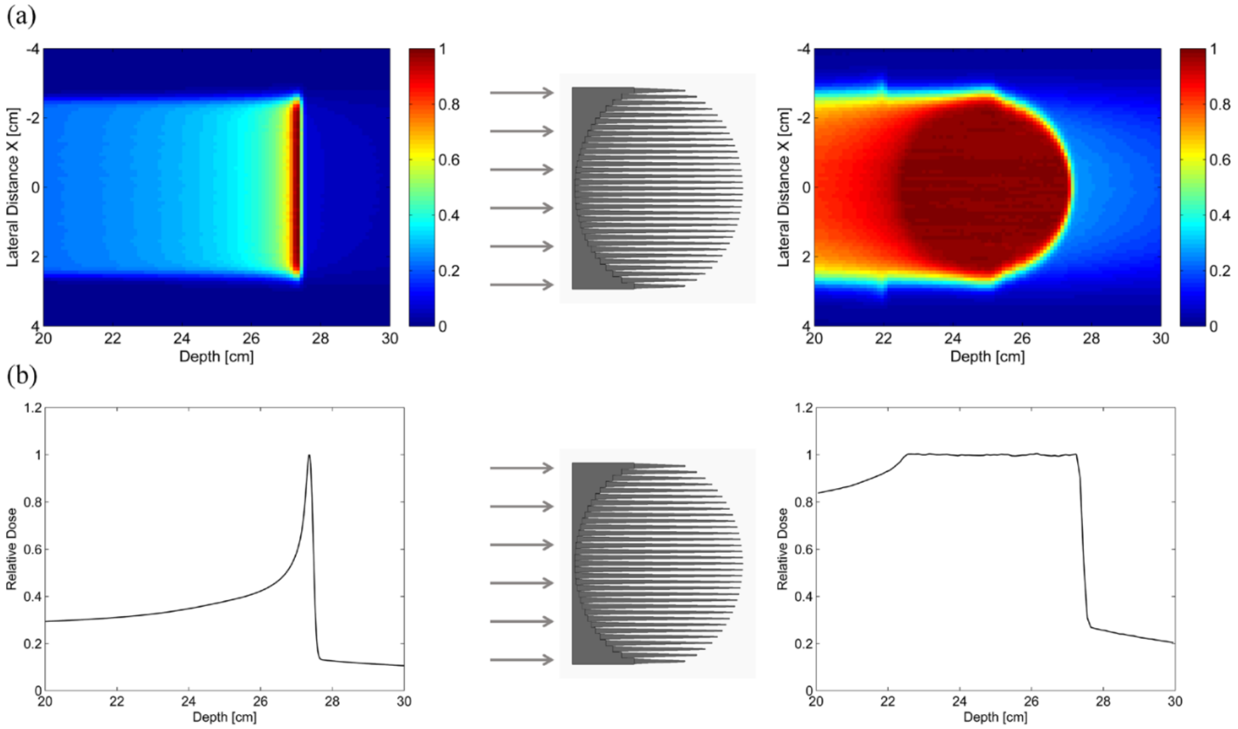

Figure 3.12: Principle of the 3D range-modulator for a spherical tumor (d = 5cm) (47)

The third part is the collimator, and its role is really important because the hedgehog will also scatter the protons outside of the target volume. The role of the collimator is to stop the protons that are not following the direction of the target volume. This is why this collimator is usually made of tungsten, a high-density material (19,3 [g.cm^{-3}] at 20°C).

3.4.2 Optimization of the hedgehog

Within the context of FLASH therapy, the optimization process involves optimizing both the treatment plan and the hedgehog. This implies optimizing two variables: the weights of the beamlets (w) that are typically optimized in all treatment plans, and the height of the hedgehog tower (h), which is specific to FLASH therapy.

In this section, we shall present the optimization of a hedgehog in openTPS which is an open-source Treatment Planning System (TPS) for research in proton therapy and will be better presented in section 4.2.1. This optimization process is conducted according to Sylvain Deffet and al in (39). But in general, the optimization of a hedgehog in other softwares may not use exactly the same algorithm or the same cost functions, but the main idea is the same.

Before explaining the optimization process described in Figure 3.13, it is necessary to define the objective function. The objective is to penalize the deviation of the dose from the prescribed dose. Since we wish to ensure that the dose reaches a minimum D_{min} everywhere and that the dose does not reach a maximum D_{max}, we define f_{min} 3.4 and f_{max} 3.5 as follows

$$f_{min}(w,h) = \frac{1}{N_r}\Sigma_{i=1}^{N_r} max_{w,h}(0, D_{min} - D_i(w,h))^2 \tag{3.4}$$

$$f_{max}(w,h) = \frac{1}{N_r}\Sigma_{i=1}^{N_r} max_{w,h}(0, D_i(w,h) - D_{max})^2 \tag{3.5}$$

Where $N_r = |ROI|$.

Note that we use a dilated Region Of Interest (ROI) for the optimization, which is the same ROI but with 3 more voxels in each dimension. We do this to ensure homogeneity even at the edges.

The final objective function to be minimized is the sum of those two functions.

$$f_{obj}(w,h) = f_{min}(w,h) + f_{max}(w,h) \tag{3.6}$$

Once this is set, we can introduce the optimization algorithm 3.13. The main idea is to first optimize the weight of the spot according to Baraggan and al (48), then optimize the height of the tower in the hedgehog using the gradient descent method.

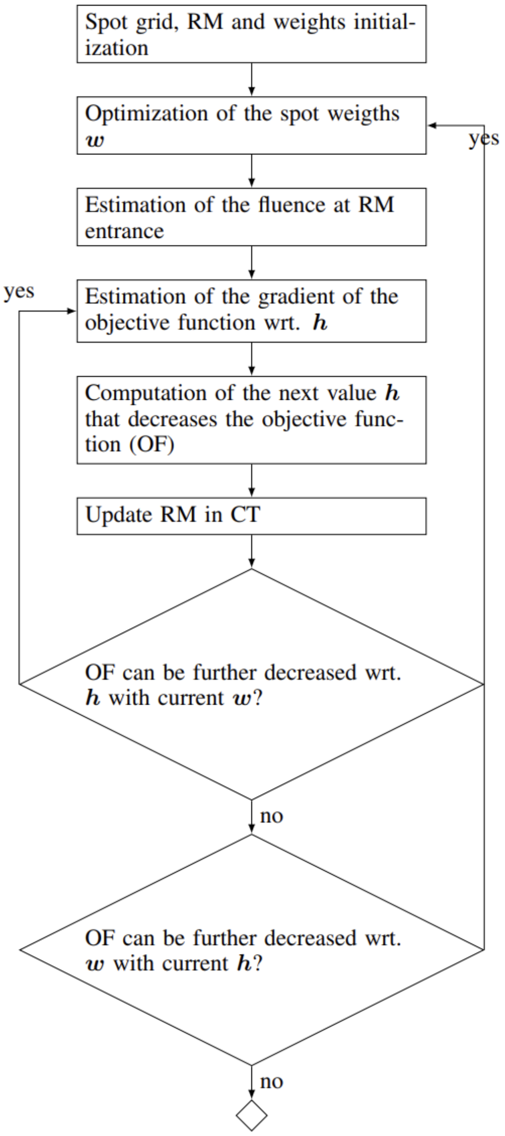

Figure 3.13: Iterative optimization of the individual heights of the hedgehog (patient-specific range modulator)

The first step in this algorithm is to initialize the spot grid according to the beam angle, the range modulator and to make an initial guess of what the hedgehog could be. Usually, we just initialize all the towers to the same height. We also define the region of interest as well as its dilated version and set D_{min} and D_{max} according to the prescription. In our case, they are respectively 54 and 54.5 Gy.

We then perform a first optimization of the spots which involves a gradient descent with regard to w. The concept of the gradient descent method will be explained later with the optimization of h.

The next step is the estimation of the fluence at the range modulator entrance given the beam model in order to produce the classical inputs used by MCsquare (a Fast Monte Carlo simulation for proton PBS).

After this, we begin the gradient descent process for the height optimization by computing the derivative of the objective function 3.6 with regard to h. This gives us :

$$\begin{aligned}\Delta f_{obj} = & \frac{2}{N_r}\Sigma_{i=1}^{N_r} max_h(0, D_i(w,h) - D_{max})\frac{\delta D_i(w,h)}{\delta h} + \\ & \frac{2}{N_r}\Sigma_{i=1}^{N_r} max_h(0, D_{min} - D_i(w,h))\frac{\delta D_i(w,h)}{\delta h}\end{aligned} \tag{3.7}$$

The next step is to update the h vector by this equation :

$$h_{n+1} = h_n - \alpha_n \Delta f_{obj}(h_n, w) \tag{3.8}$$

where α_n is either a fixed step size or a learning one.

We then proceed to update the range modulator in the Computed Tomography (CT) by incorporating the new values for the tower heights. At this stage, certain conditions are imposed so as to determine whether the value of h_{n+1} is acceptable. These conditions can be based on various criteria, such as the magnitude of $h_{n+1} - h_n$ being sufficiently low, or imposing constraints on the objective function, or setting a limit on the number of iterations. Different conditions apply to the optimization process for h compared to those for w. If the conditions related to h are not satisfied, we return to the estimation of the gradient step and repeat the process until these conditions are met.

If the conditions for h are satisfied but not the conditions for w, we return to the step of optimizing spot weights. Subsequently, we repeat the process of estimating the fluence step, as shown in Figure 3.13.

We iterate the algorithm until both the conditions for h and w are satisfied, indicating the completion of the hedgehog optimization and the treatment plan optimization.

Chapter 4

Robustness analysis of 3D patient-specific range modulators

This chapter marks the initiation of the experimental phase in this master's thesis. It is divided into 3 main sections:

1. Objective of this study
2. Materials and methods
3. Results of range modulators robustness study

The second section, Materials and methods, first details the software used to compute all our results, how range modulators are implemented in this software and how the set-up was designed. Secondly, a complete description of the methodology applied to each experiment is provided.

The third section, Results of range modulators robustness study, presents all our results and also contains comments and discussion.

4.1 Objective of this study

As explained in the previous chapter, the FLASH delivery technique requires administering a high dose within a narrow time window. To effectively address this constraint while adequately irradiating the entire tumor, a novel component known as a 3D patient-specific range modulator or hedgehog is used. This range modulator replaces the conventional energy selection system and enables the generation of a SOBP to deliver the radiation dose to the tumor, penetrating it at various depths.

With the addition of this new component to the nozzle, additional uncertainties will occur during the delivery of radiation. These uncertainties must be carefully considered and accounted for prior to administering the treatment to the patient, ensuring consistency between the planned dose and the delivered dose. It is crucial to investigate the impact of incorporating this new component into the treatment apparatus, particularly since it is adapted to each patient and may vary in quality and dose conformity across various patients.

In this master's thesis we investigated 3 types of uncertainties:

1. Impact of spot size
2. Impact of spot position
3. Impact of the presence of air inclusions in the hedgehog after the 3D impression

By selecting these parameters, we examined various types of uncertainties. The first of these can occur when there is a small difference in the initial conditions, resulting in our measuring tools producing parameters that are not exactly the same as in reality. The second measures the impact of a misalignment between the hedgehog and the nozzle. The last one evaluates the effects of 3D printing imperfections, such as the presence of air inclusions, which can introduce density variations and therefore a change in the energy delivered by protons.

Examining these uncertainties will give us an idea of the quality and robustness of this delivery method. If the impact is significant and there are important differences between the desired dose to the target and the actual dose that should be delivered to the patient, this indicates a lack of dose conformity. In such cases, certain actions must be taken to ensure proper coverage of the target. This may involve options such as reprinting the hedgehog, verifying its position on the nozzle, adapting the treatment plan, and so on.

4.2 Materials and methods

In this section, we will begin by discussing the materials employed in our study. Specifically, we used a Treatment Planning System (TPS) called OpenTPS for conducting all our simulations. Additionally, we will provide a detailed description of how the range modulator is implemented within this software. To establish a connection between the materials section and the methods section, we will outline the specific set-up that was implemented in computing our results. Finally, we will delve into a comprehensive explanation of the methods used for each of the three types of simulations.

4.2.1 OpenTPS

Throughout this master's thesis, we used the OpenTPS software to compute all our results. OpenTPS is an open-source TPS for research in PT. It was developed in Python with a special focus on simplifying contribution to the core functions in order to allow the users to develop their own features (49).

The library behind OpenTPS is composed of 2 main parts:

- OpenTPS core, containing all the functions used for performing Monte Carlo (MC) simulations.
- OpenTPS GUI, which incorporates various functions aimed at facilitating the graphical user interface, as depicted in Figure 4.1.

We essentially worked on a sub-branch of the OpenTPS core, the FLASH branch, which includes all the functions related to the research in FLASH therapy.

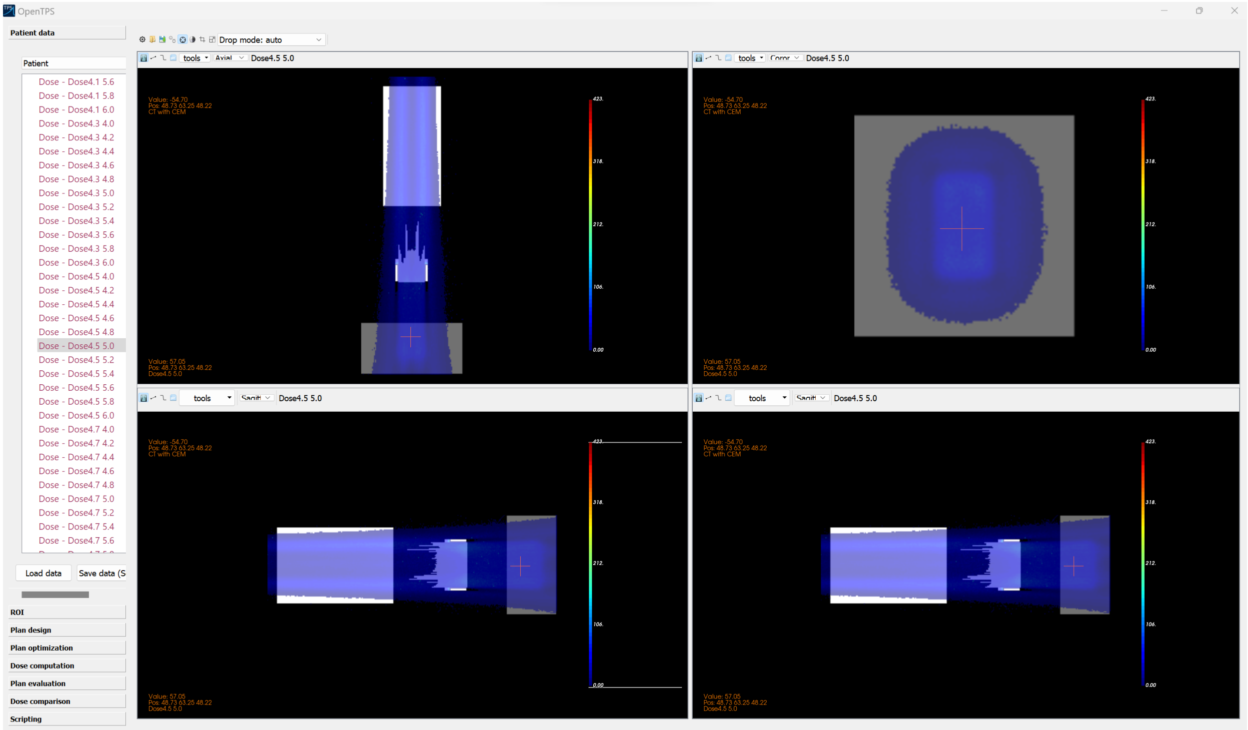

Figure 4.1: Graphic User Interface (GUI)

Another very important feature and which is still implemented in OpenTPS is the conversion between Hounsfield units (HU) and actual material density.

In fact, a Monte Carlo simulation requires the determination the elementary composition of each voxel. In MCsquare, the CT is converted using 2 tables which are given as inputs. The first table does the mapping between HU and mass density, and the other one does the mapping between HU and elementary composition.

HU conversion

The Hounsfield unit (HU) is a relative quantitative measure of radio density used by radiologists to interpret CT images. It is derived from the absorption/attenuation coefficient of radiation within tissues during CT reconstruction, which produces a grayscale image. The HU value is determined through a linear transformation of the baseline linear attenuation coefficient of the X-ray beam via the following formula ([50])

$$HU = \left(\frac{\mu_{material} - \mu_{water}}{\mu_{water}} \right) \times 1000 \tag{4.1}$$

where $\mu_{material}$ and μ_{water} represent the linear attenuation coefficient of the tissue (in a voxel) and water, respectively.

In this scale, the density of distilled water at Standard Temperature and Pressure (STP) is assigned a value of 0 HU, while the density of air at STP is defined as -1000 HU ([50]) ([51]). Figure 4.2 shows various human tissues with their corresponding HU values.

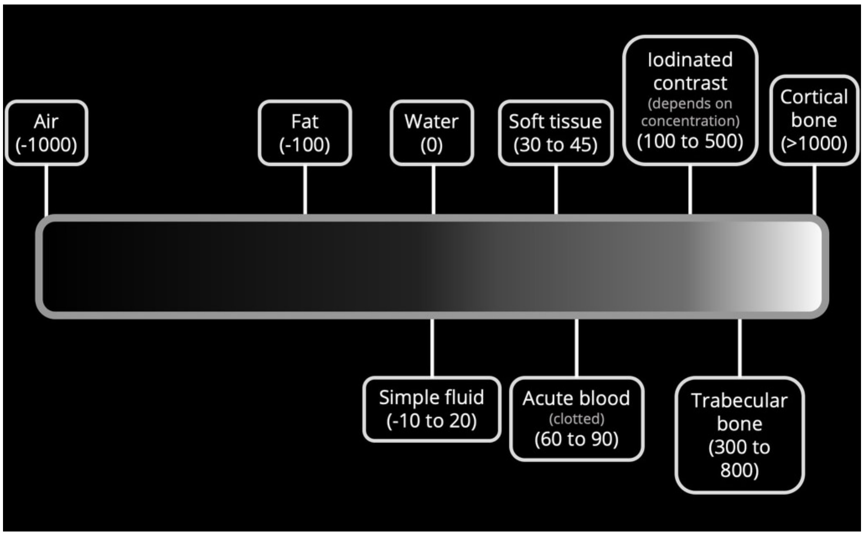

Figure 4.2: Hounsfield scale for different structures ([52])

Conversion of values between real density and HU is essential for treatment planning. Since tissues have varying densities along the proton path, they will not be attenuated uniformly, which can significantly affect the delivered dose. The physician typically delineates the PTV based on CT images.

But in our case, we had to do the inverse conversion, e.g. we knew the density of the hedgehog but we needed the corresponding HU to put it in the CT.

4.2.2 Modelling of the hedgehog in OpenTPS

We shall now going to present the way in which the hedgehog is implemented in OpenTPS.

In OpenTPS, the hedgehog is implemented directly into the CT and the beam's eye view. This approach eliminates the need for transformations between multiple reference grids, as all pixels are referenced within the same grid.

We opted for a 1mm voxel size resolution, which is a reasonable choice as it allows us to obtain hedgehogs that are certainly achievable by a 3D printer.

Furthermore, the reason for applying the transform on the CT and not on the binary mask of the hedgehog is that we expect that any rotation applied to the mask could yield dramatic changes to its geometry. For instance, when examining Figures 4.3, 4.4, and 4.5, it is obvious that deviating from a perpendicular or parallel gantry angle in relation to the patient table while retaining the original grid and applying an affine transformation to the binary mask defining the hedgehog would result in significant degradation in quality, as demonstrated in Figure 4.4.

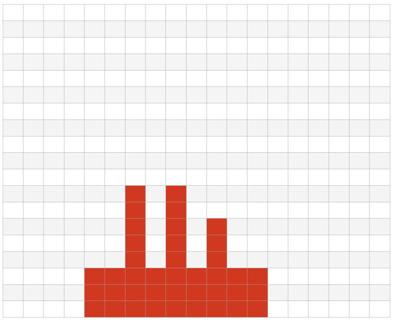

Figure 4.3: Hedgehog modelled with a 0 degree gantry angle

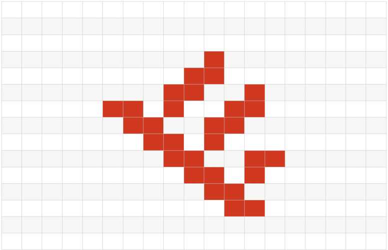

Figure 4.4: Hedgehog modelled with a 45 degree gantry angle but same grid than 0 degree angle

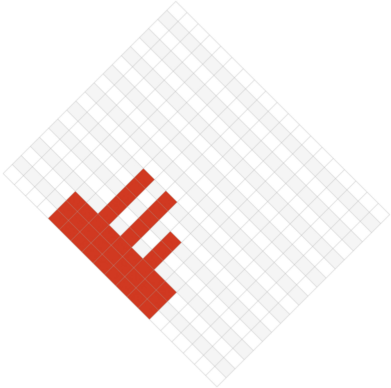

Figure 4.5: Hedgehog modelled with a 45 degree gantry angle but implemented in the beam's eye view

If, instead, we adopt the approach currently implemented in OpenTPS, which involves preserving the binary mask in its reference frame and simply rotating it, we achieve a scenario, as depicted in Figure 4.5, where there is no loss of quality in the hedgehog. However, since the only stationary element is the patient, the affine transformation is applied to the patient and consequently to the tumor. As illustrated in Figure 4.6, specifically at the bottom right of the image, the patient's skin appears to be somewhat uneven, which can be attributed to this affine transformation.

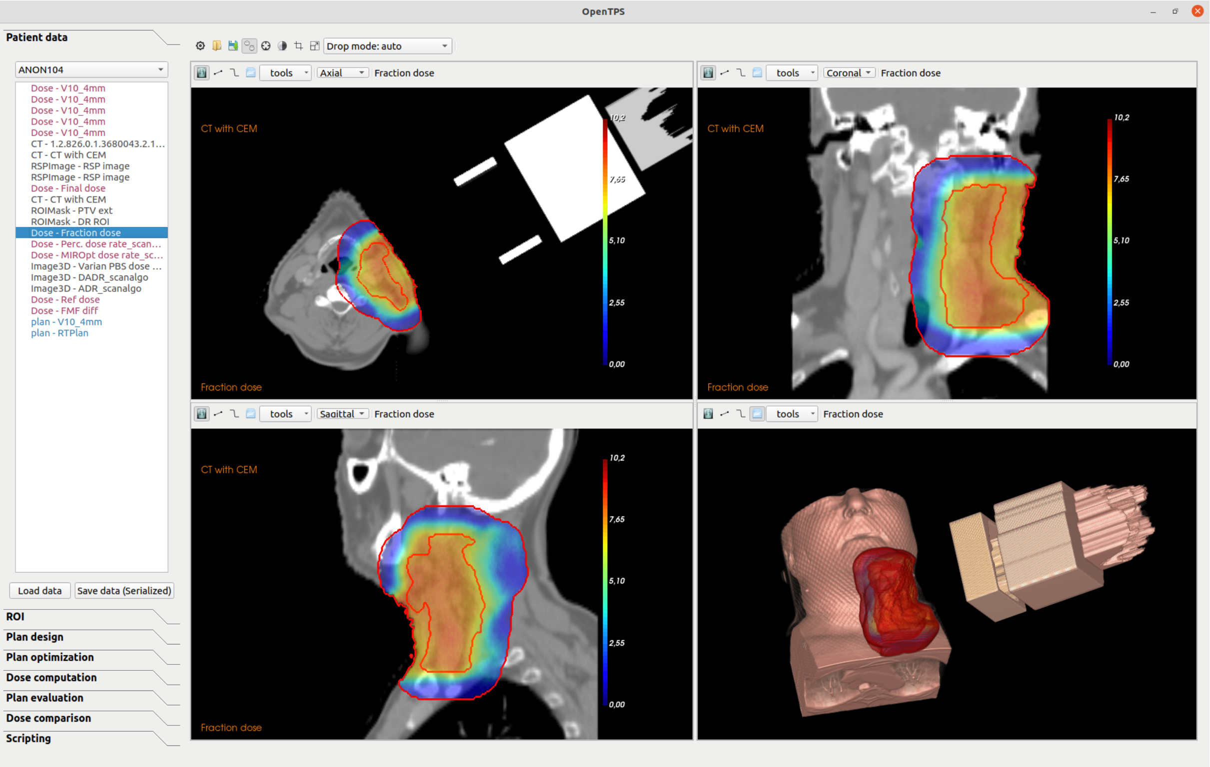

Figure 4.6: Example of a 60 degrees gantry angle treatment in OpenTPS

We might initially perceive this as a problem since it could lead to approximations and a loss of quality in the delineation of the medically defined contours (GTV, CTV, and PTV, as discussed in Section 2.3.3). However, this is not a significant concern for several reasons. First, the contours are not precisely defined to begin with due to the use of a grid, and tumors often exhibit non-cubic shapes, resulting in an inherent loss of accuracy. Secondly, even though these contours may not be exact, they serve the purpose of accounting for uncertainties and play a similar role in mitigating the impact of the quality loss in those contours. Lastly, this does not significantly affect the primary objectives of the treatment, as the worst-case scenario would involve slight deviations in dose delivery at the boundary of these volumes. Furthermore, FLASH therapy is specifically designed to better preserve healthy tissues, and it is in these contour regions that healthy tissues are typically found. Therefore, the impact on the central region of the tumor, which remains the most critical aspect, is minimal.

4.2.3 Experimental Set-up

In this section, we present a detailed description of the experimental set-up employed in this thesis, outlining the software, procedures, and variables involved. By elucidating the experimental framework, we aim to provide readers with a comprehensive understanding of the methods employed and ensure transparency and reproducibility of our findings.

First of all, we all used the Pycharm software to write the code and compile our simulations. Also, we used the OpenTPS library as already presented in section 4.2.1 to perform all our simulations.

Throughout our experimentations, we used as target a rectangular parallelepiped in a water box to facilitate the readability and visibility of our results. This region of interest was a 20x25x40 mm rectangular box as shown in Figure 4.7 with the number 4.

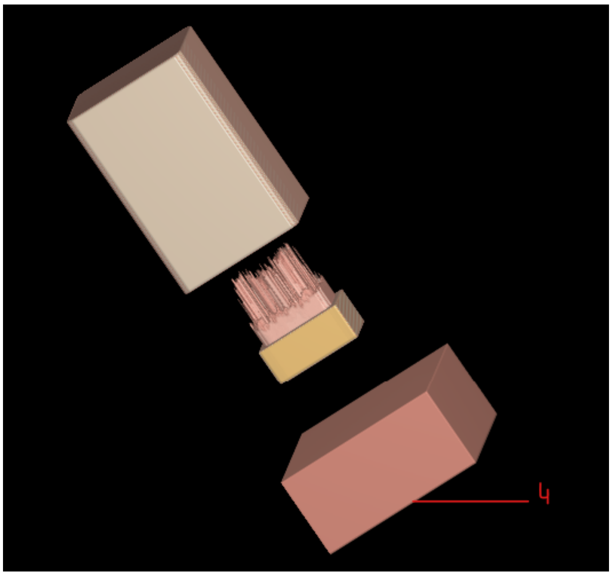

Figure 4.7: 3D image of an optimized hedgehog in OpenTPS

During the treatment optimization, we did not optimize the gantry angle, but decided to use only a 0-degree angle. To compute the various simulations of this study we used the Monte Carlo dose enginenamed MCSquare.

MCsquare is a new fast Monte Carlo code and has been developed to simulate proton PBS treatments with the accuracy and calculation speed required in the clinic.

The BDL in MCSquare

The MCsquare software incorporates the Beam Data Library (BDL), which serves as a lookup table containing beam parameters for various energy settings. These parameters need to be adjusted to ensure accurate alignment between MCsquare simulations and experimental measurements. The commissioning procedure involves a series of steps that must be followed in a specific order ([53]):

1. Optimization of the BDL parameters
    (a) Phase space calculated at the exit of the nozzle
    (b) Energy Spectrum represented as a Gaussian with a mean and a standard deviation of the proton energy
    (c) Absolute dose calibration
2. Validation of the generated beam model

The phase space sub-step within the BDL optimization process allows the extraction of optical parameters (such as spot sizes, divergences, and correlations) at the nozzle exit. The measured spot fluences can be accurately modelled using single or double 2D Gaussian distributions.

By using the Courant-Snyder equations, MCSquare is able to convert the optical parameters computed with the BDL from the isocenter to the nozzle position. The Courant-Snyder equations are described as follows.

$$\sigma_x^2(z) = \sigma_x^2(0) - 2\rho_{x\theta}(0)\sigma_x(0)\sigma_\theta(0)z + \sigma_\theta^2(0)z^2 \tag{4.2}$$

$$\sigma_y^2(z) = \sigma_y^2(0) - 2\rho_{y\phi}(0)\sigma_y(0)\sigma_\phi(0)z + \sigma_\phi^2(0)z^2 \tag{4.3}$$

where z is the distance between the isocenter and the nozzle, σ_θ the beam divergence in x direction, σ_ϕ the beam divergence in y direction, $\rho_{x\theta}$ the correlation coefficient in x direction and $\rho_{y\phi}$ the correlation coefficient in y direction.

These equations give the spot size at position z as a function of the spot size, divergence and correlation at the isocenter (z=0).

Once all parameters of the Courant-Snyder equations are determined at the isocenter, the formula is used to extrapolate the optical parameters to the nozzle exit. Correlation and divergence can be found, for x, by using the following equations ([53])

$$\rho_{x\theta}(z) = \frac{\rho_{x\theta}(0)\sigma_x(0) - \sigma_\theta(0)z}{\sigma_x(z)} \tag{4.4}$$

$$\sigma_\theta(z) = \sigma_\theta(0) \tag{4.5}$$

and similarly for y.

In our case, the distance from the nozzle exit to the isocenter is configured to be 410.0mm.

The BDL is a text file that provides a comprehensive description of the beam parameters at the nozzle. For our simulations, we used a specific BDL with the characteristics shown in Table 4.1. It is important to note that the energy of this BDL was consistently set at 226 MeV.

BDL parameters		
Name	Description	Values
NominalEnergy	The nominal energy (in MeV) as specified in the treatment plan.	225.0 MeV
MeanEnergy	The actual mean energy (in MeV) that should be simulated to reproduce the proton range measured in water.	225.217 MeV
EnergySpread	The standard deviation of the Gaussian distribution used to model the energy spectrum at the exit of the nozzle (in % of the nominal energy).	0.268174
ProtonsMU	The number of protons delivered per MU at this specific nominal energy.	152880000.0
Weight1	The weight of the first Gaussian for the double Gaussian optical model. The sum of Weight1 and Weight2 should be 1.0.	0.968
SpotSize1x	The in air spot size (in mm) along the x direction at the nozzle exit (for the first 2D Gaussian).	4.0 mm
Divergence1x	The spot divergence (in rad) along the x direction (for the first 2D Gaussian).	0.00392 rad
Correlation1x	The correlation between the spot size and the divergence along the x direction (for the first 2D Gaussian). Its value must lie between -0.99 and 0.99.	0.449243
SpotSize1y	The in air spot size (in mm) along the y direction at the nozzle exit (for the first 2D Gaussian).	5.5 mm
Divergence1y	The spot divergence (in rad) along the y direction (for the first 2D Gaussian).	0.002592 rad

Correlation1y	The correlation between the spot size and the divergence along the y direction (for the first 2D Gaussian). Its value must lie between -0.99 and 0.99.	-0.24634
Weight2	The weight of the second Gaussian for the double Gaussian optical model. The sum of Weight1 and Weight2 should be 1.0.	0.032
SpotSize2x	The in air spot size (in mm) along the x direction at the nozzle exit (for the second 2D Gaussian).	11.631725 mm
Divergence2x	The spot divergence (in rad) along the x direction (for the second 2D Gaussian).	0.0096 rad
Correlation2x	The correlation between the spot size and the divergence along the x direction (for the second 2D Gaussian). Its value must lie between -0.99 and 0.99.	0.565136
SpotSize2y	The in air spot size (in mm) along the y direction at the nozzle exit (for the second 2D Gaussian).	10.688153 mm
Divergence2y	The spot divergence (in rad) along the y direction (for the second 2D Gaussian).	0.009301 rad
Correlation2y	The correlation between the spot size and the divergence along the x direction (for the second 2D Gaussian). Its value must lie between -0.99 and 0.99.	0.145048

Table 4.1: The parameters of the BDL used in each simulation ([53])

The parameters for the range shifter, the hedgehog, and the aperture are shown in Table 4.2.

Range shifter parameters	
Material	Aluminium
density	2.7 g/cm^3
Hedgehog parameters	
Material	Accura ClearVue (SLA)
density	1.2 g/cm^3
Aperture parameters	
Material	Tungsten
density	19 g/cm^3

Table 4.2: Characteristics of the range shifter, the hedgehog and the aperture

The hedgehog was optimized to deliver a prescription dose with a minimum of 54Gy and a maximum of 54.5Gy throughout the ROI.

4.2.4 Spot size

Before explaining the method used to compute uncertainties related to spot size, we will explain the definition of spot size and the mathematical link between results at the nozzle and at the isocenter.

Definition of spot size

As mentioned in section 4.2.3, the beam, or the spot fluence, can be modeled by a double Gaussian as can be seen in Figure 4.8.

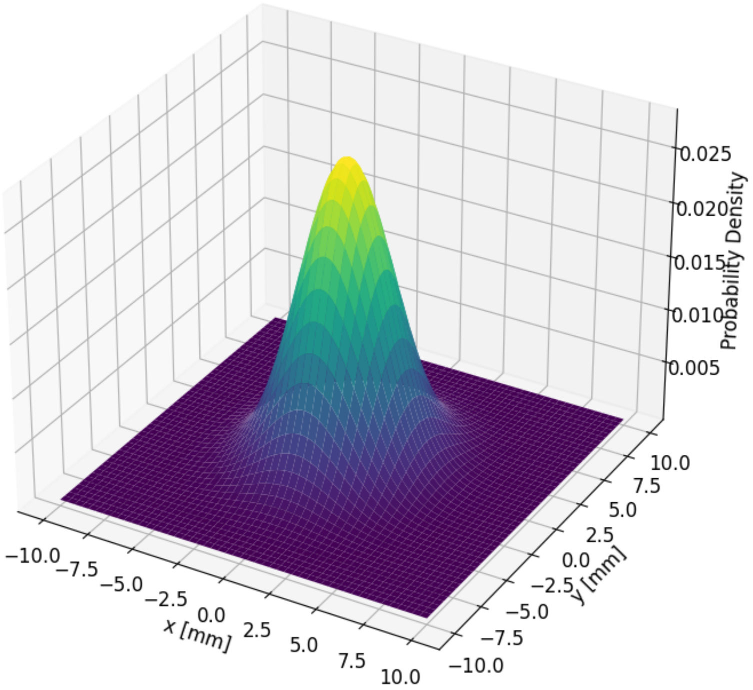

Figure 4.8: Beam model represented by a double Gaussian

The double Gaussian model is used to capture the dose distribution more accurately via two overlapping Gaussian curves instead of a single one. Each Gaussian curve is associated with a weight that influences the overall distribution. In this particular model, the first Gaussian curve has a weight of approximately 0.95, while the second one has a weight of approximately 0.05 as shown in Table 4.1. Based on this distribution, we made the decision to exclusively modify the characteristics of the first Gaussian curve for the remaining duration of the experiment, as it is the most representative component.

Since the beam is represented by Gaussian curves, the spot size technically extends to infinity. However, for practical purposes, we focus only on the regions where the dose is significant. To determine the size of the spot, we consider the threshold of one standard deviation (sigma σ) of the most heavily weighted Gaussian, which is the first Gaussian. This threshold allows us to determine the spot size, as illustrated in Figure 4.9.

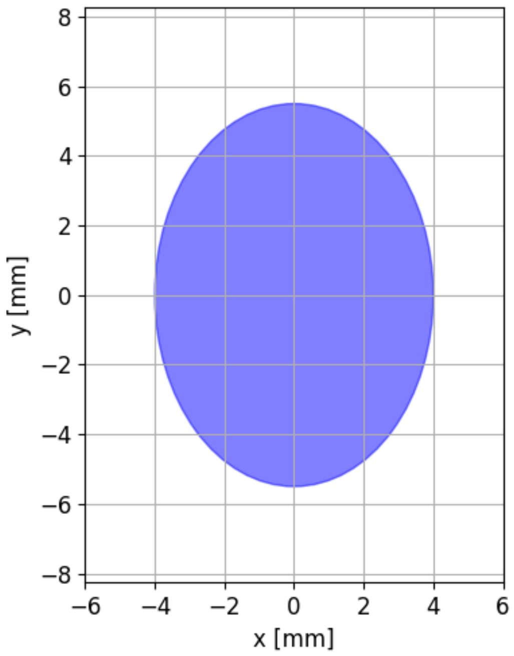

Figure 4.9: 2D spot size

Nozzle vs Isocenter

As mentioned previously, MCsquare requires beam characteristics at the nozzle, whereas other companies describe them at the isocenter. Therefore, it is necessary to convert the results obtained at the nozzle to obtain the corresponding values at the isocenter. For instance, Raystation, a well-known competitor of the OpenTPS software, provides beam model characteristics specifically at the isocenter.

To establish the relationship between the nozzle and the isocenter, the Courant-Snyder formula is employed, as explained in section 4.2.3. This formula allows the conversion of the beam parameters between the two locations ([54]) ([55]).

The equations producing the conversion are the following

$$\sigma_x^2(z) = \sigma_x^2(0) - 2\rho_{x\theta}(0)\sigma_x(0)\sigma_\theta(0)z + \sigma_\theta^2(0)z^2 \tag{4.6}$$

$$\rho_{x\theta}(z) = \frac{\rho_{x\theta}(0)\sigma_x(0) - \sigma_\theta(0)z}{\sigma_x(z)} \tag{4.7}$$

$$\sigma_\theta(z) = \sigma_\theta(0) \tag{4.8}$$

From equations 4.7 and 4.8 it is possible to obtain a new equation, viz.

$$\rho_{x\theta}(0)\sigma_x(0) = \rho_{x\theta}(z)\sigma_x(z) + \sigma_\theta(z)z \tag{4.9}$$

By injecting equations 4.9 and 4.8 into 4.6, we obtain:

$$\sigma_x^2(z) = \sigma_x^2(0) - 2\sigma_\theta(z)z(\rho_{x\theta}(z)\sigma_x(z) + \sigma_\theta(z)z) + \sigma_\theta^2(z)z^2 \tag{4.10}$$

After distributing the parenthesis and highlighting $\sigma_x^2(0)$, we finally obtain:

$$\sigma_x^2(0) = \sigma_x^2(z) + 2\rho_{x\theta}(z)\sigma_x(z)\sigma_\theta(z)z - \sigma_\theta^2(z)z^2 \tag{4.11}$$

Since we have a second order equation, taking the square root of equation 4.11 allows us to calculate the spot size in the x direction at the isocenter. The same procedure is applied to determine the spot size in the y direction.

Consequently, it is possible to compare the spot size at the nozzle with the spot size at the isocenter.

Methods

Now that the spot size is defined, we can examine the potential effects of uncertainties related to the spot size on a patient after optimization of the range modulator.

In accordance with the IBA research and development team, we decided to make the spot vary by 1 mm in each direction.

The BDL used for this experience exhibits the parameters described in Table 4.1, viz a spot size of 4mm in the x direction (SpotSize1x) (8 mm in total) and 5.5mm in the y direction (SpotSize1y) (11 mm in total) at the nozzle exit.

Initially, we optimized the hedgehog with this BDL and its associated parameters. Then, Monte Carlo simulations were performed by adjusting the spot size in the x direction within the range of 3mm to 5mm with an increment of 0.2mm, and in the y direction within the range of 4.5mm to 6.5mm with the same increment.

The objective for the delivery beam is to have a spot size as round as possible because a pencil beam is used to cover all the targets and it is important to have a round beam shape to cover the target correctly. We studied the difference in spot size shape between the nozzle (where the beam leaves the apparatus) and the isocenter (where the beam is delivered to the patient).

Figure 4.10 shows that the spot size at the isocenter is more circular than the spot size at the nozzle.

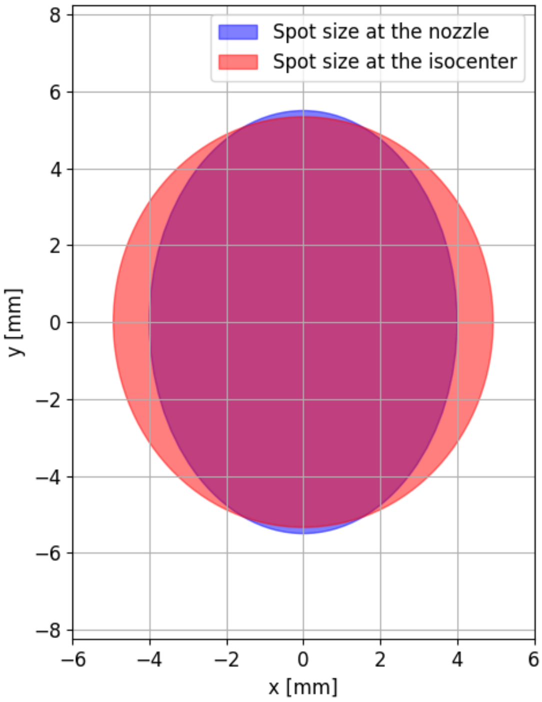

Figure 4.10: Difference of spot size for the same beam at the nozzle and at the isocenter

If we consider the double Gaussian model and make a comparison between the isocenter and the nozzle, we can observe a difference between the two. In Figure 4.11 we find the individual double Gaussian at the nozzle on the left and at the isocenter on the right.

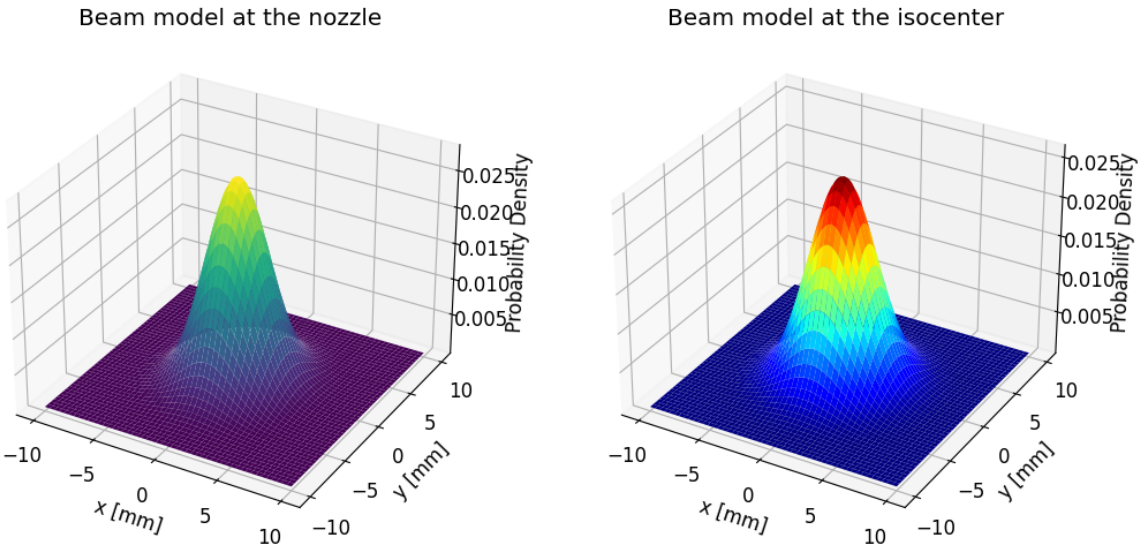

Figure 4.11: Double Gaussian beam model individually plotted at the nozzle and

If we superpose the 2 graphs (double Gaussian at the nozzle and at the isocenter) we observe again in Figure 4.12 the difference between the two. This means that, while preparing the treatment planning, we should know what the characteristics of the proton beam are and where those characteristics have been measured.

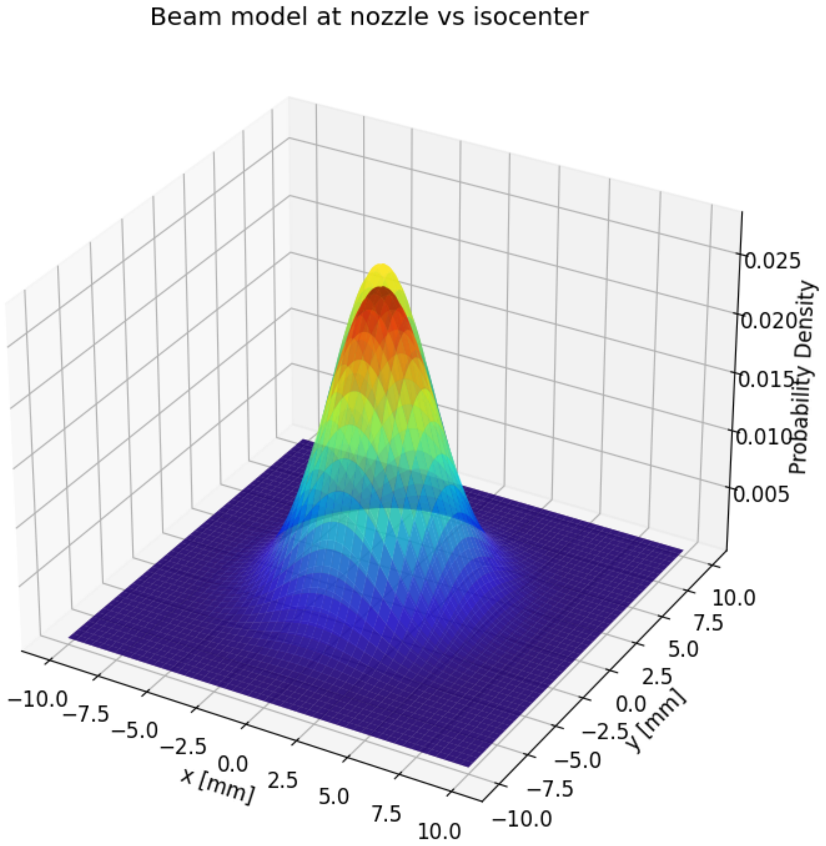

Figure 4.12: Double Gaussian beam model: superposition of the 2 graphs of Figure 4.11

4.2.5 Spot position

Methods

In this section, our objective was to investigate the effect of spot position uncertainty on the treatment outcome. During treatment planning, we optimized the dose distribution for spots positioned relative to the reference point known as the isocenter. The isocenter is located on the patient's couch, precisely where the targeted cancer is located. Afterward, equipment calibration is performed to ensure consistency between the simulation and the actual treatment. However, this calibration process may introduce uncertainties in the range of tenths-of-a-millimeter. Our focus is to assess the impact of shifting all the spots, by e.g. 0.5mm. We will analyze the resulting dose received by the ROI for each isocenter shift, including the percentage deviation from the prescribed dose and the dose homogeneity.

In Figures 4.13 and 4.14, we present the dose deposition differences between an accurate dose distribution and a dose distribution with a 3mm shift in the x and y directions. It is important to note that the chosen value of 3mm is arbitrary and not realistic in practice. In practice, small shifts are possible, but such a large shift of 3mm is purely for illustrative purposes to highlight the impact on the dose distribution. The red rectangle is the Volume Of Interest (VOI).

In our simulations, we performed spot shifts ranging from -0.5mm to 0.5mm in both the x and y directions. However, we did not display the variation in dose deposition on the target volume because the differences between the shifted and non-shifted cases were not significant for such small shifts.

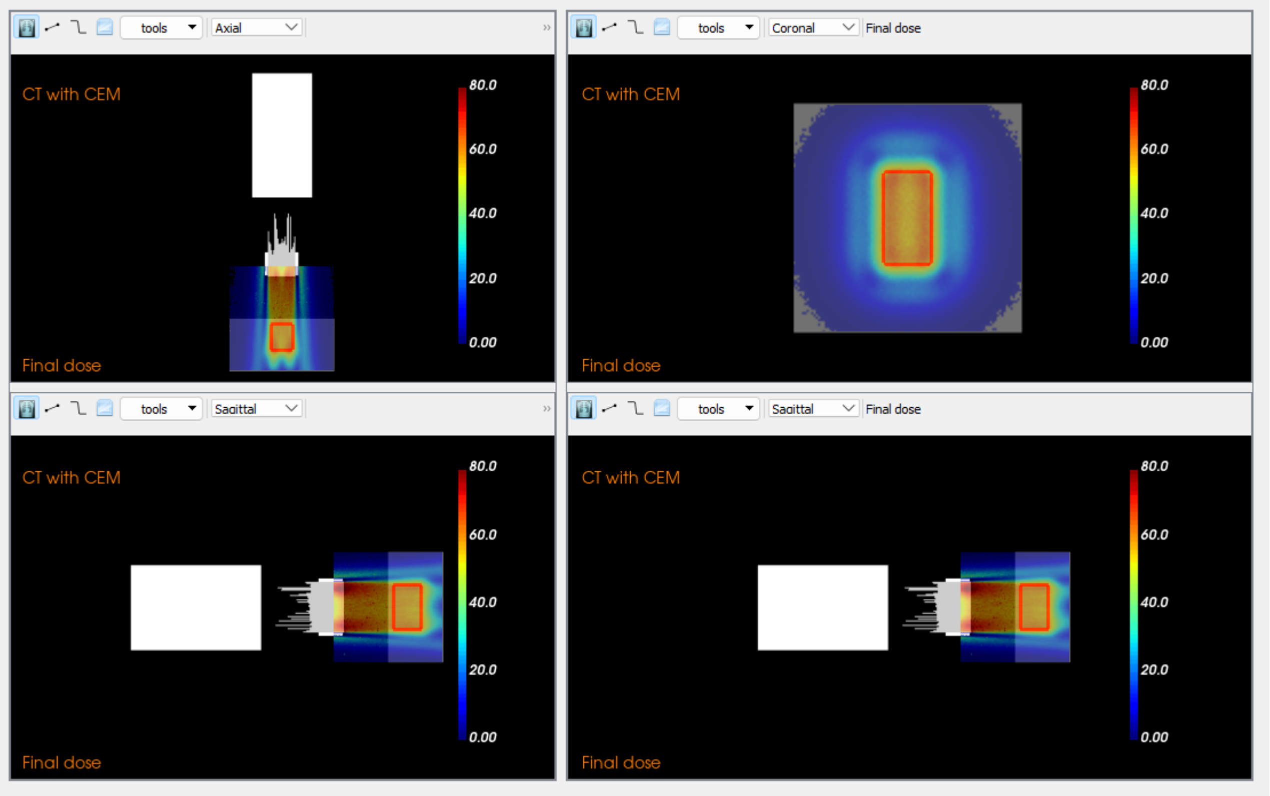

Figure 4.13: Isocenter perfectly calibrated

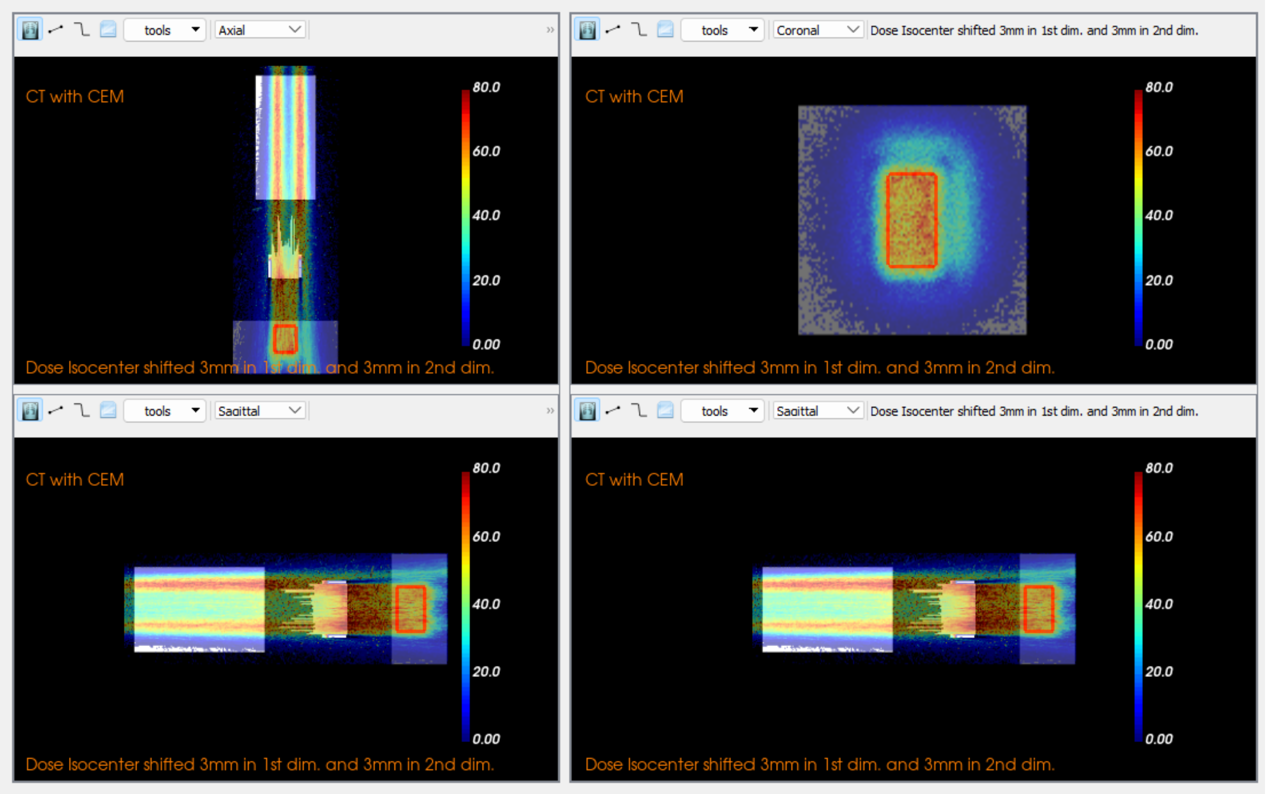

Figure 4.14: Isocenter shifted by 3mm in each direction

4.2.6 Air inclusions in the hedgehog

The last parameter we investigated is the impact of the presence of air inclusions in the range modulator. Since the hedgehog is 3D printed, it is subject to the limitations of the printing process, such as the potential inclusion of small air bubbles. The presence of these inclusions can be observed in Figure 4.15, where we can see that they are relatively abundant.

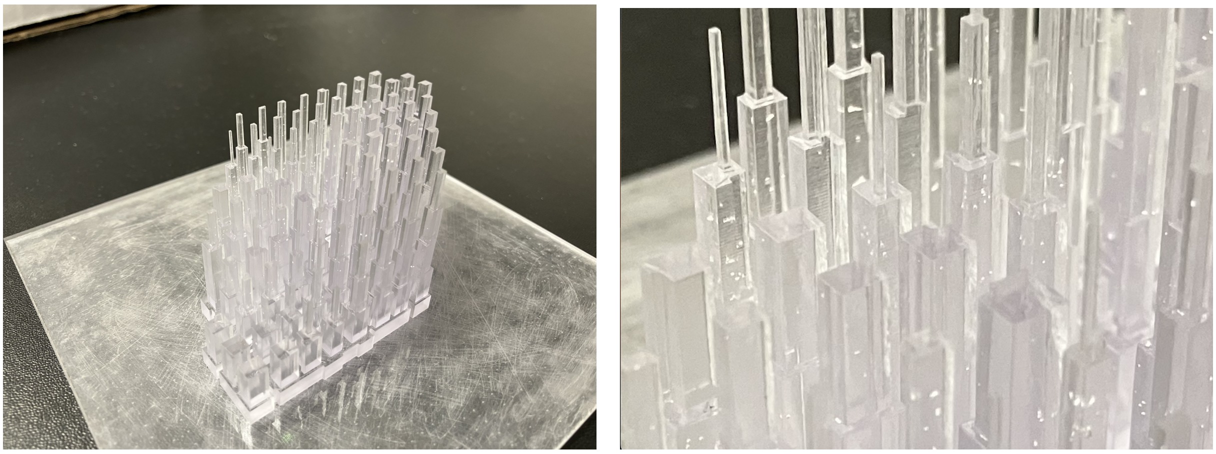

Figure 4.15: Air inclusions in a 3D printed range modulator

The presence of air inclusions can introduce variations in the materials encountered by the protons. Since these materials have different densities and stopping powers, they can potentially affect the final dose distribution.

Methods

In this experiment, we consider the presence and position of air inclusions to be random. The objective is to investigate the impact of these inclusions on the final dose delivery. However, due to the random nature of this effect, the exact number and location of the inclusions are unknown.

To study the impact of air inclusions on the dose delivery, we conducted an experiment where we controlled the number of inclusions in the hedgehog. However, the placement of the inclusions was randomized. To address placement variability, we repeated this random placement process 20 times. This approach allowed us to assess the potential significance of bubble placement in the overall results.

We conducted a series of experiments in which we progressively increased the number of inclusions in a logarithmic manner, with increments of 10. This approach allowed us to gain a comprehensive understanding of when the presence of inclusions may start to pose a significant problem. We started with a control case where no inclusions were present and then proceeded to evaluate scenarios with 10, 10^2, 10^3, and finally 10^4 inclusions.

In each scenario, except for the control, we performed 20 iterations with random placement of the air inclusions. This approach allowed us to assess the effects of increasing bubble quantity on the final dose distribution.

Moreover, because of the way we implemented the grid, the lowest resolution for these inclusions was the size of one pixel which is a 1 mm voxel. This characteristic will be discussed later.

In order to give an idea of what this looks like during the simulation, we can see an example of this hedgehog in openTPS with 10^3 air inclusions in Figure 4.16.

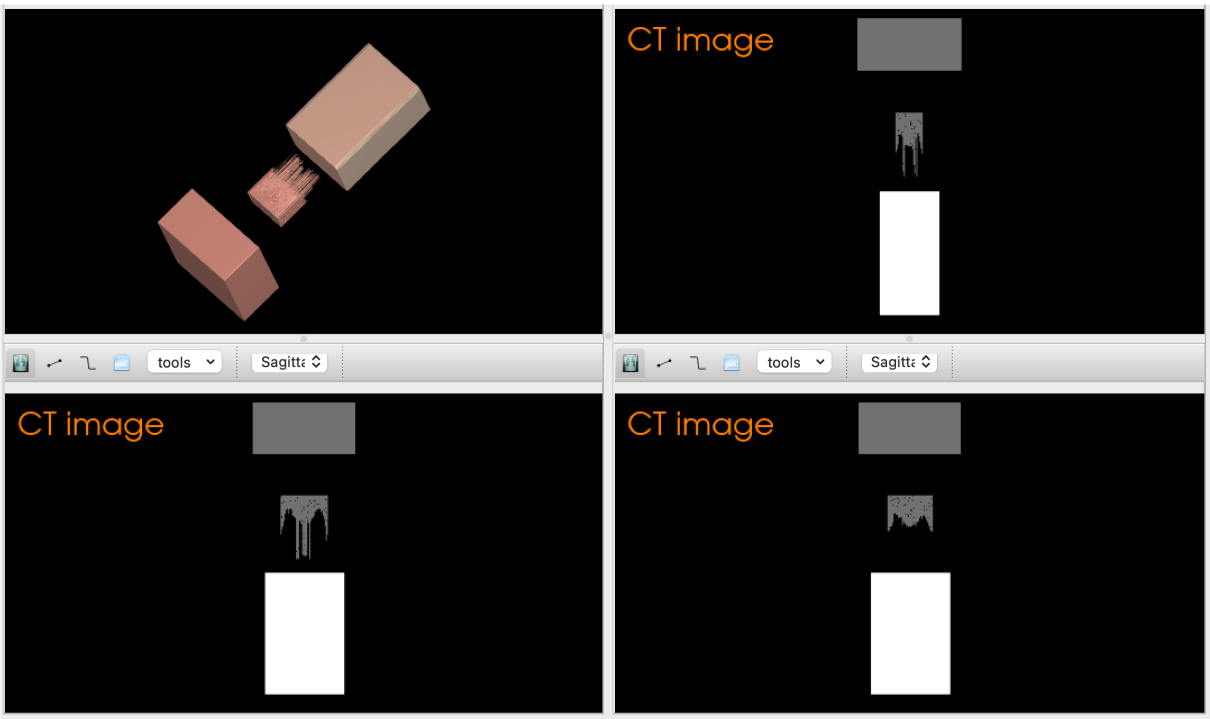

Figure 4.16: OpenTPS screenshot of the hedgehog with 10^3 air inclusions in it

4.3 Results of range modulators robustness study

In this final section, we will conduct an analysis and provide comments on the results obtained regarding the 3 types of uncertainties. These uncertainties are analyzed by evaluating various metrics, such as the percentage of deviation or the homogeneity index.

4.3.1 Spot size

As a reminder, in this study the spot size is 8 mm long in the x direction and 11 mm long in the y direction in total at the nozzle exit. We make it vary by 1 mm in each direction.

First, the most important graph is the variation of the dose metrics associated to DVH (which will be refered to as Dx from now on) according to the spot size at the nozzle. This variation is shown in Figure 4.17. We observe that the spot size has a big influence on the delivered Dx. While the D_{95} and D_{50} values show some minor variations, they remain within an acceptable range. However, the D_5 value exhibits a significant difference, with nearly a 4Gy variation between the two spot sizes. This variation can have implications for the treatment, particularly for the OAR, if the dose increases excessively between its maximum expected value and the actual delivered dose.

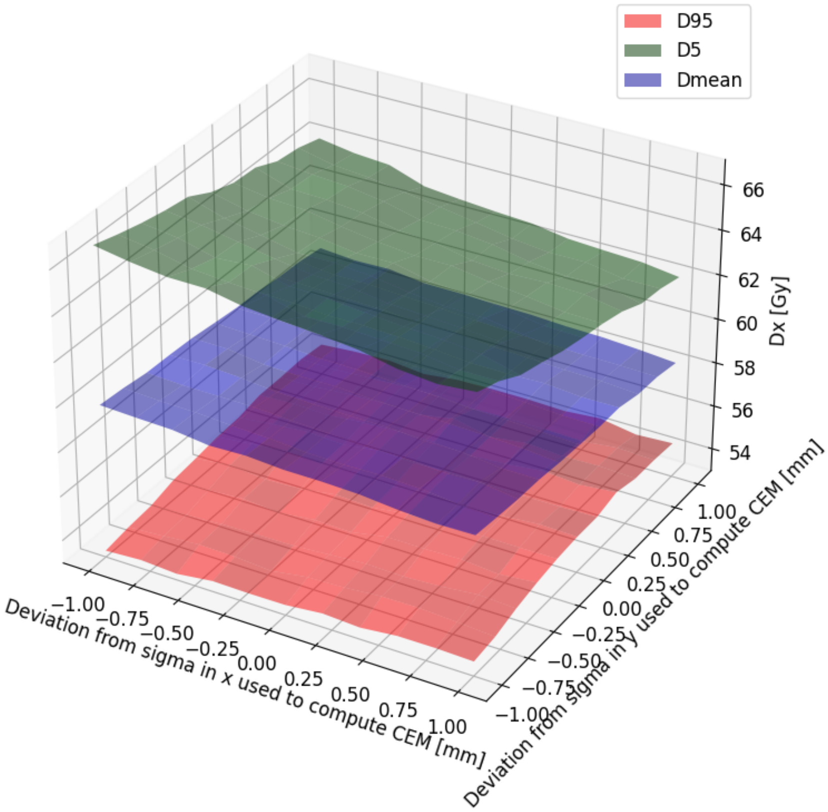

Figure 4.17: 3D dose variation according to spots size

We decided to normalize this graph by D_{50}:

$$D_{normalized} = \frac{D}{D_{50}} \times D_{50,ideal} \tag{4.12}$$

We made this decision because, if we have the possibility to evaluate the spot size just before the treatment, we could simply adjust the dose by multiplying the weight of each spot by the ratio between the actual D_{50} and the ideal D_{50}. The normalized graph is shown in Figure 4.18.

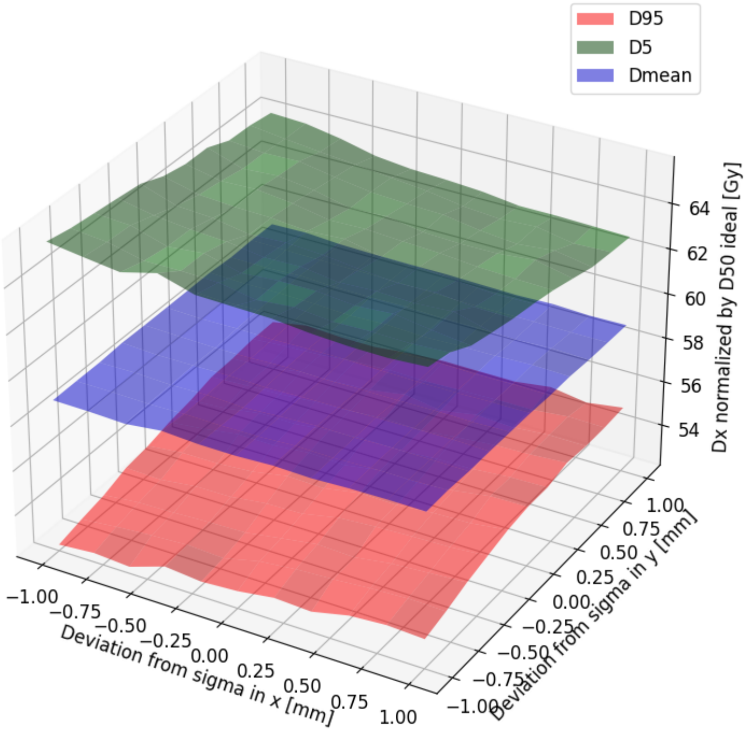

Figure 4.18: 3D dose variation normalized by D_{50} ideal

Since we have the distribution probability of the spot size at the nozzle and, the isocenter, we check whether this small modification has an impact on the dose distribution at the nozzle and the isocenter. This is shown in Figure 4.19.

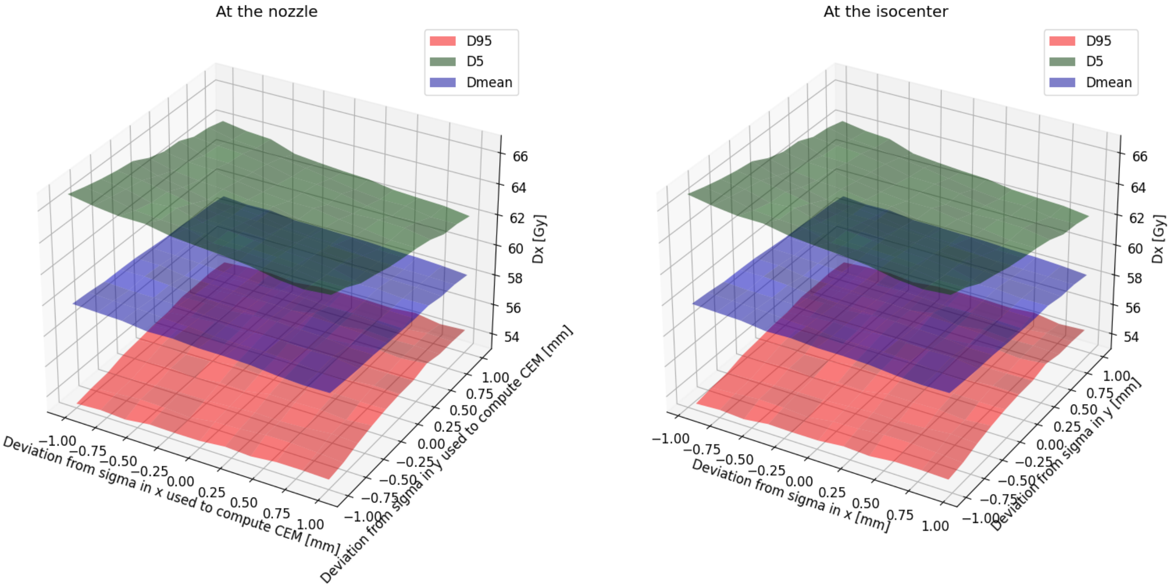

Figure 4.19: Dose distribution at the nozzle and at the isocenter

As we can see in Figure 4.19, there is no significant difference, whether the characteristics of the BDL are calculated at the nozzle or at the isocenter. This is a good thing because it means that no matter how someone is describing their study (with the characteristics at the nozzle or the characteristics at the isocenter) we can still directly interpret their results without having to recalculate them.

After several discussions with the FLASH team at IBA, they suggested we study the homogeneity. The Homogeneity Index (HI) is an objective tool to analyze the uniformity of dose distribution in the target volume ([56]). In all types of radiation treatment (RT, PT, and FLASH-PT), the objective is to deliver the maximum of the dose homogeneously to the target volume. Different formulae exist but for this study, we use the formula which the most commonly used in the literature ([56]):

$$HI = \frac{D_5 - D_{95}}{D_p} \times 100 \tag{4.13}$$

where D_5 and D_{95} are the minimum dose in the 5% and the 95% of the target volume, and D_p the prescription dose.

We can interpret this formula as aiming for a value as close to zero as possible. A value close to zero indicates that the D_5 and D_{95} values are very similar, indicating that the dose is pretty much the same everywhere over the region of interest.

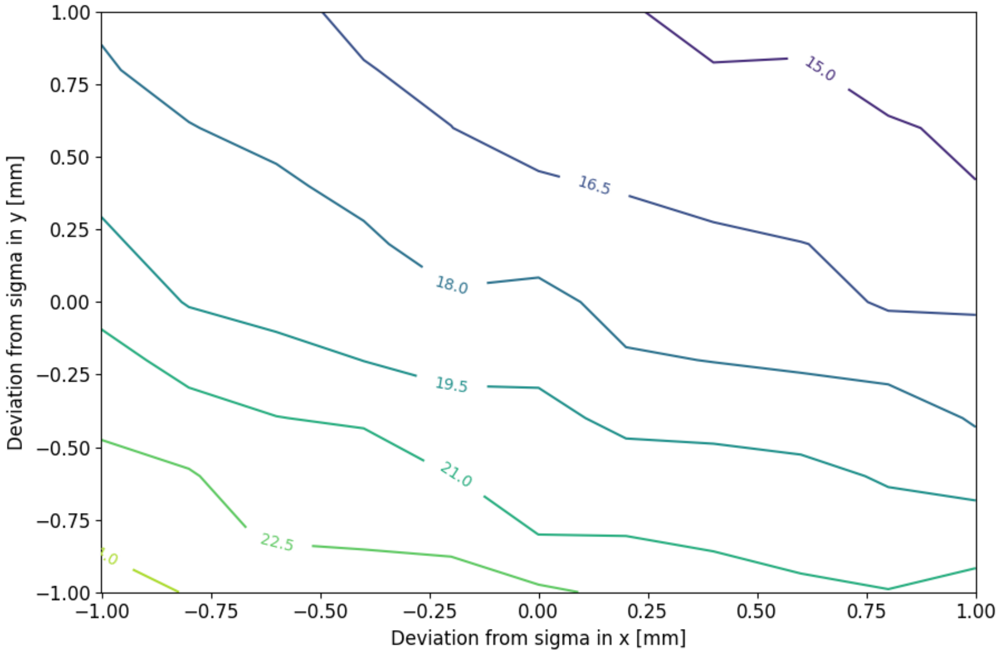

Figure 4.20: Homogeneity study of the dose through the HI

In our case, our goal is to minimize the variation of the homogeneity index when we change the spot size. This indicates that the variation in spot size does not significantly affect the homogeneity of the dose. Unfortunately, we see in Figure 4.20 that we can have a 33 % variation of the homogeneity index which is non-negligible.

The IBA team also asked us to make a graph of the D_{95} deviation according to spot size, so as to better observe in 2D when the D_{95} will be too far from the prescription. In order to do that, we computed the D_{95} deviation (dd) using this formula

$$dd = \left(\frac{D_{95}}{D_p} - 1\right) \times 100 \tag{4.14}$$

with D_p the prescribed dose.
We decided with the IBA team to set a limit at 1% of deviation from the optimized dose because it seemed a good compromise for staying close enough to the optimized dose. Over this 1% mark, we consider that the dose starts to be too different from what it should be.

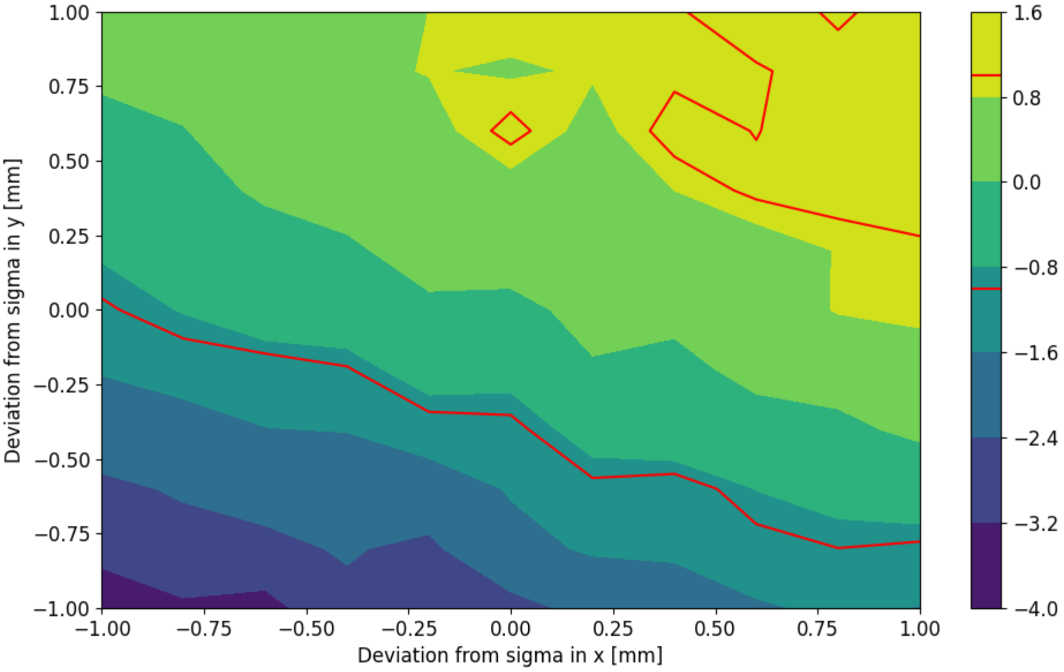

Figure 4.21: Percentage of deviation from the prescription dose

Once again, we can see that the uncertainties on the spot size will have a huge impact on the delivery dose. As we can see in Figure 4.21, the D_{95} deviation rises quite rapidly up to 1% which is not a good thing.

To conclude the results of spot size, we can state that uncertainties about spot size can have a huge impact on treatment delivery. This means that it is quite important to correctly and precisely model the BDL before optimizing the hedgehog. And most importantly it is crucial to ensure that the beams possess the same characteristics as those used for the optimization because there is not much room for error in this case.

4.3.2 Spot position

During treatment planning, the dose distribution is optimized for spots positioned according to the isocenter, which may have uncertainties in calibration in the range of tenths-of-a-millimeter. The experiment aims to study the effects of shifting all spots by a certain amount, such as 0.5mm in all directions.

Figure 4.22 depicts a three-dimensional plot illustrating the dose for each potential shift of the isocenter. As we can see, the uncertainties on the position of the spots do not have a significant impact on the Dx distribution in the ROI.

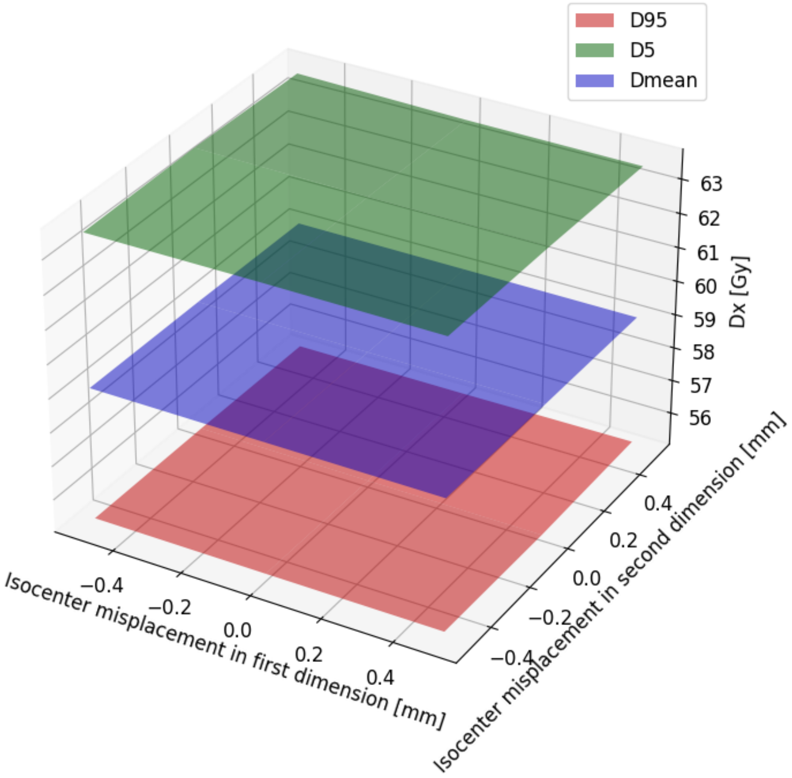

Figure 4.22: Dose variation for different spot position

Figure 4.23 shows the percentage of deviation from the prescripted dose, and we can see that even for extreme conditions the D_{95} deviates by a maximum of 0.18% which is far away from the 1% line we chose as a reference (the same line as the one we chose in the spot size section).

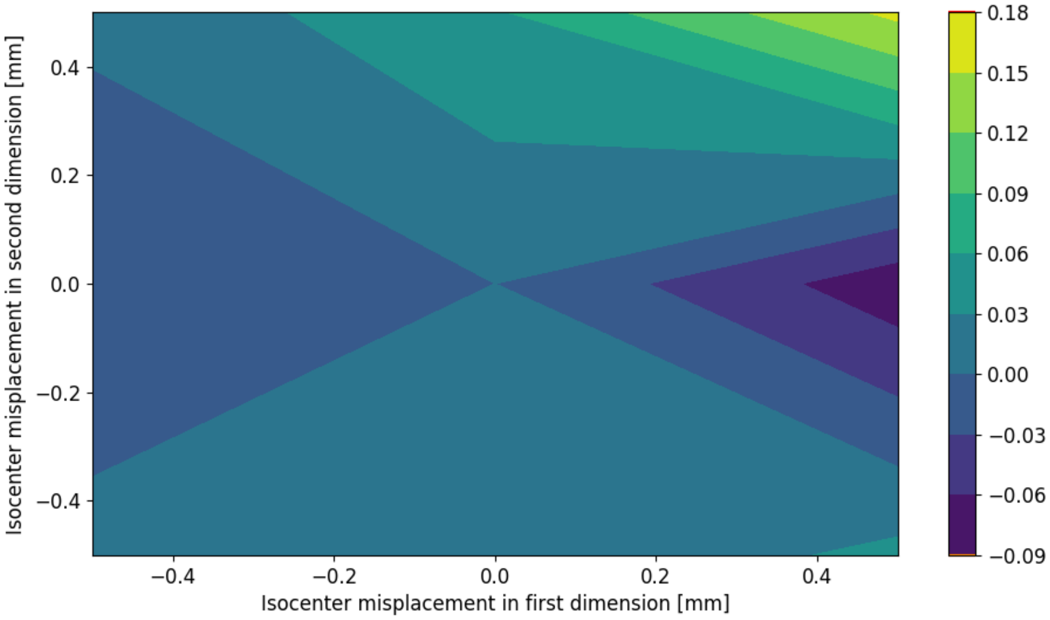

Figure 4.23: Percentage of deviation from the prescription dose

We can also observe that this type of uncertainty does not have a significant impact on the homogeneity of the dose. As shown in Figure 4.24, we find only a 1.3% difference between an extreme case of shifting and the ideal situation, and this is not much of a difference.

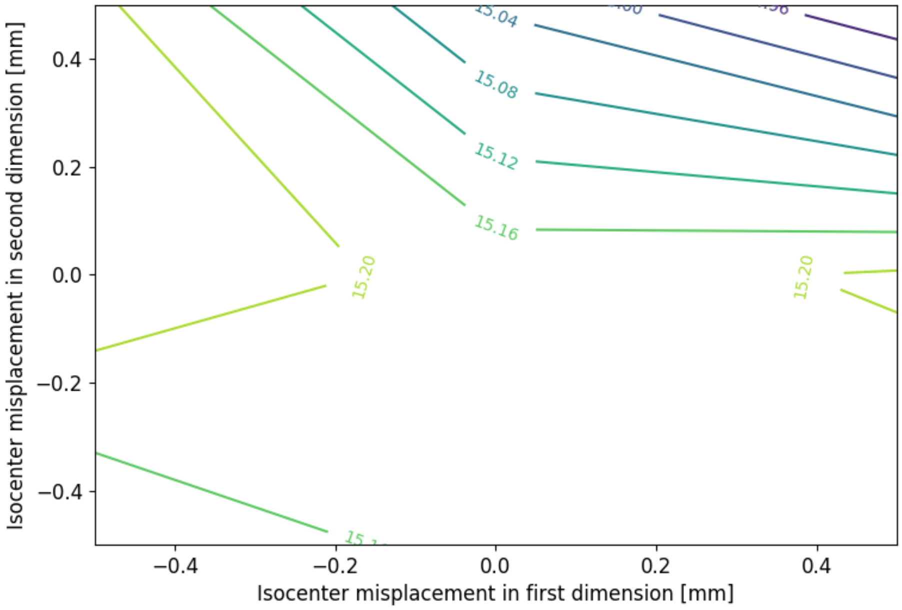

Figure 4.24: Homogeneity study of the dose through the HI

To conclude this subsection, we can state that whatever the method used to evaluate spot position uncertainties, it does not have a large impact on spot position. We can conclude that it will have a minimal impact on dose delivery. This is a really good result since it means that the actual method used to calibrate the isocenter is valid and precise enough to guarantee a good distribution of the treatment.

4.3.3 Air inclusions

In this experiment, we aimed to investigate the effect of random air inclusions on the final dose delivery. To account for the randomness of this phenomenon, we conducted an experiment where we controlled the number of added inclusions but randomized their placement. We tested for 0, 10, 10^2, 10^3, and 10^4 air inclusions with the size of a voxel (1mm large). Except for the control group without any inclusions, each condition underwent 20 iterations with randomly placed air inclusions. This approach allowed us to assess whether the placement of inclusions could significantly impact the results.

The first result we examined is the evolution of the various DVH metrics: D_{95}, D_{50}, D_{mean}, and D_5. We can observe these results in Figure 4.25. This graph is quite interesting because, first of all, it shows the mean value of the 20 iterations for each number of inclusions tested as well as the standard deviation of these values. As we can see on the graph, the standard deviation is quite small. This finding allows us to conclude that the random placement of inclusions has negligible effects and does not significantly impact the delivery of the dose.

Secondly, we can see that the metrics barely move until the number of inclusions reaches 10^3. However, after this value, the impact is quite important. However, the effect of these inclusions on D_5 is not enormous indicating that in the worst case scenario, more cells will receive some doses but none will receive a much higher dose than they should have.

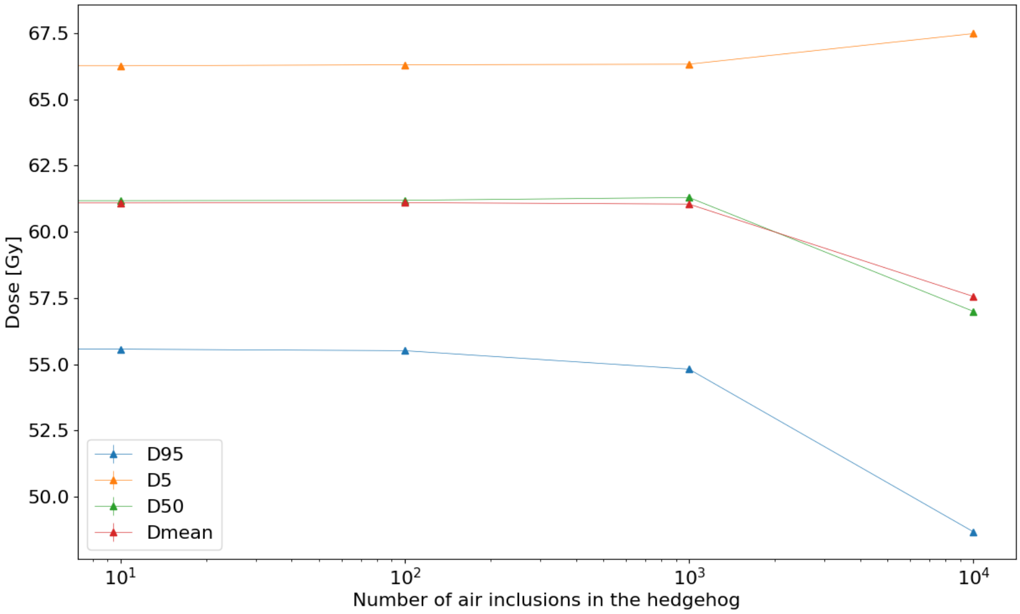

Figure 4.25: Dose metrics variations according to the number of air inclusions

These results are pretty good because, since the placement of the inclusions does not seem to have an effect on Dx but rather the number of inclusions, this means our limitation on the resolution for the air bubble is kind of sorted out. For instance, if we were to examine the impact of inclusions measuring 0.5mm in size, the results would likely be similar to those with 1mm inclusions, except that the value would be multiplied by 4. This indicates that the crucial factor is the overall volume of air remaining in the hedgehog, rather than the specific location of the air bubbles.

To further explore the relationship between the number of air inclusions and their impact on the dose, we will examine another metric: the deviation from the optimized or control scenario, where no inclusions are present in the hedgehog. This metric will provide insights into the extent to which the D95 is affected by the presence of air inclusions.

As a reminder, we used the same indicator (dd) in Equation 4.14 as for the previous results, this being:

$$dd = \left(\frac{D_{95}}{D_p} - 1\right) \times 100$$

Also note that similar to previous studies, we maintain the one percent line as a reference point for comparison

In Figure 4.26, we see that three different lines have been drawn.

The blue line represents the actual results we obtained after our simulations.
The red line is the one percent line taken as a reference to determine whether the effect is too large or not.
Finally, the green line is a linear regression of these results.

From this figure, we observe that as long as the number of air inclusions remains relatively below 10^3, we remain below the one percent line.

Although it may be difficult to observe on the graph, there is a linear relationship between the percentage of deviation and the number of air inclusions in the hedgehog. To further investigate this relationship, we conducted a linear regression analysis on the results. The regression equation is reported in Equation 4.15

$$Y = 1.22 \times 10^{-3} X - 0.0292 \tag{4.15}$$

with Y the percentage of deviation from the D_{95} received with the optimized hedgehog, and X the number of 1 mm large air inclusions in the hedgehog. Since the placement of the latter has no direct incidence, the X can be interpreted as a volume in mm^3.

These results are encouraging because it seems first of all that the hedgehog is robust against these air inclusions when their number does not exceed 10^3. Secondly, once we receive a hedgehog, a CT scan could determine the volume of air it contains, and we can already be prepared for the consequences that this could cause.

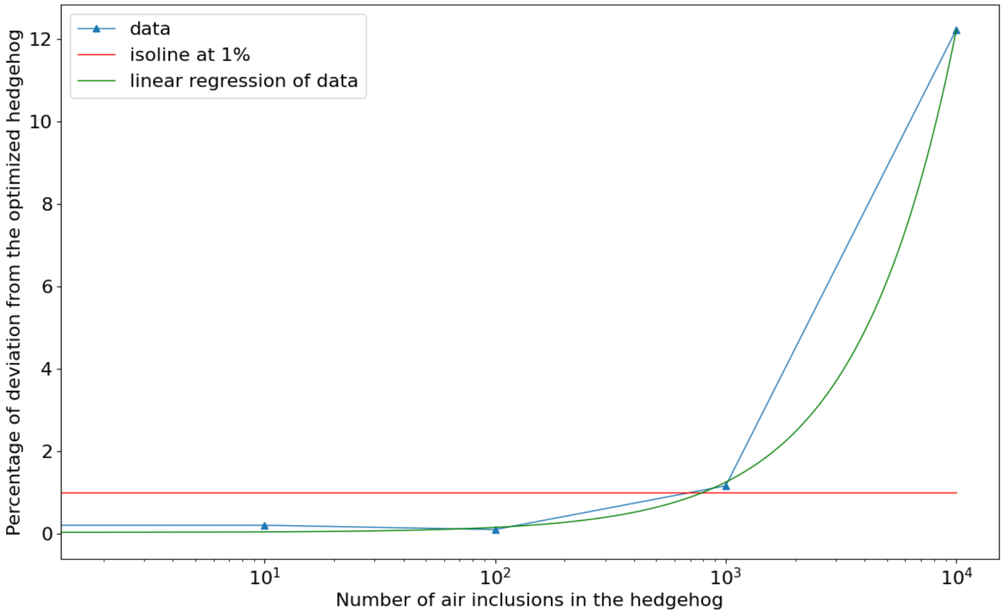

Figure 4.26: Dose deviation in percentage from the prescription

The third metric we wished to analyze is the homogeneity index (HI) of the dose in the ROI. This is calculated as before, according to Equation 4.13 which is:

$$HI = \frac{D_5 - D_{95}}{D_p} \times 100$$

The results are shown in Figure 4.27. As can be observed, the graph has the same profile as the one for dose deviation. We can thus assume that the homogeneity index is linearly correlated to the volume of residual air in the hedgehog. But once again, it appears that when the number of air inclusions in the hedgehog is higher than 10^3, this begins to have a serious impact compared to the optimized version of the hedgehog.

This result goes parallel to the previous ones, and we can state that finally, the hedgehog is pretty robust to this phenomenon, since it allows IBA to require this type of quality in their order, and it seems that asking to have less than 1000 mm^3 of air inclusions is not an impossible task to do.

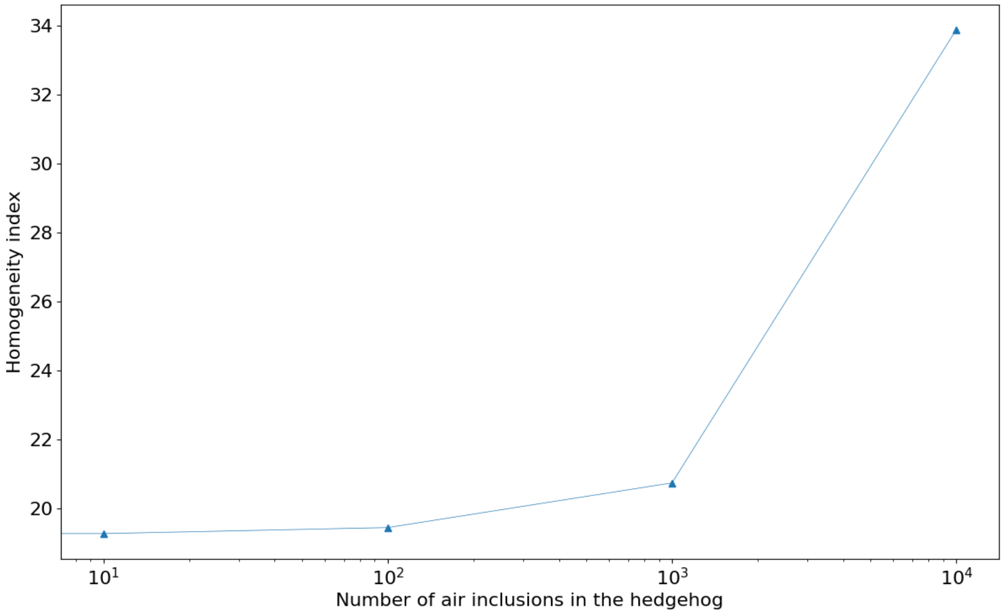

Figure 4.27: Homogeneity index of the dose in the region of interest

In this section on air inclusions, we would like to get a visual idea of the effect, the changes that these air inclusions have on the hedgehog.

This is why we will analyze a new parameter that has not been previously examined. Before conducting this analysis, we will introduce a relevant concept associated with this parameter. Specifically, we wish to introduce the concept of water equivalent thickness.

Water Equivalent Thickness (WET)

The WET is a measure used in radiation therapy to describe the amount of material that is capable of attenuating or stopping a beam of radiation.

Globally, the WET considers both the physical thickness and the radiation absorption properties of a specific material compared to these of water. Water is commonly used as a reference material because it closely approximates human tissue's average radiation absorption characteristics.

So, to calculate the WET, the actual physical thickness of the material (in millimeters, for example) is multiplied by the relative proton stopping power.

In our case, we wish to analyze the attenuation loss that the hedgehog undergoes with air inclusions. We first determine the WET of the hedgehog with various numbers of air inclusions and then compare it to the optimized case.

Of course, since the hedgehog is a complex object that does not have the same thickness throughout, we compiled a 2D map where the WET is calculated for each pixel of the hedgehog base as can be seen in Figure 4.28, 4.29, 4.30 and 4.31.

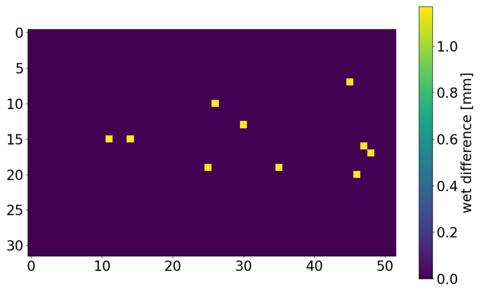

Figure 4.28: 2D WET difference with 10 air inclusions

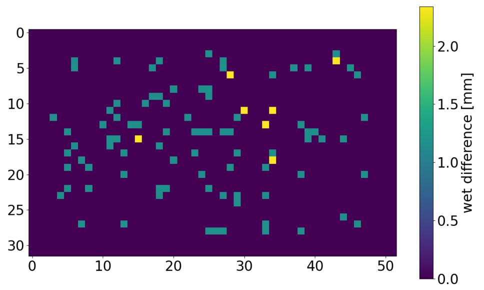

Figure 4.29: 2D WET difference with 10^2 air inclusions

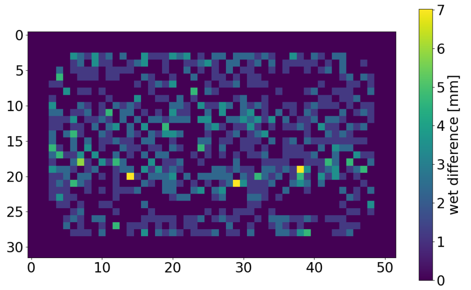

Figure 4.30: 2D WET difference with 10^3 air inclusions

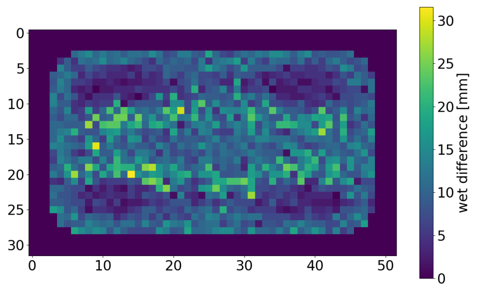

Figure 4.31: 2D WET difference with 10^4 air inclusions

From this 2D map, we examined the mean difference that these inclusions make in the WET and the maximum difference that they usually create. That is represented in Figure 4.32.
We see that the relation between the mean difference and the number of air inclusions appears to be linear.

Also, we see that when there are 10^3 air inclusions, there is a mean difference of 1 mm in the WET, which is our resolution, and that the medium we are shooting at is water.

So we might think that our results for the dose computation when there are less than 10^3 air inclusions are not very precise because the loss of thickness is on average less than our resolution. But when we examine the maximum difference, we see that for each case, the value is always at least 1 mm, and this is due to the fact that the wet factor of the hedgehog is quite close to 1. That means that even though on average we are dealing with values that are below our resolution, we can still interpret the results because the individual values that are used are in our resolution range.

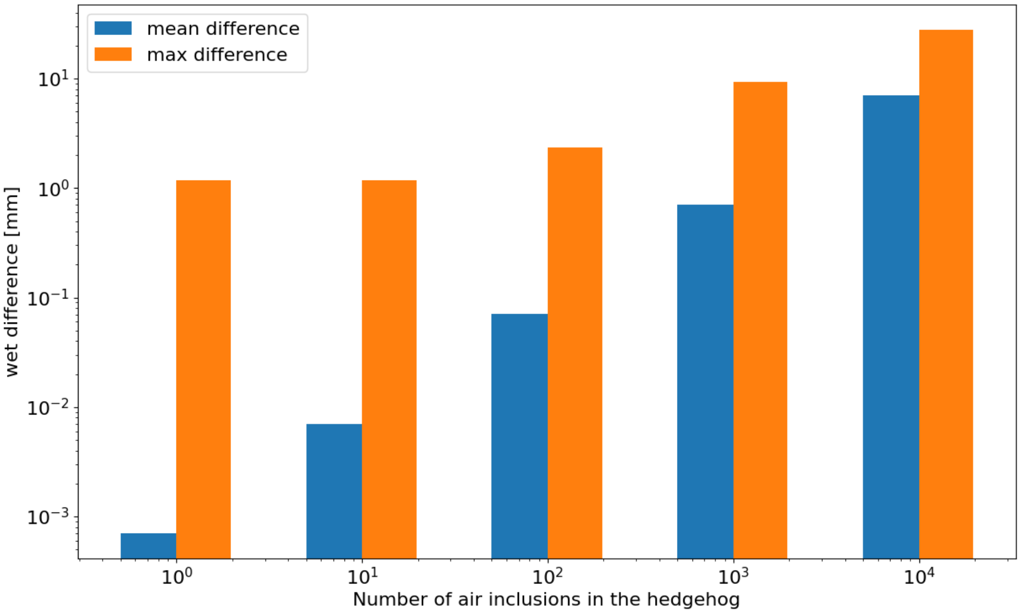

Figure 4.32: Mean and max value of the 2D WET difference map of the different hedgehog

In view of the results, it could be said that the placement of the air inclusions does not seem to have an impact, but rather the total air volume. It also seems that it is when we have a total of 1000 mm^3 of air that arises a problem. All in all, we could say that the hedgehog is quite robust against these air inclusions since first of all 1000 mm^3 of air seems to be an odd number in reality. Secondly, this could just be a specification required by IBA from their manufacturer.

One could still dispute whether the resolution used during our simulations could cause a bias in our results but we still consider that it was the best resolution to use.

To conclude this section about the results of the study, we can say that variations in spot size have a significant impact on dose delivery. Therefore, it is crucial to manage and control these variations prior to dose administration to ensure consistent treatment outcomes. On the other hand, uncertainties related to spot position and air inclusions have minimal effects on dose distribution, as long as they remain within a reasonable range of values.

Chapter 5

Conclusion and perspectives

In recent times, there has been growing interest in FLASH radiation therapy due to its potential to reduce the side effects commonly associated with conventional dose rate radiation therapy. To qualify as a FLASH treatment, a high dose of radiation is delivered over a short period of time. While more research is needed to fully comprehend the benefits and limitations of FLASH proton therapy (FLASH-PT) and its underlying mechanisms, an increasing number of studies are now focusing on treatment planning and delivery in this field. Increasing the dose involves the use of a new component which can create uncertainties in dose delivery.

In this master's thesis, we conducted three types of experiments. The first one focused on assessing the influence of spot size on dose coverage and its the conversion from the nozzle to the isocenter. The second experiment examined the impact of positional shifts between the target and the beam delivery, which could arise from a misplacement of the isocenter. Lastly, we investigated the effects of air inclusions present in the 3D-printed range modulator.

In the first experiment, we observed a significant impact on the dose distribution when changing the spot size. Deviations from the prescribed dose increased by more than 1%, and degradation of the dose homogeneity up to 33%, when the uncertainty is 1mm, which is considerable. This emphasizes the importance of keeping the same spot size during the optimization and treatment delivery. However, due to the low values of the divergence of the beam usually used for this treatment, the range of acceptable uncertainties in the spot size is the same whether this characteristic is taken at the nozzle or at the isocenter.

In the second experiment, we assessed the impact of spot position due to shifts of the target. We observed that small shifts within a range of 0.5mm in all directions did not significantly affect the dose distribution. In practical scenarios, it would be challenging to have misplacements of the range modulator component on the nozzle or the patient, thanks to the rigorous calibration settings and verifications performed prior to treatment delivery. The impact on dose delivery was minimal, and even with small shifts, the prescribed dose remained largely unchanged. We can state that the hedgehog is quite robust to this uncertainty, certainly by its nature. Since the hedgehog is used to degrade the energy, it will induce scattering that will eliminate the small uncertainties on the initial conditions of the isocenter placement.

The final parameter we examined was the impact of air inclusions in the printed range modulator. The 3D printing process can introduce imperfections such as air inclusions. These inclusions can affect the path of protons due to the density difference between the Accura ClearVue material and air. Based on the results of our air inclusion simulations, we observed that for a number of inclusions less than 10^3, the dose closely matched the prescribed one. However, when the number of air inclusions exceeded 10^3, the dose deviated significantly from the prescription, the homogeneity of the dose distribution was no longer maintained, and the deviation from the prescription increased drastically. All these characteristics show that the treatment requires quality controls to ensure target coverage and treatment efficiency.

Based on our current findings, it can be concluded that, if the level of uncertainty observed is within an acceptable range and can be addressed prior to treatment delivery, there is no immediate need to reprint the range modulator using a 3D printer. However, further testing is required to more accurately assess the quality of dose delivery and its conformity to the prescribed dose. It is important to note that the treatment planning already incorporates a margin to account for uncertainties. Furthermore, it is worth considering that the addition of the range modulator may introduce other types of uncertainties. Exploring the impact of other types of uncertainties in the context of FLASH proton therapy could be an interesting avenue for future research if this technique were to be adopted in clinical practice.

An interesting prospect is to integrate this type of tool with the optimization of treatment plans in order to achieve a robust optimization of the FLASH plan. In this type of option, the aim is to obtain the most robust plan with respect to the uncertainties considered. The robust plan is evaluated in the same way as we did, by introducing errors and evaluating deteriorations in the quality of the plan, in particular using DVH. However, this means that the more uncertainty you consider, the longer it takes to optimize the plan, and this can quickly take several hours. It is therefore important to first determine the parameters that have the greatest impact on the dose and to quantify this impact so as not to consider sources of uncertainty that have little impact.

Our investigation work presents an approach and some insight into the robustness study of the FLASH method. But it is important to recall that, first, this work did not treat every uncertainty related to this method. Among others, the impact related to the quality of the impression of the hedgehog (tower too high or too wide, the curvature of the hedgehog, ...) remains to be studied.

Moreover, it would be important to better quantify the uncertainty sources since the currently utilized ranges may not provide sufficient assurance that broader ranges should be disregarded.

Finally, it would also be interesting and necessary to consider a wide variety of cases, including clinical cases and not only synthetic cases.

References

[1] World Health Organization. (2022, Feb. 3). *Cancer*. Available: `https://www.who.int/news-room/fact-sheets/detail/cancer`

[2] International Agency for Research on Cancer. (2020, Dec.) *All cancers*. Available: `https://gco.iarc.fr/today/data/factsheets/cancers/39-All-cancers-fact-sheet.pdf`

[3] National Cancer Institute. (2021, Oct. 11). *What Is Cancer?*. Available: `https://www.cancer.gov/about-cancer/understanding/what-is-cancer`

[4] AACR American Association for Cancer Research. *What Is Cancer?*. Available: `https://www.aacr.org/patients-caregivers/about-cancer/what-is-cancer/`

[5] Douglas Hanahan, Robert A. Weinberg. *Hallmarks of Cancer: The Next Generation*. Cell, vol. 144, n°5, mars 2011, p. 646-74. DOI.org (Crossref), https://doi.org/10.1016/j.cell.2011.02.013

[6] Mayo Clinic. *Cancer treatment*. Available: `https://www.mayoclinic.org/tests-procedures/cancer-treatment/about/pac-20393344#:~:text=Chemotherapy%20uses%20drugs%20to%20kill,inside%20your%20body%20(brachytherapy).`

[7] Cancer council. *Radiation therapy*. Available: `https://www.cancer.org.au/cancer-information/treatment/radiation-therapy`

[8] National Cancer Institute. *External Beam Radiation Therapy for Cancer*. (2018, May 1). Available: `https://www.cancer.gov/about-cancer/treatment/types/radiation-therapy/external-beam`

[9] Edmond Sterpin. *General introduction to radiotherapy and proton therapy*. UCLouvain. Engineering issues in proton therapy, LGBIO2070.

[10] Themes, U.F.O. *11: Radiation Treatment of Cancer*. Radiology Key, 8 janvier 2016. Available: `https://radiologykey.com/11-radiation-treatment-of-cancer/`

[11] Jihye Cha, Jinsil Seong, Ki Chang Keum, Chang Geol Lee, Woong Sub Koom. *Comparison of Elective Inguinal Node Irradiation Techniques in Anal Cancer*. Radiation Oncology Journal, vol. 29, n°4, 2011, p. 236. DOI.org (Crossref), https://doi.org/10.3857/roj.2011.29.4.236

[12] Mayo Clinic. *Intensity-modulated radiation therapy (IMRT)*. Available: `https://www.mayoclinic.org/tests-procedures/intensity-modulated-radiation-therapy/about/pac-20385147`

[13] Cancer Research UK. *Intensity modulated radiotherapy (IMRT).* Available: `https://www.cancerresearchuk.org/about-cancer/treatment/radiotherapy/external/types/intensity-modulated-radiotherapy-imrt#:~:text=Volumetric%20modulated%20arc%20radiotherapy%20(VMAT)%20or%20Rapid%20Arc&text=VMAT%20is%20different%20to%20normal,it%20moves%20around%20the%20body.`

[14] Andrea Holt, Dirk Van Gestel, Mark P Arends, Erik W Korevaar, Danny Schuring, Martina C Kunze-Busch, Rob JW Louwe and Corine van Vliet-Vroegindeweij. *Multi-institutional comparison of volumetric modulated arc therapy vs. intensity-modulated radiation therapy for head-and-neck cancer: a planning study.* Radiation Oncology, vol. 8, n°1, janvier 2013, p. 26. BioMed Central, https://doi.org/10.1186/1748-717X-8-26.

[15] Manjit Dosanjh. *The changing landscape of cancer therapy.* (2018, Jan. 15). CERN Courier. Available: `https://cerncourier.com/a/the-changing-landscape-of-cancer-therapy/`

[16] Melissa R. Young, James B. Yu. *Intensity Modulated Radiotherapy and Image Guidance.* Prostate Cancer, Elsevier, 2016, p. 413-26. DOI.org (Crossref), https://doi.org/10.1016/B978-0-12-800077-9.00045-1

[17] Emory University. *Power & Precision.* Available: `https://news.emory.edu/features/2018/11/proton-therapy-center/index.html`

[18] S. Bijan Jia, F. Romano, Giuseppe A.P. Cirrone, G. Cuttone, M.H. Hadizadeh, A.A. Mowlavi, L. Raffaele. *Designing a Range Modulator Wheel to Spread-out the Bragg Peak for a Passive Proton Therapy Facility.* Nuclear Instruments and Methods in Physics Research Section A: Accelerators, Spectrometers, Detectors and Associated Equipment, vol. 806, January 2016, p. 101-08. ScienceDirect, https://doi.org/10.1016/j.nima.2015.10.006.

[19] Hui Liu, Joe Y. Chang. *Proton therapy in clinical practice.* Chinese Journal of Cancer, vol. 30, n°5, May 2011, p. 315-26. DOI.org (Crossref), https://doi.org/10.5732/cjc.010.10529

[20] Patricia van Marlen, Max Dahele, Michael Folkerts, Eric Abel, Ben J Slotman and Wilko Verbakel. *Ultra-High Dose Rate Transmission Beam Proton Therapy for Conventionally Fractionated Head and Neck Cancer: Treatment Planning and Dose Rate Distributions.* Cancers, vol. 13, n°8, April 2021, p. 1859. PubMed, https://doi.org/10.3390/cancers13081859

[21] Simon Deycmar, Erica Faccin, Tamara Kazimova, Philip A. Knobel, Irma Telarovic, Fabienne Tschanz, Verena Waller, Rona Winkler, Carmen Yong, Dario Zingariello, Martin Pruschy. *The Relative Biological Effectiveness of Proton Irradiation in Dependence of DNA Damage Repair.* The British Journal of Radiology, vol. 93, n°1107, March 2020, p. 20190494. DOI.org (Crossref), https://doi.org/10.1259/bjr.20190494

[22] Glennda Chui. *The Power of Proton Therapy.* Symmetry Magazine. Available: `https://www.symmetrymagazine.org/article/december-2008/the-power-of-proton-therapy`

[23] Steven van de Water, Hanne M. Kooy, Ben J.M. Heijmen and Mischa S. Hoogeman. *Shortening Delivery Times of Intensity Modulated Proton Therapy by Reducing Proton Energy Layers During Treatment Plan Optimization.* International Journal of Radiation Oncology*Biology*Physics, vol. 92, n°2, June 2015, p. 460-68. DOI.org (Crossref), https://doi.org/10.1016/j.ijrobp.2015.01.031

[24] Dongxu Wang. *A Critical Appraisal of the Clinical Utility of Proton Therapy in Oncology.* Medical Devices: Evidence and Research, 0ctober 2015, p. 439. DOI.org (Crossref), https://doi.org/10.2147/MDER.S65594.

[25] Melissa A.L. Vyfhuis, Nasarachi Onyeuku, Tejan Diwanji, Sina Mossahebi, Neha P. Amin, Shahed N. Badiyan, Pranshu Mohindra and Charles B. Simone. *Advances in Proton Therapy in Lung Cancer.* Therapeutic Advances in Respiratory Disease, vol. 12, January 2018, p. 175346661878387. DOI.org (Crossref), https://doi.org/10.1177/1753466618783878

[26] Daniel E. Hyer, Patrick M. Hill, Dongxu Wang, Blake R. Smith, and Ryan T. Flynn. *A Dynamic Collimation System for Penumbra Reduction in Spot-Scanning Proton Therapy: Proof of Concept.* Medical Physics, vol. 41, n°9, August 2014, p. 091701. DOI.org (Crossref), https://doi.org/10.1118/1.4837155

[27] Bethany Rothwell, Matthew Lowe, Erik Traneus, Miriam Krieger and Jan Schuemann. *Treatment Planning Considerations for the Development of FLASH Proton Therapy.* Radiotherapy and Oncology, vol. 175, octobre 2022, p. 222-30. DOI.org (Crossref), https://doi.org/10.1016/j.radonc.2022.08.003

[28] Ahmad Neishabouri, Niklas Wahl, Andrea Mairani, Ullrich Köthe and Mark Bangert. *Long Short-term Memory Networks for Proton Dose Calculation in Highly Heterogeneous Tissues.* Medical Physics, vol. 48, n°4, April 2021, p. 1893-908. DOI.org (Crossref), https://doi.org/10.1002/mp.14658

[29] Edmond Sterpin. *PTV margins: concepts and practicalities.* UCLouvain. Technology, dosimetry and treatment planning in radiotherapy, WRDTH3160.

[30] William Parker and Horacio Patrocinio. *Clinical treatment planning in external photon beam radiotherapy.* Review of Radiation Oncology Physics: A Handbook for Teachers and Students, chap. 7.

[31] Giampaolo Bolzicco1, Maria Silvia Favretto, Ninfa Satariano, Enrico Scremin, Carmelo Tambone and Andrea Tasca. *A Single-Center Study of 100 Consecutive Patients with Localized Prostate Cancer Treated with Stereotactic Body Radiotherapy.* BMC Urology, vol. 13, n°1, December 2013, p. 49. DOI.org (Crossref), https://doi.org/10.1186/1471-2490-13-49

[32] Sylvain Deffet, Valentin Hamaide and Edmond Sterpin. *Definition of FLASH dose rate in pencil beam scanning: a comparative study.* (2023, Feb. 28). https://doi.org/10.48550/arXiv.2303.02056

[33] Binwei Lin, Feng Gao, Yiwei Yang, Dai Wu, Yu Zhang, Gang Feng, Tangzhi Dai and Xiaobo Du. *FLASH Radiotherapy: History and Future.* Frontiers in Oncology, vol. 11, May 2021, p. 644400. PubMed Central, https://doi.org/10.3389/fonc.2021.644400

[34] Anna A. Friedl, Kevin M. Prise, Karl T. Butterworth, Pierre Montay-Gruel and Vincent Favaudon. *Radiobiology of the FLASH Effect.* Medical Physics, vol. 49, n°3, March 2022, p. 1993-2013. DOI.org (Crossref), https://doi.org/10.1002/mp.15184

[35] M.-C. Vozenin, J.H. Hendry, and C.L. Limoli. *Biological Benefits of Ultra-high Dose Rate FLASH Radiotherapy: Sleeping Beauty Awoken.* Clinical oncology (Royal College of Radiologists (Great Britain)), vol. 31, n°7, July 2019, p. 407-15. PubMed Central, https://doi.org/10.1016/j.clon.2019.04.001

[36] Till Tobias Böhlen, Jean-François Germond, Jean Bourhis, Marie-Catherine Vozenin, Esat Mahmut Ozsahin, François Bochud, Claude Bailat and Raphaël Moeckli. *Normal Tissue Sparing by FLASH as a Function of Single-Fraction Dose: A Quantitative Analysis.* International Journal of Radiation Oncology*Biology*Physics, vol. 114, n°5, December 2022, p. 1032-44. DOI.org (Crossref), https://doi.org/10.1016/j.ijrobp.2022.05.038

[37] L. G. Marcu. *The Role of Amifostine in the Treatment of Head and Neck Cancer with Cisplatin-Radiotherapy.* European Journal of Cancer Care, vol. 18, n°2, March 2009, p. 116-23. DOI.org (Crossref), https://doi.org/10.1111/j.1365-2354.2008.01032.x

[38] Jean Bourhis and al. *Clinical Translation of FLASH Radiotherapy: Why and How?.* Radiotherapy and Oncology, vol. 139, October 2019, p. 11-17. DOI.org (Crossref), https://doi.org/10.1016/j.radonc.2019.04.008

[39] Sylvain Deffet, Kevin Souris, and Edmond Sterpin.*Optimization of patient-specific range modulators for conformal FLASH proton therapy.* (2023, Mar. 15). DOI.org (Crossref), https://doi.org/10.48550/arXiv.2303.08649

[40] G. Kourkafas, J. Bundesmann, A. Denker, T. Fanselow, J. Heufelder, J. Röhrich and A. Weber. *A 3D RANGE MODULATOR FOR ULTRA-SHORT PROTON FLASH IRRADIATION.* Physica Medica, vol. 94, February 2022, p. S64-65. DOI.org (Crossref), https://doi.org/10.1016/S1120-1797(22)01578-2

[41] Wayne D Newhauser, Rui Zhang. *The physics of proton therapy.* Physics in Medicine and Biology, vol. 60, n°8, April 2015, p. R155-209. DOI.org (Crossref), https://doi.org/10.1088/0031-9155/60/8/R155

[42] Edmond Sterpin. *Interactions of protons with matter.* UCLouvain. Engineering issues in proton therapy, LGBIO2070.

[43] A. Schüller, and al. *The European Joint Research Project UHDpulse – Metrology for Advanced Radiotherapy Using Particle Beams with Ultra-High Pulse Dose Rates.* Physica Medica, vol. 80, December 2020, p. 134-50. ScienceDirect, https://doi.org/10.1016/j.ejmp.2020.09.020

[44] Vadim P. Moskvin, Neil C. Estabrook, Chee-Wai Cheng, Indra J. Das and Peter A. S. Johnstone. *Effect of Scanning Beam for Superficial Dose in Proton Therapy.* Technology in Cancer Research & Treatment, vol. 14, n°5, October 2015, p. 643-52. DOI.org (Crossref), https://doi.org/10.7785/tcrt.2012.500435

[45] Muhammad Ramish Ashraf and al. *Dosimetry for FLASH Radiotherapy: A Review of Tools and the Role of Radioluminescence and Cherenkov Emission.* Frontiers in Physics, vol. 8, August 2020, p. 328. DOI.org (Crossref), https://doi.org/10.3389/fphy.2020.00328

[46] Rodrigo José Santo, Steven Habraken, Sebastiaan Breedveld and Mischa Hoogeman. *Improved Dose Rate by Scanning-Pattern Optimization in FLASH Proton Therapy of Small Lung Lesions.* Radiotherapy and Oncology, vol. 170, May 2022, p. S242-43. DOI.org (Crossref), https://doi.org/10.1016/S0167-8140(22)02540-3

[47] Yuri Simeonov, Uli Weber, Petar Penchev, Toke Printz Ringbaek, Christoph Schuy, Stephan Brons, Rita Engenhart-Cabillic, Jens Bliedtner and Klemens Zink. *3D range-modulator for scanned particle therapy: development, Monte Carlo simulations and experimental evaluation.* Physics in Medicine & Biology, vol. 62, n°17, August 2017, p. 7075-96. DOI.org (Crossref), https://doi.org/10.1088/1361-6560/aa81f4

[48] Ana María Barragán Montero, Kevin Souris, Daniel Sanchez-Parcerisa, Edmond Sterpin and John Aldo Lee. *Performance of a Hybrid Monte Carlo-Pencil Beam Dose Algorithm for Proton Therapy Inverse Planning.* Medical Physics, vol. 45, n°2, November 2017, p. 846-62. DOI.org (Crossref), https://doi.org/10.1002/mp.12688

[49] OpenTPS. `http://opentps.org/`

[50] Tami D. DenOtter and Johanna Schubert. *Hounsfield Unit.* StatPearls Publishing, 2023. PubMed, http://www.ncbi.nlm.nih.gov/books/NBK547721/

[51] Wikipedia. *Hounsfield Scale.* Available: `https://en.wikipedia.org/w/index.php?title=Hounsfield_scale&oldid=1072238718`

[52] Francis Fortin. *Hounsfield Scale (Diagram).* Radiopaedia, https://doi.org/10.53347/rID-77397

[53] MCSquare - Commissioning procedure. `http://www.openmcsquare.org/documentation_commissioning.html`

[54] Sheng Huang, Minglei Kang, Kevin Souris, Christopher Ainsley, Timothy D. Solberg, James E. McDonough, Charles B. Simone II and Liyong Lin. *Validation and Clinical Implementation of an Accurate Monte Carlo Code for Pencil Beam Scanning Proton Therapy.* Journal of Applied Clinical Medical Physics, vol. 19, no 5, September 2018, p. 558-72. DOI.org (Crossref), https://doi.org/10.1002/acm2.12420

[55] E.D. Courant and H.S. Snyder. *Theory of the Alternating-Gradient Synchrotron.* Annals of Physics, vol. 3, n°1, January 1958, p. 1-48. DOI.org (Crossref), https://doi.org/10.1016/0003-4916(58)90012-5

[56] Tejinder Kataria, Kuldeep Sharma, Vikraman Subramani, K. P. Karrthick and Shyam S. Bisht. *Homogeneity Index: An objective tool for assessment of conformal radiation treatments.* Journal of Medical Physics / Association of Medical Physicists of India, vol. 37, n°4, 2012, p. 207-13. PubMed Central, https://doi.org/10.4103/0971-6203.103606

UNIVERSITÉ CATHOLIQUE DE LOUVAIN
École polytechnique de Louvain
Rue Archimède, 1 bte L6.11.01, 1348 Louvain-la-Neuve, Belgique | **www.uclouvain.be/epl**